UC Irvine

UC Irvine Previously Published Works

Title

A comprehensive review of advanced manufacturing techniques, ai-enabled design, and mechanical characterization of nature-inspired helicoidal hybrid composites for impact-resistant applications

Permalink

https://escholarship.org/uc/item/8770k7wq

Journal

Advanced Composites and Hybrid Materials, 9(6)

ISSN

2522-0128

Authors

Kakur, N

Nguyen, AT

Sarmiento, E

et al.

Publication Date

2026-12-01

DOI

10.1007/s42114-026-02122-w

Copyright Information

This work is made available under the terms of a Creative Commons Attribution-NonCommercial-NoDerivatives License, available at https://creativecommons.org/licenses/by-nc-nd/4.0/

Peer reviewed

eScholarship.org Powered by the California Digital Library
University of California

Advanced Composites and Hybrid Materials

REVIEW | Article in Press

A comprehensive review of advanced manufacturing techniques, ai-enabled design, and mechanical characterization of nature-inspired helicoidal hybrid composites for impact-resistant applications

Naresh Kakur · Andrew Tran Nguyen · Ezra Sarmiento · David Kisailus

Received: 29 May 2026 / Revised: 2 October 2026 / Accepted: 5 October 2026
© The Author(s) 2026

Abstract

Helicoidal structures mimic nature and are evident in plant cell walls, lamellar bone, and the shell structures of mantis shrimp and beetles. These nature-inspired helicoidal composites are widely used in impact-resistant applications. Traditional hand-layup methods for producing layered helicoidal composites can introduce defects such as gaps, overlaps, and wrinkles, which can be mitigated using Automated Fiber Placement (AFP). Optimizing AFP process parameters, including pressure, temperature, and layup speed, is crucial. While experimental optimization is costly and time-consuming, Artificial Intelligence (AI)-based design offers a more efficient alternative. This narrative review explores the inspiration behind helicoidal structures and their application fields. It also covers advanced manufacturing of hybrid long-fiber layered composites using AFP + autoclave/hot press, ceramic filler-based nanocomposites using direct ink writing (DIW), and multi-walled carbon nanotube (MWCNT)-based nanocomposites using digital micromirror device (DMD). Furthermore, it discusses the roles of machine learning and deep learning, coupled with finite element modeling, in minimizing process-induced defects. Compared with conventional AFP inspection techniques such as laser profilometry and thermography, a defect-detection algorithm based on PointNet + +, a convolutional neural network (CNN), can be tailored for 3D point cloud segmentation, offering a cost-effective, user-friendly alternative. Next, the mechanical and microstructural properties of helicoidal composites, compared with those of traditional laminates, are discussed to evalaute impact performance. Helicoidal composites with low inter-ply angles up to 20° consistently outperform conventional lay-ups under quasi-static and impact loading, due to a crack-twisting mechanism and superior out-of-plane properties. Incorporating nylon 6 powder microparticles into carbon/epoxy and glass/epoxy helicoidal composites subjected to impact loading significantly improves their toughness through self-healing, compared with virgin helicoidal composites. Carbon/epoxy helicoidal composites with low inter-ply angles of up to 9° are prone to extensive matrix cracking and minor fiber damage, while self-healing in carbon/epoxy composites also helps minimize matrix cracking but does not reduce fiber damage. In contrast, self-healing significantly decreases overall damage in glass/epoxy composites. Self-healing is more effective at eliminating damage in glass/epoxy than in carbon/epoxy, primarily because the former exhibits higher ductility (% elongation) than the latter.

This Article in Press is shared early to give you faster access to new research. It is citable and carries a permanent DOI. The final edited version will replace it automatically.



Published online: 23 October 2026

Highlights

- This review article comprehensively covers a wide range of biological materials documented over the past decade that inspire helicoidal structures.
- The manufacturing of helicoidal hybrid composites using conventional and advanced manufacturing techniques is discussed.
- The use of machine learning and deep learning to optimize AFP and 3D printing process parameters, and thereby reduce defects in helicoidal composites, is discussed.
- The role of deep learning in data segmentation and the reduction of computational time for helicoidal composites is discussed.
- The properties of helicoidal composites under low-velocity impact, high-velocity impact, and high strain rates are discussed.

Keywords Bio-inspired composites · Helicoidal hybrid composites · Advanced manufacturing · Finite element analysis · Artificial intelligence · Mechanical properties

Nomenclature

FRP	Fiber-reinforced polymer
CFRP	Carbon fiber-reinforced polymer
GFRP	Glass fiber-reinforced polymer
FFRP	Flax fiber-reinforced polymer
Al_2O_3	Aluminum Oxide
MWCNTs	Multi-walled carbon nanotubes
UHMWPE	Ultra-high molecular weight polyethylene
NFRCs	Natural fiber-reinforced polymer composites
SFRCs	Synthetic fiber-reinforced polymer composites
Polyamide 6	PA6, also known as Nylon 6
PBO	Poly(p-phenylene-2,6-benzobisoxazole), also known as Zylon
BS	Bouligand structures, also known as helicoidal structures
ABM	Aligned brick-and-mortar (ABM)
NL	Nacre-like
CP	Cross-ply
QS	Quasi-isotropic
VSCH	Variable-stiffness curvilinear helicoidal
FGP	Functionally graded pitch
SH	Single-helicoidal
DH	Double-helicoidal
HR	Helicoidal-Recursive
HE	Helicoidal-Exponential
HE	Helicoidal-Semicircular
AFP	Automated fiber placement
ATL	Automated tape laying, also called automated tape layup
TFP	Tailored fiber placement
AM	Additive manufacturing
CAD	Computer-aided design
3D	Three-dimensional
DT	Destructive testing
NDT	Non-destructive testing
AI	Artificial intelligence

ML	Machine learning
DL	Deep learning
FEA	Finite element analysis
OoA	Out-of-autoclave
VBO	Vacuum-bag-only
RTM	Resin transfer molding
HPRTM	High-pressure resin transfer molding
VARTM	Vacuum-assisted resin transfer molding
HAO	Hot air oven
ALM	Additive layer manufacturing
DMD	Digital micromirror device
DLP	Digital light processing
DIW	Direct Ink Writing
FDM	Fused deposition modeling
SEM	Scanning electron microscopy
OM	Optical microscopy
μCT	X-ray computed tomography
ET	Electron tomography
HRTEM	High-resolution transmission electron microscopy
MRI	Magnetic resonance imaging
VI	Visual inspection
ANNs	Artificial neural networks
GANs	Generative adversarial networks
GNNs	Graph neural networks
CNNs	Convolutional neural networks
DBNs	Deep belief networks
AEs	Autoencoders
RNNs	Recurrent neural networks
LVI	Low-velocity impact
HVI	High-velocity impact
V_b	Ballistic limit
EA	Energy absorption
SEA	Specific energy absorption
V_i	Impact velocity
V_r	Residual velocity
BFS	Back face signature
CAI	Compression after impact
FAI	Flexural after impact
SHPB	Split-Hopkinson pressure bar

1 Introduction

Researchers have been developing fiber-reinforced polymer (FRP) composites for years, aiming to combine high strength and stiffness without compromising toughness [1–3]. However, these challenges persist. For instance, carbon fiber-reinforced polymer (CFRP) exhibits high strength and stiffness but low toughness (low impact resistance) [4, 5], whereas glass fiber-reinforced polymer (GFRP) shows the opposite trend [4]. Composites are

susceptible to delamination, a primary damage mechanism that compromises structural integrity [5]. Conversely, nature offers biological materials that combine outstanding mechanical properties, including high strength, stiffness, toughness, and exceptional impact resistance [6–8]. Nacre-inspired aluminum oxide (Al_2O_3) ceramic-filled carbon fiber/epoxy-based hybrid nanocomposites significantly increase toughness, addressing the poor toughness of carbon/epoxy composites [9]. These impressive qualities have inspired researchers to develop next-generation high-performance composite structures for diverse applications [10–13]. For example, nacre was found in mollusk shells [7], Bouligand structures (BS), also known as helicoidal structures [14, 15], are hierarchical structures that are found in exoskeletons in a large variety of biological microstructures (arthropod phylum, crustaceans, insects, etc.,) [16, 17], coelacanth fish [18], especially in dactyl limbs of the mantis shrimp (Odontodactylus scyllarus) [19]. Most species exhibit periodic helicoidal structures that confer excellent toughness and damage tolerance [8, 12, 20]. For instance, the mantis shrimp's dactyl club can move at high speeds (~14–23 m/s) and deliver a burst of energy in just 2. 7 ms, enduring impacts of over 10 kg without structural damage [21, 22]. Consequently, traditional laminate configurations (such as cross-ply (CP) or quasi-isotropic (QI) layups) are increasingly being replaced by helicoidal composite structures in applications including aircraft and automotive load-bearing components, engine casings, wind turbine blades, and biomedical implants [1, 23–25]. These benefits arise from helicoidal structures, which offer enhanced out-of-plane properties, a crack-twisting mechanism, and shear-wave filtering, thereby outperforming conventional laminates [12, 26–29]. Moreover, in constructing many modern buildings, helicoidal structures have been used [30, 31], for example, Eco-Tower, Taiwan [32], Amazon's HQ2 in Arlington, Virginia [33], Meixi Urban helix, China [34], entrance staircase in the Louvre, France [35], etc. These architectural features reduce interior space, thereby lowering costs [36]. In particular, helicoidal laminate configurations manufactured with ultra-high molecular weight polyethylene (UHMWPE) are widely used in various defense applications because of their excellent specific energy absorption capability [2, 37–40]. However, UHMWPE composites are very expensive, and their manufacture requires high-pressure (approximately 165–600 bar) curing machines, such as hot press [38, 39, 41] and hydroclave [42]. To match the same impact performance of UHMWPE, it is important to develop hybrid composites by adding nanofillers in other synthetic (carbon, glass, and Kevlar) and natural (flax and basalt) fiber-based composites [43].

However, studies on the broader use of natural fiber-reinforced helicoidal composite structures across various applications remain limited, with only a few papers [44–47] available, compared with studies on synthetic fiber-reinforced helicoidal composite structures [20, 48–51]. Natural fiber-reinforced polymer composites (NFRCs) offer several benefits, including biodegradability, sustainability, CO_2 reduction, low cost, and lower density, compared with synthetic fiber-reinforced polymer composites (SFRCs) [52–54]. Agro-based NFRCs can reduce automotive component cost and weight by 20% and 30%, respectively, compared to petrol-based SFRCs [55, 56]. Components manufactured with plant fiber (flax, hemp, sisal, etc.)-based NFRCs can be 40% to 50% less dense than GFRP [57]. In particular, basalt rock fiber and flax fiber are replacing E-glass fiber in aerospace and automotive applications because they offer higher mechanical and physical properties at the same or lower cost [58–60]. Liu et al. [47] reported in a recent article that helicoidal composites manufactured from a hybrid of 70 wt% flax fiber/epoxy prepreg and 30 wt% glass fiber/epoxy prepreg exhibited 15% higher impact perforation energy than their quasi-isotropic counterparts. Recently, NFRCs have gained widespread use in soft body armor due to their excellent mobility, flexibility, ballistic performance, and low cost. Gowda and Bhat [61] developed helicoidal hemp/basalt/polyurethane rubber bio-composites for soft body armor applications. Moreover, researchers are hybridizing these natural fibers with carbon fiber to reduce costs, enhance the impact resistance of SFRCs [61, 62], and with glass fiber to reduce density and increase strength [62], which bridge the gap between carbon and glass fibers [58, 63, 64].

In recent times, helicoidal lay-ups are being manufactured not only with conventional hand-layup techniques [16, 44] but also using advanced manufacturing techniques, such as automated fiber placement (AFP), automated tape laying (ATL), tailored fiber placement (TFP) [5, 26, 65], and additive manufacturing (AM) techniques [66–68]. These advanced manufacturing techniques rely on computer-aided design (CAD) drawings, enabling rapid, accurate manufacturing of double-curvature or variable-angle tow geometries [56]. Further details about

these advanced manufacturing techniques are discussed in a recent article by Carosella et al. [69]. In recent years, these techniques have been widely used across industries, including Airbus Helicopters, Fraunhofer, TU Dresden, and the German Aerospace Center (DLR), for manufacturing helicopter tail booms and for space and aviation applications [70, 71]. The main advantage of these advanced manufacturing techniques over hand layup is reduced material waste, especially for complex-geometry parts, and reduced human error [70], thereby lowering void content and defects in composites [72]. As a result, it is possible to produce repeatable, high-quality parts while digitally tracing defects, reducing labor costs and increasing production rates, thereby further lowering overall costs. Additive manufacturing methods offer an advantage over traditional techniques because they do not require a mold [73]. However, voids may occur during the three-dimensional (3D) printing process due to its layer-by-layer approach [21]. Researchers can study these voids and other microstructural changes using destructive testing (DT) and non-destructive testing (NDT) methods [74, 75]. However, compared with destructive testing, NDT methods provide more information and do not affect the residual properties of composites [76–78]. Nonetheless, both methods are valuable for supplying input data to model composites and predict their mechanical properties through finite element analysis (FEA) [79, 80]. This approach to predicting mechanical properties using FEA simulation software packages, such as Abaqus, Ansys, SolidWorks, and LS-DYNA, saves time, experimental costs, and manpower [79, 81, 82]. Moreover, a few researchers [83] compared FEA simulation results with experimental results using X-ray computed tomography (μCT) NDT technique. However, FEA simulation studies on helicoidal composite structures are limited. Further studies are needed in this area, beyond a few papers on high-velocity impact [38, 83, 84] and the high-strain-rate properties of helicoidal composites to minimize the number of experimental trials, as a result, production rate can be increased [84].

Moreover, scanned composite sample data from DT and NDT techniques are very large and require significant post-processing time [85]. Therefore, deep learning-based convolutional neural network algorithms are important for analyzing the data and reducing post-processing time [86]. In recent years, researchers have used artificial intelligence (AI)-enabled design to develop bioinspired helicoidal composites [87, 88]. AI-enabled material design can also support multiscale modeling of hierarchical structures [89]. However, little research has examined coupling AI-enabled design with automated manufacturing (AM, AFP, ATL, TFP) processes, which further reduces time and labor costs [90, 91].

The various scales of biological hierarchical structures are shown in Fig. 1a [92]. As shown in Fig. 1a, biomineral crystals exist at the atomic scale, while nanograins in nacre, collagen fibrils in fish scales, and nanoparticles in the mantis shrimp are found at the nanoscale. At the microscale, structural elements include the lamella in bone, tubules in horn, sutures in boxfish scales, and herringbone patterns in the mantis shrimp. At the macroscale, however, natural organisms are classified based on different loading conditions; specifically, the dactyl club of the mantis shrimp and the woodpecker beak are categorized under high-velocity impact loading. The AI-enabled material design of hierarchical structures at various scales, ranging from the nanoscale (nanocomposites) to the microscale (surface modification of fibers) to the macroscale (laminated composites) [89], are shown in Fig. 1b [90].

Property optimization (mechanical, interface, dynamic, and shape-morphing) can be achieved through AI-driven material design at different scales [88, 92]. (i) Nanoscale: property enhancement by modifying resin and surface modification of nanofillers [94]; (ii) Microscale: property enhancement through surface modification of fibers. This improves interfacial bonding between the fiber and resin and can be achieved through physical, chemical, and biological treatment methods [91, 95, 96]. Additionally, fibers are treated with nylon microparticles to enhance their toughness and self-healing abilities [97, 98]; (iii) Mesoscale: property enhancement through ply-level modification (based on tow orientations, such as unidirectional, bi-directional, triaxial, or hybridization of different tow materials (intra-ply)) [78]; (iv) Macroscale – property enhancement through laminated level composites (layered and twisted composites) by using automated manufacturing and lay-up techniques (AFP and AM) [88, 99, 100].

Although Ning et al. [12] reviewed the impact performance of conventional and additively manufactured helicoidal hybrid composites, literature addressing AI- and FEA-driven designs that combine AFP for layered

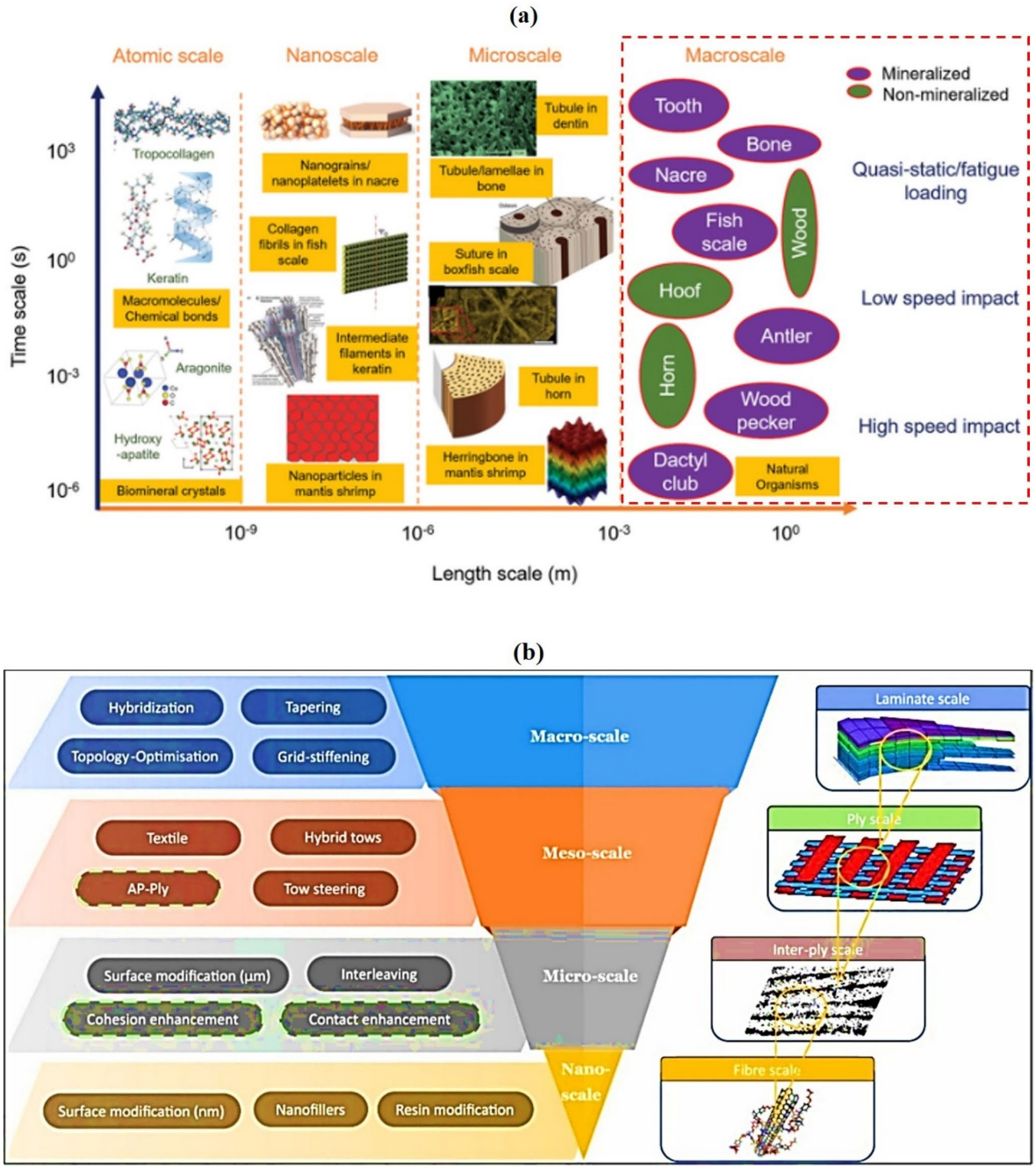


Fig. 1 Various scales of biological hierarchical structures are classified from the atomic scale to the macroscale (**a**) [93] and AI-enabled material design in studying various scales of hierarchical structures (**b**) [90]

composites and AM for particle-filled polymer composites remains scarce. Consequently, further research is required to integrate AI-driven optimization with these automated manufacturing techniques to develop next-generation hybrid structures. This review is narrative rather than systematic. In this review, Sects. 2 and 2.1 discuss the inspiration and applications of helicoid structures in manufacturing various FRP composites using conventional and advanced manufacturing techniques. In Sect. 2.2, classification and toughening mechanisms of helicoid composite structures are discussed. In Sect. 2.3, helicoid biocomposites and the hybridization approach to synthetic/natural fiber-reinforced helicoid composites are discussed; these studies are very limited [46]. In Sect. 2.4, the manufacturing of particle-filled polymer composites using additive manufacturing techniques is discussed. In Sects. 3.0–3.2, the use of NDT and DT techniques to capture and understand the microstructural changes in helicoid structures, and the modeling of helicoid structures using FEA analysis, are discussed. In Sects. 4.0 and 4.1, AI-enabled machine learning and deep learning algorithms are discussed that optimize AFP and 3D printing process parameters to minimize experimental costs and processing defects in composites. In Sect. 4.2, the application of deep learning to composites and the use of deep learning algorithms to analyze NDT and DT data and reduce computation time are discussed. In Sect. 5.0, the mechanical properties of helicoid composite structures are discussed in detail. In Sect. 6.0, future perspectives are discussed in detail, including research gaps in manufacturing and mechanical characterization (Sect. 6.1), optical property characterization (Sect. 6.2), and in artificial intelligence-based modeling of helicoid composites (Sect. 6.3). The advanced manufacturing techniques, FEA, and AI-based modeling of helicoid structures discussed in this review offer new directions for researchers seeking to rapidly and effectively manufacture high-strength, high-stiffness, and impact-resistant composites for the aerospace, defense, and sports industries.

2 Inspiration and applications of helicoidal structures

Helical architecture appears in nature across length scales, from molecular to macroscopic, for example, in DNA molecules, plant roots, and spiral nanoribbons [101, 102]. For example, helicoidal structures can be inspired by natural materials, such as lamellar bone [17], cell walls of plants and wood [103], leaves (Diplazium crenatoserrarum, Lindsaea lucida, etc.), flowering plants (Phyllagathis rotundifolia), Pollia condensata fruit, etc. [104]. Moreover, the helicoidal structures are inspired from nature through several shell structures of biological materials [40], such as the dactyl club of Mantis shrimp [27], prawn exoskeleton [105], elytral cuticle of beetles (Scarab beetles [106] or Chrysina gloriosa beetle [107], Macraspis lucida beetle [108], Japanese jewel beetle [109], etc.) [110], weevils [111], fish scales (Coelacanth-fish [18], Arapaima gigas scales [112, 113], Pagrus major, Latimeria chalumnae, Shark [114]), sea and land snails (Bertia cambojiensis) [115], the cuticle of Scorpio Maurus Palmatus tarsus (endocuticle) [116], arthropod cuticle [117, 118], Lobster cuticle [119], Scarabaei cuticle [66], Crustacean [120], claw of crabs [121], etc.

Figures 2a-e and 3a-e show the biological structures that inspired the helicoidal composite structure (Figs. 2f and 3c). Moreover, Figs. 2h-l and 3f and g show numerous applications in which helicoidal composite structures are used. In our recently published US patent, the use of helicoidal technology across various applications, especially for leading-edge protection of aerodynamic structures, was highlighted [122]. Moreover, helicoidal composites have recently been used in the hockey industry (Fig. 2m) [123] and in a DNA-inspired soft actuator for soft-robot applications (Fig. 2n) [124]. Helicoidal composites have also been used in bioinspired lattice applications to develop bioinspired skyscrapers in London, UK [125]. Figure 3g shows helicoidal technology in cement-based composites for modern construction and buildings [126], including helicoidal and nacre-inspired hybrid composites, which delay catastrophic failure and possess excellent toughness properties [9, 127].

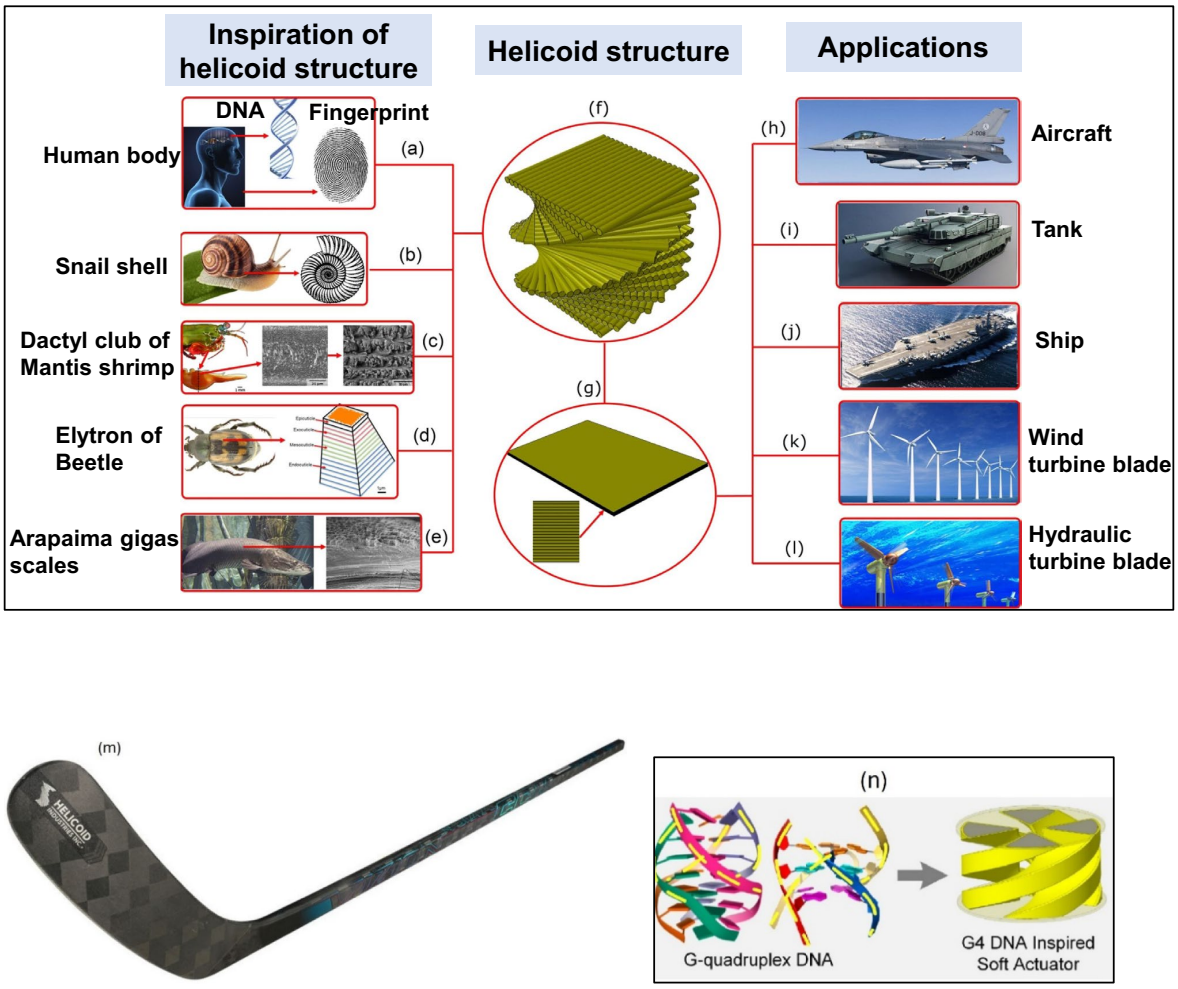


Fig. 2 Inspiration of helicoidal structures from various biological structures (**a**-**e**) [67, 112, 128], Schematic of helicoidal composite structure (**f**-**g**) and applications of helicoidal composite structures in aircraft, tank, ship, wind, and hydraulic turbine blades (**h**–**l**) [129], hockey stick (**m**) [123] and soft actuator for soft robots (**n**) [124]

2.1 Manufacturing of helicoidal composite structures

Helicoid composites can be manufactured using the autoclave and out-of-autoclave (OoA) manufacturing techniques. Common OoA manufacturing techniques include vacuum-bag-only (VBO) prepreg, liquid composite molding, hot press, and filament winding. Liquid composite molding can be further classified as resin transfer molding (RTM), high-pressure RTM (HP-RTM), and resin infusion (RI), also known as vacuum-assisted RTM (VARTM) [130, 131]. In RTM and high-pressure RTM (HP-RTM), the resin system, which usually uses a low-viscosity thermoset such as epoxy or polyurethane, is preheated and premixed in a mixing chamber before injection into the mold. Injection pressures range from 1 to 20 bar for standard RTM, and reach up to 200 bar for HP-RTM [132]. Autoclave, high-pressure RTM, hot press, and filament winding have very high capital costs. In contrast, VBO prepreg and resin infusion techniques are inexpensive and can produce larger parts than autoclave processing [133]. However, these techniques produce porosity greater than 1% because the maximum applied

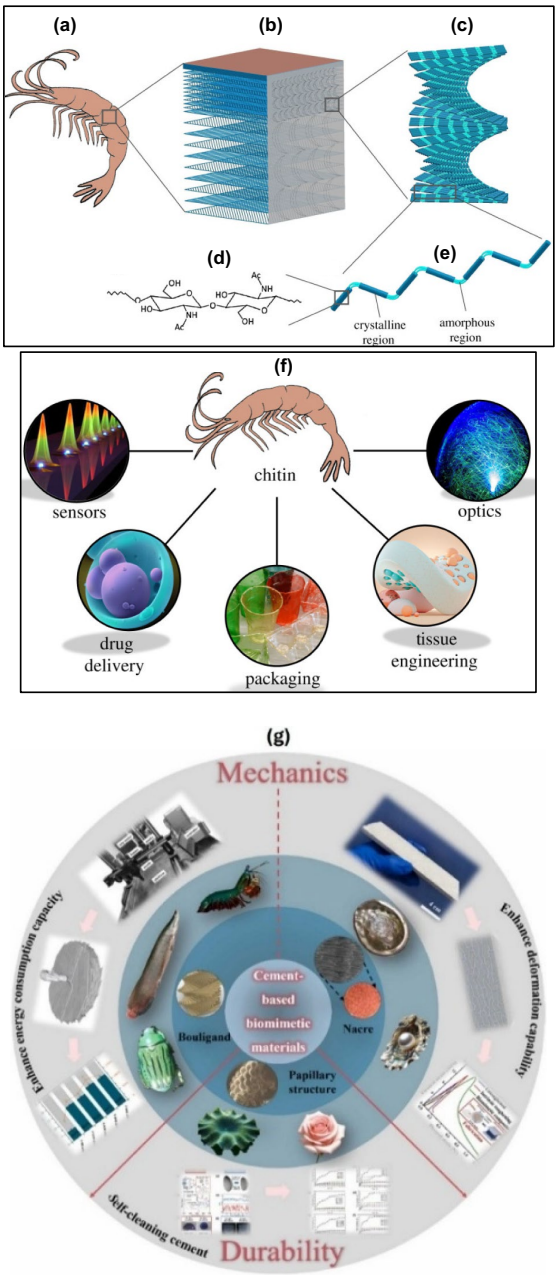


Fig. 3 Prawn exoskeleton (**a**); the macrostructure of prawn exoskeleton reinforced with layered chitin/proteins/calcium carbonate (**b**); helicoidal structure of layered chitin (**c**); chitin crystalline chains are bundled into nanofibrils and its chemical composition (**e**); various applications of layered chitin helicoidal structure (**f**) [105] and cement-based biomimetic materials (**g**) [126]

pressure is 1 bar, while autoclave processing produces porosity less than 1% due to its high applied pressure [134, 135]. Table 1 compares the process and output parameters of autoclave and OoA manufacturing techniques.

In recent years, the hand-layup technique has been replaced by the AFP technique to manufacture helicoidal layups, which minimizes ply-drop gaps and enhances the impact resistance of parts [5, 65, 136]. The AFP technique automatically places tows using a robotic system guided by a computer-aided design (CAD) model [54]. As shown in Figs. 4a–c, the AFP machine consists of a robotic arm, a compaction roller, and an AFP head that holds the prepreg material [137]. Additionally, Fig. 4d illustrates the automation trend in AFP across various sectors

Table 1 Autoclave and out-of-autoclave (OoA) manufacturing techniques and their process and output parameters [91, 140–142]

Manufacturing techniques, process and output parameters	Prepreg-based manufacturing		Liquid composite molding		Wet compression molding and Prepreg compression molding	Wet winding (fiber) and dry winding (Prepreg)
	Vacuum bag + autoclave curing	VBO prepreg + oven curing	HP-RTM	Resin infusion + oven post-cure	Hot press	Filament winding + thermal curing via heated ovens or infrared lamps
Critical processing paramters	Vacuum pressure, autoclave Internal Pressure and temperature, dwell time	Vacuum pressure and oven temperature, dwell time	Mold shape, resin rheology, fiber permeability, injection pressure and temperature, gel time	Resin rheology, fiber permeability, vacuum pressure, gel time and oven temperature	Mold shape, hydraulic pressure and temperature, dwell time	Winding speed, winding angle, fiber tension, oven temperature, dwell time
Energy consumption	Very high	Low	Very high	Low	High – Very high	Medium—high
Best geometry	Flat and Complex curves	Flat and shallow curve	Panels and shells	Flat and shallow curve	Flat and shallow curve	Cylinder and pressure vessel
Part size	Small-medium	Very large	Small-medium	Very large	Small-medium	Medium—large
Surface quality	Best	Medium	Good	Medium	Good	Good
Fiber control	High	Medium—high	Medium—high	Medium	Medium—high	Strongest
Fiber volume fraction	55–65%	55–65%	50–60%	45–60%	40–70%	60–70%
Consistency	Highest	Medium–high	Medium–high	Low-Medium	High	Very high
Cost	Very expensive	Inexpensive	Very expensive	Inexpensive	Very expensive	Very expensive

of the composite manufacturing industry aimed at increasing production rates [138]. By utilizing the built-in resistance scanner in the AFP system, researchers can leverage the electrical conductivity of prepregs for the real-time, in-situ monitoring of defects such as porosity, delamination, gaps, overlaps, tape breakage, twisting, and wrinkling [139]. AFP usage has increased year over year. Figure 4e displays the number of articles published from 1972 to the present, showing a rise over the last five years [131].

Despite its advantages, AFP still faces several challenges, as tow-placement quality depends on several parameters, including compaction pressure, temperature, and lay-up speed (Fig. 23) [90], particularly during curvilinear tow placement for manufacturing fiber-steered composites or variable stiffness fiber-placed composites, which requires complex path planning. During non-linear tow placement, the path length discrepancy between the inner and outer radii of a steered tape induces severe localized shear stresses and asymmetric tension distributions. As a result, common manufacturing problems during placement of these curvilinear tows include local tow gaps and misalignment, steering overlaps, and wrinkling [143]. Therefore, combined approaches that model AFP tow-placement processing conditions using FEA simulations and optimize AFP process parameters using AI-enabled machine learning and deep learning are essential to address these issues [144–146]. Recently, several researchers [147, 148] have integrated machine learning and deep learning algorithms to optimize AFP process parameters and minimize processing defects. Further details on modeling AFP tow-placement processing conditions using FEA simulations are discussed in the literature [134, 135]. The optimization of AFP process parameters using AI-enabled machine learning and deep learning is discussed in Sect. 4.1.

The curing process for AFP-stacked samples can be performed in a hot press, an autoclave, or a hot air oven (HAO), depending on the application and required manufacturing pressure. Dyneema-based UHMWPE composites can be cured only by hydroclave [42] or hot press (HP) [38, 39] techniques because they require very high pressure, approximately 165 bar [43]−600 bar [44], as used in ballistic armor applications [41, 149]. However, conventional autoclave (maximum pressure of approximately 16 bar) [150] or HAO (maximum pressure of 1 bar) techniques cannot cure these UHMWPE composites, limiting their use to lower-pressure applications. However, most synthetic and natural fiber-reinforced polymer composites, other than UHMWPE composites, can



Fig. 4 AFP machine (**a**-**c**) [137], automation trend in AFP (**d**), and number of articles published related to AFP (**e**) [138]

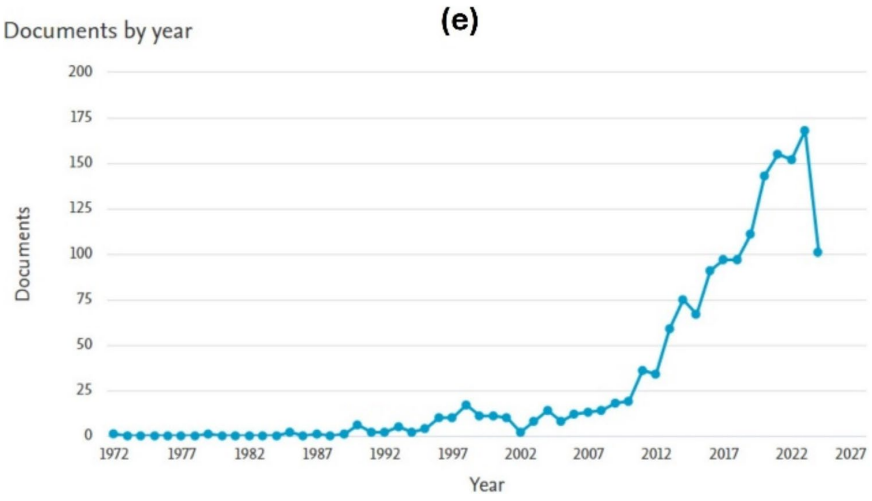


Fig. 4 (continued)

be cured within autoclave-curing pressure limits. More importantly, hybrid composites, synthetic fiber/synthetic fiber [151] and synthetic fiber/natural fiber [47] and synthetic fiber/ceramic nano-filler [9] helicoidal hybrid composites can be cured using hot press or autoclave techniques. However, all these hybrid composites have been manufactured using hand layup followed by hot press or autoclave curing; further studies are required to replace hand layup with the AFP technique.

Figure 5a-i shows the manufacturing process for typical variable-stiffness curvilinear helicoidal (VSCH) composites, from layup unit to layer stacking using the AFP technique, to the hot-press curing cycle, to the final product. However, the capital investments in autoclaves and hot presses are high. To reduce costs, researchers

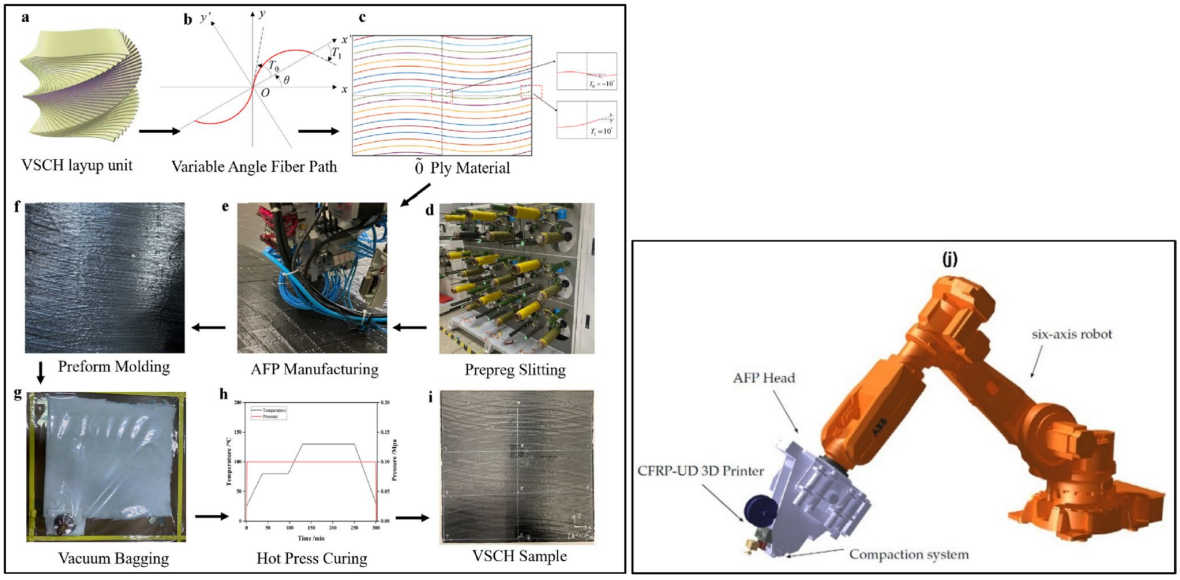


Fig. 5 Manufacturing steps of variable-stiffness curvilinear helicoidal (VSCH) composites using the AFP technique, followed by the hot press curing (**a-i**) [65], and the combination of AFP and ALM (**j**) [153]

increasingly combine AFP with additive layer manufacturing (ALM) [138, 152, 153], as shown in Fig. 5j. Several researchers have been inspired by biological materials in manufacturing FRP composites, as presented in Table 2.

In general, among many biological structures, the dactyl clubs of Mantis shrimp are the most commonly used source of inspiration for the manufacturing of helicoidal composite structures [51, 128]. Figure 6a shows the Mantis shrimp and its dactyl clubs, which are indicated by white arrows, from which the helicoidal structure is inspired by several researchers [19, 161]. Figure 6b shows the optical microscopy (OM) images of the cross-section of the dactyl clubs, which have several regions, namely impact, periodic, and striated regions. Accordingly, the periodic region is used to design the helicoidal structures, as shown in Fig. 6c, and the coronal cross-section of the backscattered scanning electron (BSE) image is shown in Fig. 6d. Figure 6e and f show the crack twisting mechanisms of helicoidal laminate, and Fig. 6g shows the crack propagation without a twisting mechanism in traditional laminate. Figure 6h and i show that the nacre-like (NL) basalt/epoxy composite delays crack propagation and prevents catastrophic failure under low-velocity impact, exhibiting superior impact resistance and energy absorption compared with the aligned brick-and-mortar (ABM) basalt/epoxy composite [162].

Table 2 Manufacturing FRP helicoidal composite structures through bio-inspired biological structures

Biological materials	Adopted material	Manufacturing technique	Reference
Coelacanth-fish	Carbon/polyamide (PA) 6	Hand-layup + hot press	Yin et al. [154]
	UHMWPE	Hand-layup + hot press	Hu et al. [38]
Mantis shrimp	Flax/epoxy	Hand-layup + autoclave	Chew et al. [44]
	Glass/epoxy, Glass/urethane, Kevlar/epoxy, and Kevlar/urethane;	Hand-layup + wet layup + HAO	Rivera et al. [51]
	Basalt/epoxy	Hand-layup + hot press	Han et al. [45, 46]
	UHMWPE	Hand-layup + hot press	Sreekantha Reddy et al. [37] and Karthikeyan et al. [155]
Crustaceans	Aramid/epoxy	Hand-layup + hot press	Wang et al. [156]
	Carbon/epoxy	Hand-layup + HAO	Liu et al. [157]
	Carbon/epoxy	Hand-layup + hot press	Liu et al. [158]
	Glass/epoxy	Hand-layup + autoclave	Liu et al. [98]
Dactyl clubs and exoskeletons of mantis shrimps	Carbon/epoxy	AFP + hot press	Liu et al. [65]
	Carbon/epoxy	AFP + autoclave	Whitehouse et al. [5]
Odontodactylus scyllarus	Carbon/epoxy	Hand-layup + autoclave	Mencattelli and Pinho [50]
	Carbon/epoxy	Hand-layup + HAO	Grunenfelder et al. [128]
Odontodactylus japonicas	Carbon/PA 6	Fused Deposition Modeling (FDM)	Yin et al. [21]
Peacock mantis-shrimp	Carbon/epoxy	Hand-layup + hot press	Liu et al. [159]
	CFRP (USN 15000/6511/RC33)	Hand-layup + autoclave	Ouyang et al. [160]
Homarus americanus, Callinectes sapidus, and Popillia japonica	S2-glass/epoxy	Hand-layup + HAO	Cheng et al. [16]
Cuticle of the Figeater beetle (Cotinis mutabilis)	VeroWhite/TangoPlus	3D printing	Zaheri et al. [67]
Beetle's elytron	Carbon/PP, glass/PP, and hybrid carbon/glass/PP	Hand-layup + hot press	Wang et al. [151]
Fish scales (Pagrus major, Latimeria chalumnae, Shark)	Tungsten/copper composites	Hand-layup + infiltration	Zhang et al. [114]

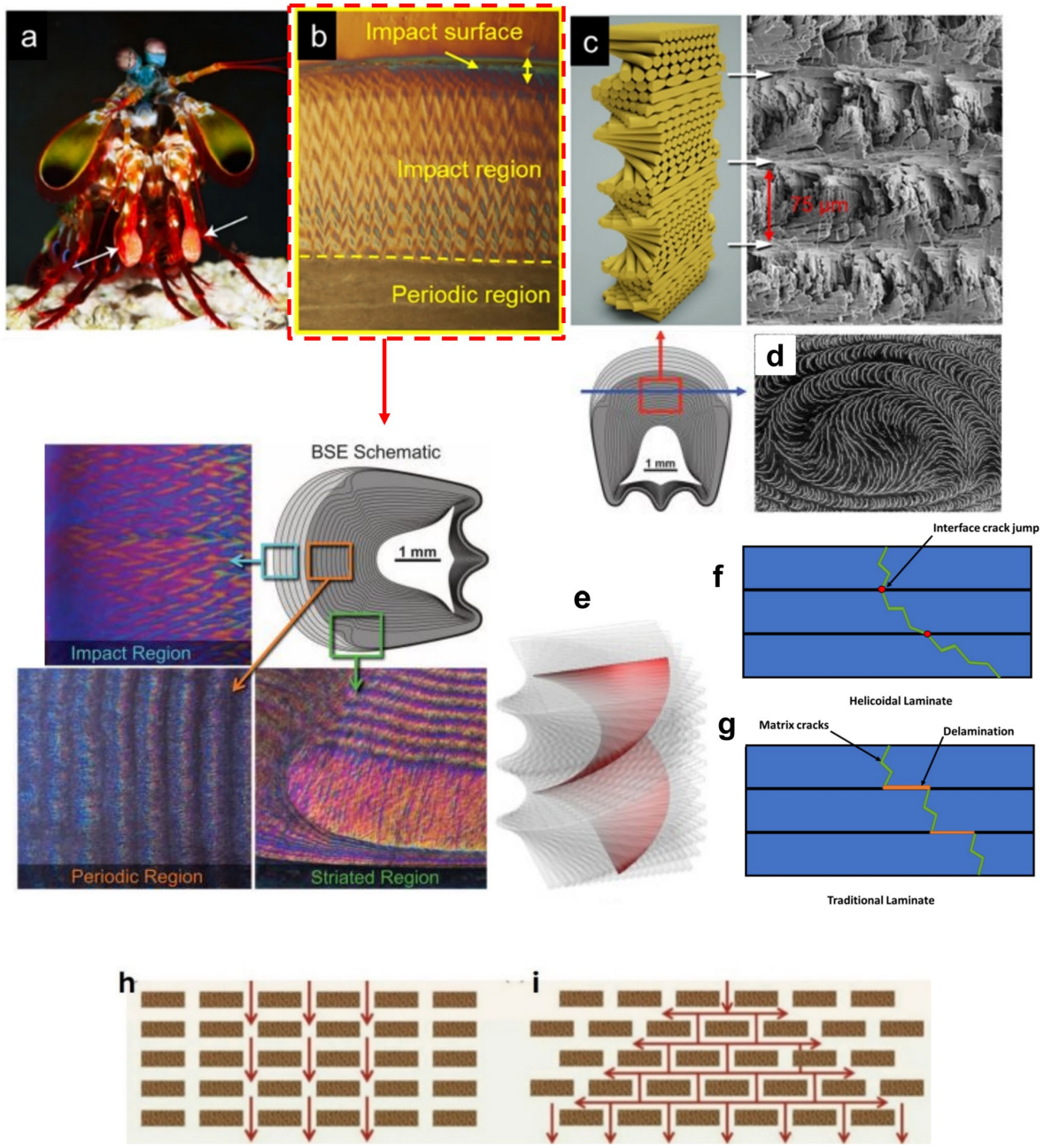


Fig. 6 Mantis shrimp and its dactyl clubs (**a**); optical microscopy images of the cross-section of the dactyl clubs (**b**); schematic and SEM picture of helicoidal structure (**c**) [161]; coronal cross-section of dactyl clubs (**d**); Crack twisting mechanism in helicoidal laminate (**e**, **f**); matrix crack propagation in traditional laminate (**g**) [163] and energy dissipation path between the ABM and NL design structures in the basalt/epoxy prepreg composites (**h** and **i**) [162]

2.2 Classification and toughening mechanisms of helicoidal composite structures

The helicoidal laminates can be divided into two types based on layup orientation, namely linear-helicoidal (LH) and nonlinear-helicoidal (Helicoidal-recursive (HR), Helicoidal-exponential (HE), Helicoidal-semicircular (HS), Fibonacci helicoidal) [164, 165]. The helicoidal structure is characterized by stacking layers, each gradually rotated about its normal direction relative to the adjacent layer [16], as shown in Fig. 2f. Helicoidal structures show lower strain-stiffening values and fewer fiber reorientation angles than mono-balanced structures [166]. Through this smaller inter-ply angle rotation mechanism in the helicoidal approach, cracks can be twisted within the structure during in-plane and out-of-plane loading [28]. Therefore, crack propagation can be controlled to protect the structure from catastrophic failure, reducing delamination areas and increasing energy absorption and toughness [20, 167]. Moreover, Grunenfelder et al. [128] reported that damage was more widely distributed in helicoidal laminates, whereas a quasi-isotropic laminate showed localized, narrowly distributed damage that resulted in a higher dent depth. Similarly, Ouyang et al. [168] observed that damage in cross-ply laminates is localized and concentrated, while double-helicoidal (DH) configurations develop widespread, asymmetric damage fields. Therefore, the helicoidal structure concept is widely adopted in manufacturing FRP composite structures [52] to overcome the lower mechanical properties of traditional fiber-orientation concepts, such as cross-ply [158] and quasi-isotropic [51].

Figure 7a and b show the conventional (unidirectional, cross-ply, and quasi-isotropic) and helicoidal layup configurations, respectively, along with their polar properties [169]. The elastic moduli (E_1 and E_2) and shear modulus (G_{12}) of composites depend on fiber orientation. Composite failure mechanisms depend on the fiber, matrix, and interphase, as well as the loading direction [129]. As shown in Fig. 7b, the elastic moduli (E_1 and E_2) are aligned with the cross-ply and quasi-isotropic layup orientations; however, these properties differ markedly between the linear and nonlinear helicoidal orientations.

Helicoidal laminates can also be classified as single-, double-, quadruple-, octuple-, and cross-helicoidal types [168, 170]. Inter-ply angles between 2.5° and 5° induce severe spiraling matrix splits that compromise laminate integrity. Conversely, when angles reach 20° or greater, the laminate's resistance to spiraling matrix splits becomes too high to develop; as a result, fiber damage becomes dominant, causing the failure mechanisms of the helicoidal laminate to resemble those of a quasi-isotropic laminate [128, 171]. Identifying the optimal inter-ply angle is essential to improve out-of-plane properties, as helicoidal laminates exhibit poor out-of-plane performance at both extreme ends: very small [44, 129] or very large inter-ply angles [48]. In comparison, Liu et al. [157] reported an optimal inter-ply angle of approximately 5º to 10º, while other studies suggest values up to 20º [154, 172, 173]. However, this optimum depends on several parameters, including fiber and matrix selection, laminate thickness, loading mode, and impact conditions [157, 160, 174].

Moreover, several researchers reported that helicoidal laminates with non-uniform variation in inter-ply angles exhibited better out-of-plane properties than those with uniform variation [156, 163]. Smaller inter-ply angles control delamination, while larger inter-ply angles control matrix splitting; thus, Liu et al. [159] suggested designing a helicoidal laminate with larger inter-ply angles at the bottom and smaller inter-ply angles at the top to control both delamination and matrix splitting, thereby increasing composite toughness. Lin et al. [154] performed quasi-static three-point bending and Charpy impact tests on both single- and double-helicoidal laminate configurations. Results showed that single-helicoidal configurations are affected by inter-ply angles, mid-plane architecture, and strain rate, while double-helicoidal configurations are unaffected by these factors.

The toughening of helicoidal composites can be analytically predicted using the crack-bridging model [175]. The toughening ratio of helical fibers depends on the length-to-diameter (L/D) ratio of fibers. A higher L/D ratio provides greater toughening of fibers, as it increases with fiber length and decreases with fiber diameter, as shown in Fig. 8a and b. For the same fiber volume fraction, the toughening efficiency can be measured based on the crack-bridging stress intensity factors of helical and straight fibers using Eq. (1):

https://doi.org/10.1007/s42114-026-02122-w

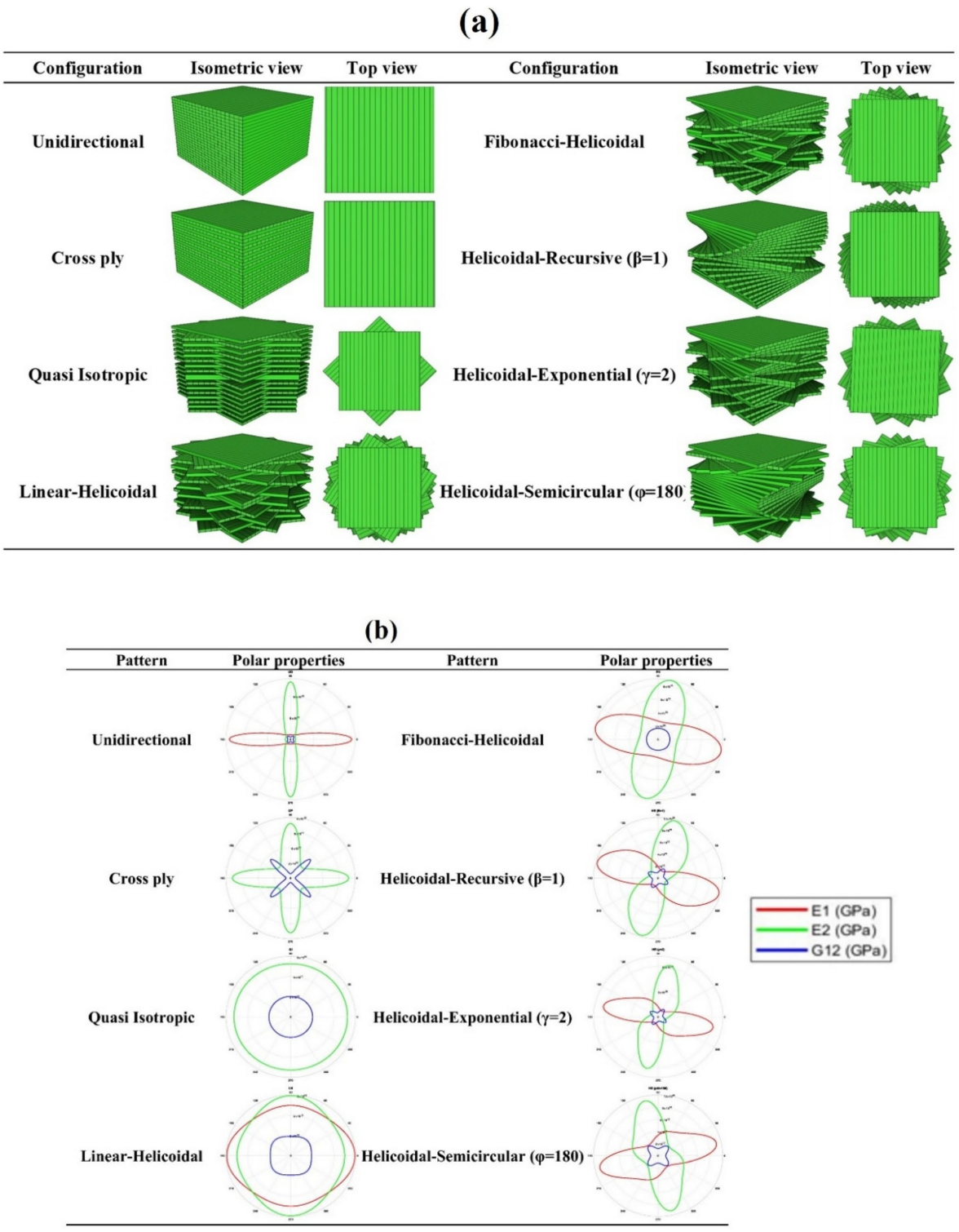


Fig. 7 Schematic representation of conventional and helicoidal layup configurations (**a**) and their polar properties (**b**) [169]

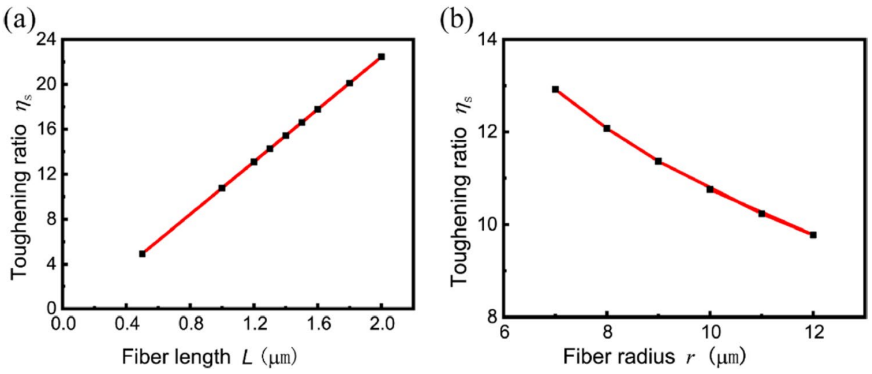


Fig. 8 Effect of L/D ratio on the toughening ratio of helical fibers [175]

$$\Psi = \frac{K_1(_{helical})}{K_1(_{straight})} = \frac{\eta_s(_{helical})}{\eta_s(_{straight})} \quad (1)$$

where Ψ is the toughening efficiency of helical fibers; $K_1(_{helical})$ and $\eta_s(_{helical})$ are the crack-bridging stress intensity factor and toughening ratio of helical fibers, respectively. $K_{1(straight)}$ and $\eta_s(_{straight})$ are the crack-bridging stress intensity factor and toughening ratio of straight fibers, respectively.

Toughening of helicoidal composites can be increased by the hybridization approach, such as hybridizing synthetic fibers (e.g., UHMWPE/CFRP prepregs, Kevlar/carbon fabrics), combining natural and synthetic fibers (e.g., flax/glass fabrics, basalt/carbon fabrics), and reinforcing nanofillers with synthetic and natural fiber-reinforced composites. However, studies on the mechanical properties of natural fiber-reinforced (NFR) helicoidal biocomposites are very limited, except in very few papers [44–46], compared to synthetic fiber-reinforced (SFR) helicoidal composites. More importantly, studies on nanofillers added to NFR helicoidal composites are not available in the literature. The advantages, limitations, and applications of hybrid composites are discussed in the next section.

2.3 Helicoidal concept in Biocomposites

Figures 9a-c show the classifications of biocomposites, fibers, and polymers, respectively. Biocomposites can be divided into two groups: (i) partially biodegradable, in which either fiber or polymer can be biodegradable, and (ii) completely biodegradable, in which both fiber and polymer are biodegradable. All natural fibers (vegetable and animal) shown in Fig. 9b are biodegradable, while mineral and synthetic fibers are non-biodegradable. Moreover, some polymers are biodegradable, and others are non-biodegradable, as shown in Fig. 9c. Basalt fiber is a natural mineral fiber manufactured by melt-drawing igneous basalt rock at around 1500 °C [58]; This is an industrially processed inorganic mineral fiber and differs fundamentally from lignocellulosic fibers. However, by reinforcing it with biodegradable polymers allows partial biodegradability. Several researchers have manufactured helicoidal laminates and investigated their mechanical properties. More importantly, several researchers have investigated the mechanical properties of SFR thermoset and thermoplastic polymer helicoidal structures [21, 49, 51]. However, to the authors' knowledge, these studies are limited to helicoidal composites with NFR thermoset polymers (flax/epoxy) [44, 47], and basalt/epoxy [45]), and to NFR thermoplastic polymer helicoidal composites, for which studies are not available.

Thermoplastic polymers offer several advantages over thermoset polymers, including recyclability, self-healing, design flexibility, and excellent surface finish. Driven by innovations in automated tape laying, in-situ consolidation, and additive manufacturing, thermoplastic polymers have successfully transitioned from low-volume specialized uses to high-caliber, industrial-scale production [97, 176]. Liu et al. [98, 158, 171] developed self-healable helicoidal CFRP and GFRP structures by using combined thermoset (epoxy) and thermoplastic (Nylon

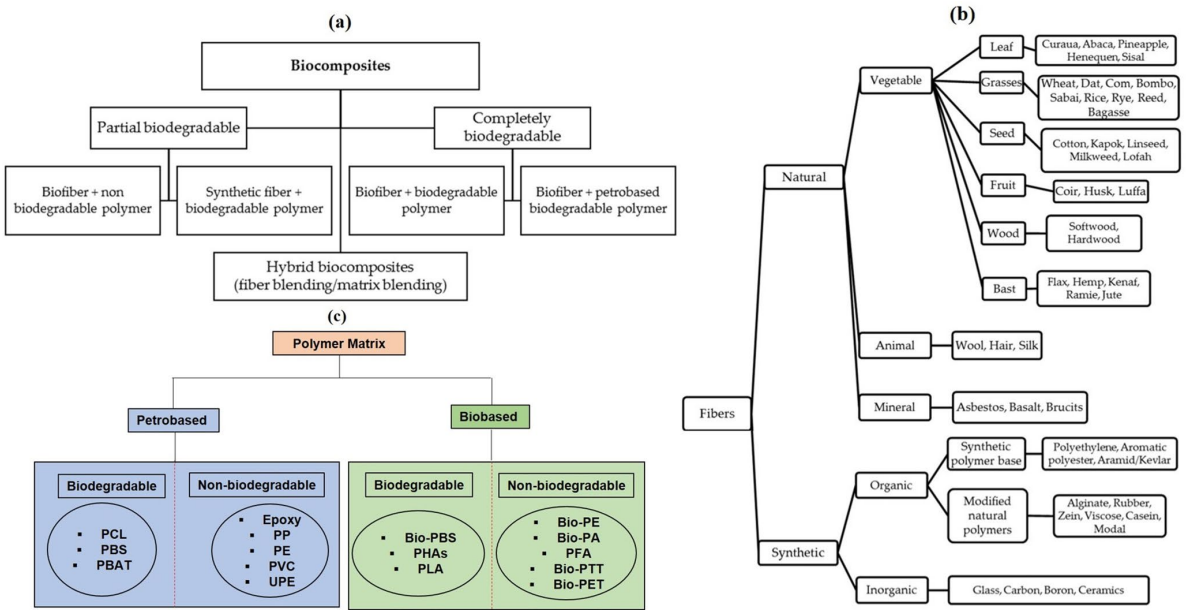


Fig. 9 Classifications of biocomposites (**a**) [177], fibers (**b**) [177] and polymers (**c**) [178]

6) matrices. However, these SFRCs are not biodegradable. Therefore, it is important to manufacture NFR biodegradable thermoplastic (polylactic acid (PLA), polycaprolactone (PCL), polybutylene succinate (PBS), polybutyrate adipate terephthalate (PBAT), etc.) polymer helicoidal composites to achieve complete biodegradability.

2.3.1 Surface treatment and hybridization of natural fibers in manufacturing high-performance helicoidal biocomposites

The main constituents of vegetable or plant natural fibers are cellulose, hemicellulose, and lignin, as shown in Fig. 10a. Natural fibers offer several advantages over synthetic fibers, including biodegradability, sustainability, low density, and lower cost; therefore, NFRCs are widely used in various applications, as shown in Fig. 10b. However, the mechanical and thermal properties of most NFRCs are lower and more sensitive to environmental factors (temperature, low thermal stability, moisture absorption, water absorption, etc.) than those of synthetic fiber-reinforced polymer composites. This can be attributed to hemicellulose in natural fibers, which increases hydrophilicity and reduces compatibility between the fiber and the matrix [179]. Removing hemicellulose can reduce the hydrophilicity of natural fibers, a process that can be obtained through surface modification [180, 181]. Surface modification of natural fibers can be obtained through physical or chemical treatments. Hydrothermal treatment is a promising physical method for improving fiber-matrix compatibility [182]. However, chemical treatments provide better results. Mohit Kumar et al. [183] utilized a sodium hydroxide (NaOH) surface treatment on sisal fibers to investigate the resulting fiber-PLA matrix bonding; scanning electron microscopy images revealed significantly improved interfacial adhesion. Alkalization is the most promising and economical treatment method, removing non-cellulosic elements (pectin, wax, hemicellulose, etc.). As a result, fiber surface roughness increases, promoting interlocking between fibers and the matrix [184]. Further details regarding natural fiber treatments can be found in the literature [52, 185]. Moreover, hybridization improves the low desirable properties of NFRCs, as shown in Fig. 10c. Further details about the hybridization of natural fibers are given in the literature [186].

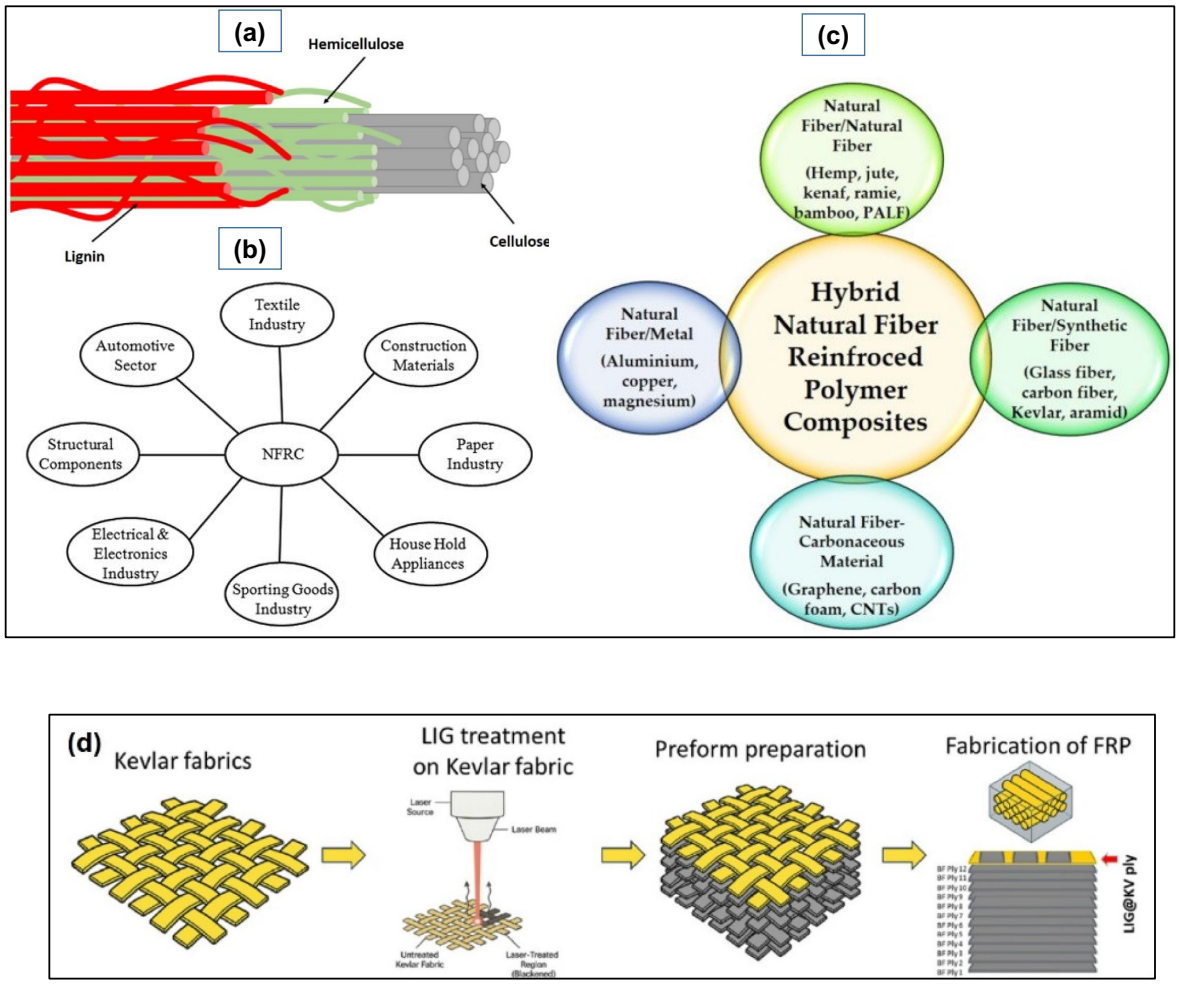


Fig. 10 Structure of natural plant fibers (**a**), Applications of NFRCs (**b**) [188], different combinations of hybrid NFRCs (**c**) [189] and LIG treatment on Kevlar fabric [3]

As shown in Fig. 10c, the hybridization of natural fibers is possible in several ways, such as natural/natural and natural/synthetic. Laser-induced graphene (LIG) is an automated fabric-treatment process that uses a laser beam to deposit graphene nanoparticles onto fabric, as shown in Fig. 10d [3]. The hybridization approach of treating fabric with a helicoidal layup orientation using nanofillers has also not performed well. Using LIG, both synthetic and natural fabric layers can be treated, and the AFP technique can then place the tows and stack the layers, minimizing processing time and defects [187]. Therefore, the hybridization approach is important for rectifying the undesirable properties of both fibers and for manufacturing high-performance helicoidal biocomposites.

Figure 11a and c show the advantages of synthetic fibers (Kevlar and carbon fibers) over aluminum and ceramics, including their higher specific strength and stiffness. Moreover, numerous natural materials exhibit excellent mechanical properties. For example, Fig. 11b shows the high fracture toughness of bone and nacre, and Fig. 9c shows the high specific stiffness of Arthropod cuticle and Beetle elytra. Therefore, combining these nature-inspired biological structures yields helicoidal hybrid composites composed of different materials that exhibit improved mechanical properties.

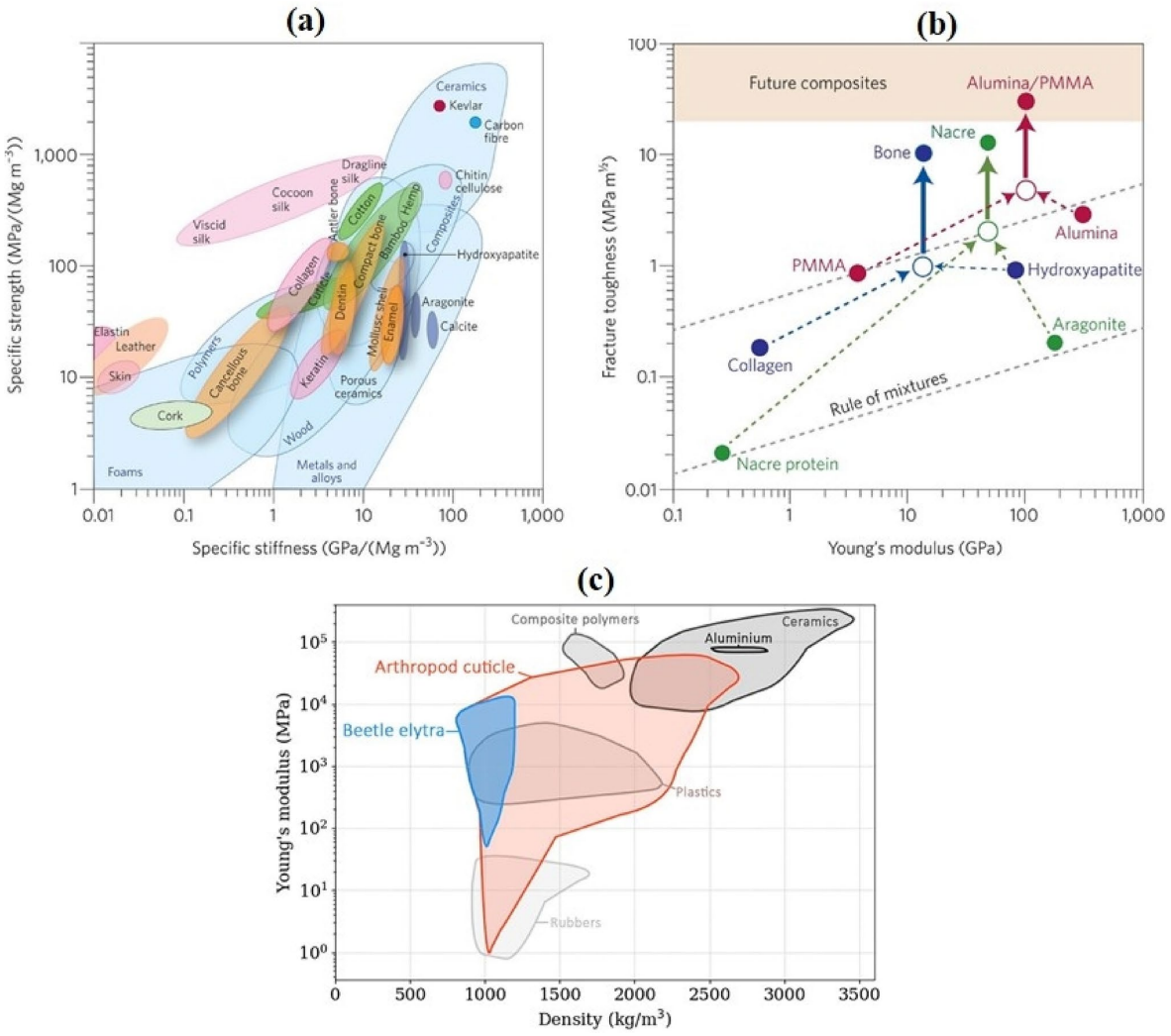


Fig. 11 Projections in developing natural and synthetic composite materials [118, 190, 191]

The hybridization approach in helicoidal laminates has been studied previously: carbon fiber/glass fiber/polypropylene (PP) [151], glass fiber/epoxy/nylon 6 and carbon fiber/epoxy/nylon 6 [97, 98, 158, 171], CFRP/Al_2O_3 particle-filled composites [99, 192], and glass fiber/flax fiber/epoxy [47]. However, further studies are needed to match the impact properties of UHMWPE composites with those of other composites, including particle-filled polymer composites for impact-resistant applications.

2.4 Manufacturing of particle-filled polymer composites using additive manufacturing (AM) techniques

Reinforcing the polymer matrix with nanoparticles and microfibers mitigates microvoid content, crack propagation, and delamination, resulting in superior impact and wear resistance [193–196]. Particle-filled polymer composites can be manufactured using various AM techniques, such as electrically assisted digital micromirror

device (DMD), magnetically assisted digital light processing (DLP), and Direct Ink Writing (DIW)-based 3D printing [100].

This section compares DLP/DMD and DIW printing processes. DLP/DMD resolution depends on the projector pixel size, while DIW resolution depends on nozzle diameter, ink rheology, and post-extrusion filament spreading. As a result, DLP/DMD can achieve resolutions below 50 µm, while DIW produces much thicker lines (over 100 µm) because of the extreme pressure and shear forces inside the tip [197]. Another advantage of DLP/DMD over DIW is that entire layers cure simultaneously; therefore, the processing is much faster [198, 199]. However, adding high-aspect-ratio materials, such as carbon nanotubes or metal fibers, quickly ruins this benefit. Because these fillers scatter and block UV light, the resin cannot cure deeply enough, capping the maximum filler loading at around 5 vol% [200]. However, DIW allows filler loadings above 50 vol% to create dense ceramic structures [201, 202]. This section discusses these manufacturing techniques.

Figure 12a shows the Homarus americanus-inspired helicoidal composites. To manufacture multi-walled carbon nanotube (MWCNT) polymer composites, the electrically assisted digital DMD technique aligns carbon nanotubes within a low-viscosity, photocurable resin by controlling the rotational movement of two parallel electrodes, as shown in Fig. 12b. These electrodes generate an electric field in response to the applied DC voltage. After manufacturing the polymer/MWCNT composites, the microstructure is examined using scanning electron microscopy (SEM) and OM for quality control, as shown in Fig. 12c. Finally, after ensuring layup quality, the layups can be stacked to generate helicoidal nanocomposites, as shown in Fig. 12d [203]. Similarly, instead of electrically assisted 3D printing, magnetically assisted DLP 3D printing is used to manufacture steel fiber-reinforced polymer helicoidal composites, as shown in Fig. 13a-d [204]. Magnetic fields generated by magnets align the steel fibers in the photocurable resin. The remaining procedure is the same as the previous one.

Ceramic-polymer composites [205] and short (chopped) fiber/ceramic-filled polymer composites [99] can be effectively produced using a ball mill followed by DIW 3D printing, as melting ceramics is not feasible with

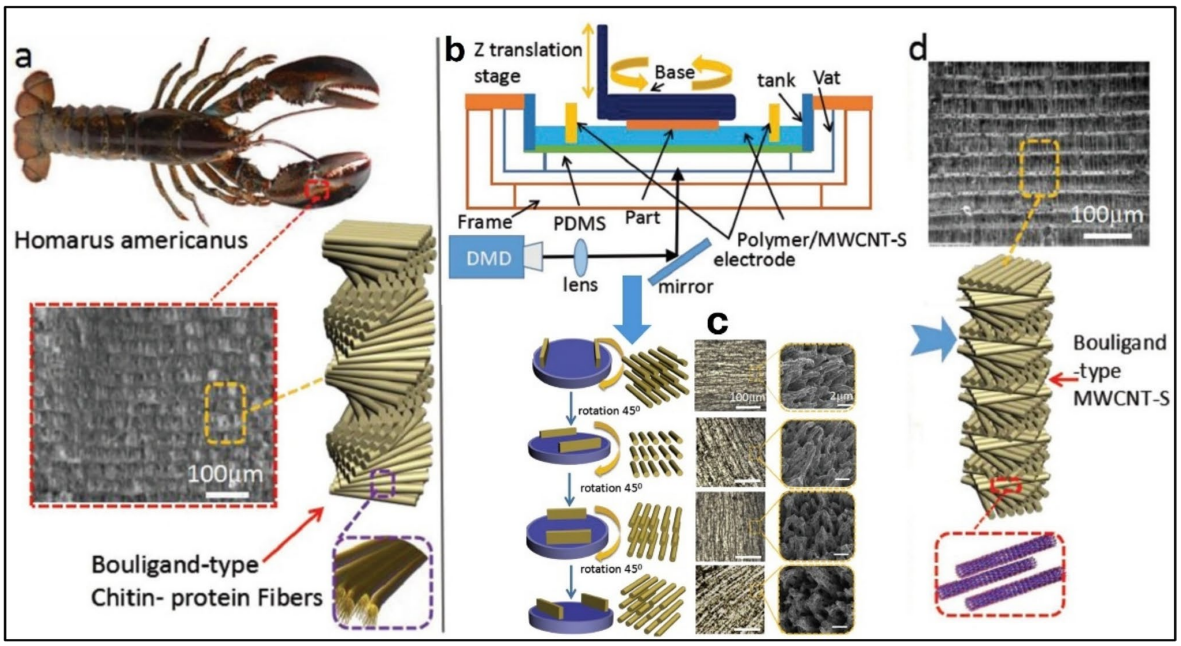


Fig. 12 Manufacturing steps of MWCNTs-reinforced polymer helicoidal composites: Homarus americanus-inspired helicoidal design (**a**), electrically-assisted digital micromirror device (DMD)- based 3D printing setup (**b**), microstructure investigation of helicoidal composites using OM and SEM images for quality checking (**c**), and layer-by-layer stacked helicoidal composites (**d**) [203]

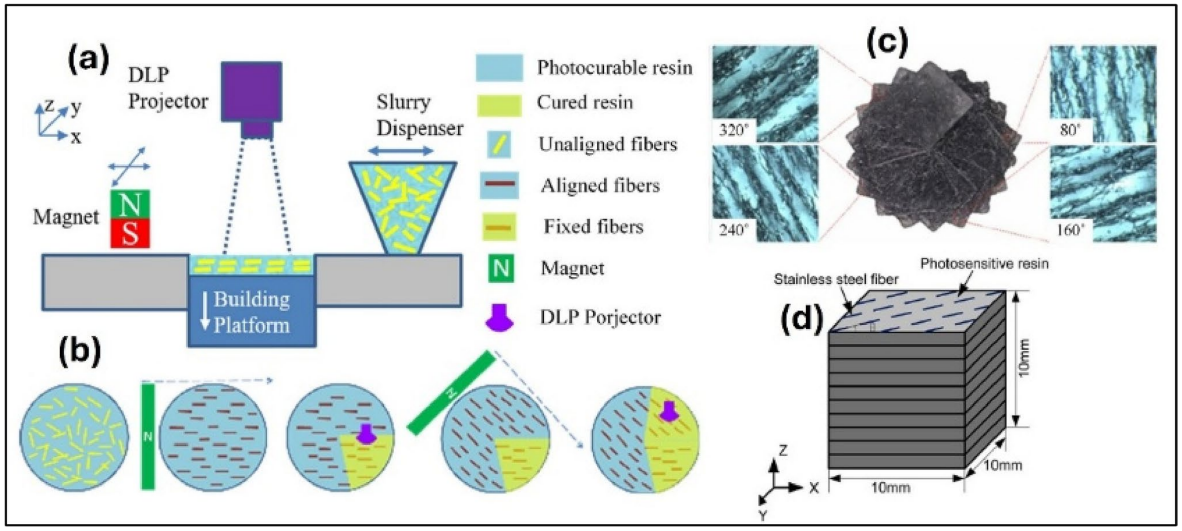


Fig. 13 Manufacturing steps of steel fiber reinforced polymer helicoidal composites: magnetically-assisted DLP 3D printing setup (**a**) and aligned fibers in the cured resin (**b**), microstructure investigation of helicoidal composites using OM for quality checking (**c**), and final part (**d**) [204]

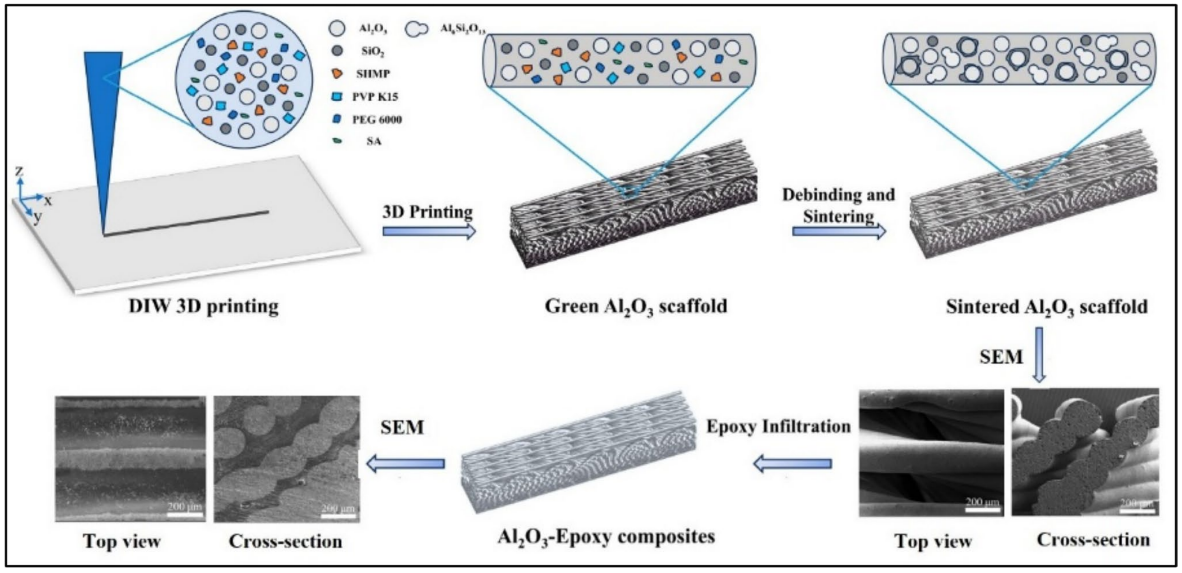


Fig. 14 Manufacturing steps of Al_2O_3-epoxy helicoidal composites using DIW 3D printing [206]

FDM 3D printing. Figure 14 shows the stepwise procedure for the preparation of Al_2O_3-epoxy helicoidal composites. First, an Al_2O_3 ceramic slurry is prepared in a ball mill; subsequently, rheology studies determine the slurry's optimal viscosity using a rheometer. The slurry is then used to create a green Al_2O_3 scaffold via DIW 3D printing. The debinding process involves gradually heating from room temperature to 300ºC and holding for 1 h, then increasing to 600ºC and holding for 2 h in a debinding furnace, and finally cooling to room temperature. Sintering follows, with a gradual temperature increase from room temperature to 300ºC, holding for 1 h, then to 600ºC, holding for 1 h, and finally to around 1600ºC, holding for 2 h. After sintering, the Al_2O_3 scaffold is cooled,

and its quality is assessed using SEM. The rigid ceramic scaffold is then resin-infiltrated, and the final product's quality is reassessed using SEM.

This section discusses the failure mechanisms that occur during debinding and sintering (Fig. 14). During debinding, pressure builds up inside the part's tiny pores as the binder burns out and produces gases. If this trapped pressure cannot escape, it causes micro-cracks. During sintering, the ceramic powder is heated until it fuses into a solid piece, causing the part to shrink. Sometimes, uneven shrinkage occurs across the structure, which leads to warpage or macro-cracking. The literature describes the detailed procedure for preparing these composites [205, 206].

3 Destructive and non-destructive testing techniques

In general, the most commonly used DT techniques for investigating FRP composites are SEM, OM, and transmission electron microscopy (TEM) [91, 131]. In contrast, the most commonly used NDT techniques are μCT, magnetic resonance imaging (MRI), ultrasonic C-scan, digital image correlation (DIC), and infrared thermography (IRT) [77, 207]. These techniques are important for studying voids, failure mechanisms, and related features that are difficult or impossible to observe using visual inspection (VI).

NDT techniques can investigate the microstructure of composite samples without damaging them, whereas DT sample preparation is lengthy and includes cutting, sectioning, polishing, etc., and requires cutting a small sample from the target sample for microstructural investigation [78, 208]. Figure 15 shows the microstructure of bio-inspired helicoidal structures captured using DT (SEM and OM) and NDT (μCT) techniques. The main advantages of μCT over SEM and OM are easy sample preparation and the ability to obtain two- and three-dimensional data, whereas DT techniques require lengthy sample preparation and provide only 2D information [91]. Figure 16a-d shows the microstructural properties of the helicoidal structure in the biological material lucida elytron, captured using non-destructive (μCT) and destructive (OM) testing techniques [108]. From the figure, OM provides poor spatial resolution, so it cannot measure ultrafine deformations. However, OM is easy to handle, inexpensive, and requires less training than μCT.

Conventional DT techniques, such as SEM and OM, are limited to 2D; however, modern technology now enables 3D visualization and analysis in DT. The next section discusses the advantages and disadvantages of 3D NDT and DT techniques.

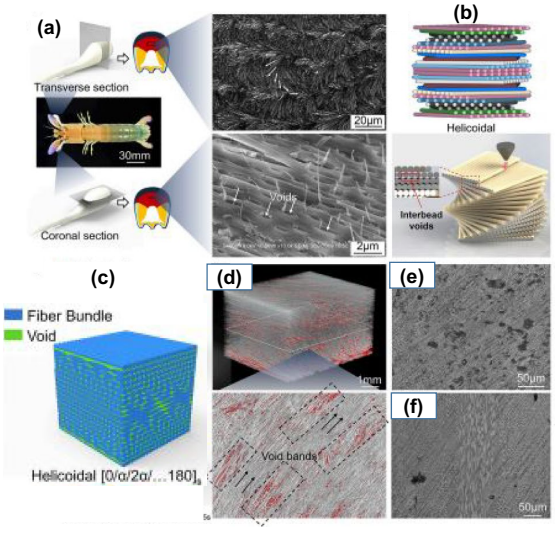


Fig. 15 DT vs. NDT: SEM images of the cross and coronal sections in the periodic region of Odontodactylus japonicas (**a**); FDM printed carbon/PA6 helicoidal laminate (**b-f**); schematic of the helicoidal laminate (**b** and **c**); μCT images—3D and 2D microstructures of void distribution (**d**); OM images—2D microstructures of void distribution in helicoidal laminate: without (**e**) and with hot pressing (**f**) [21]

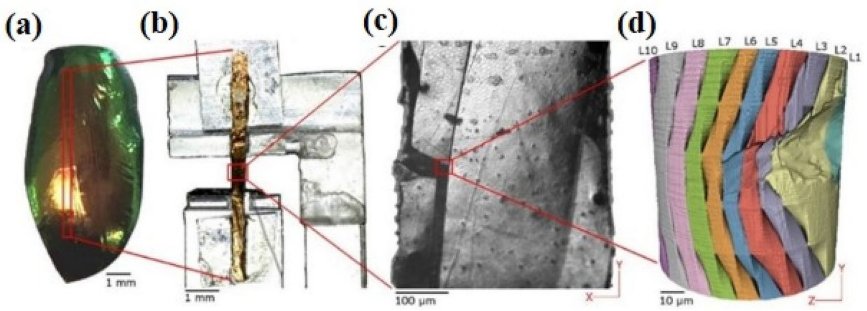


Fig. 16 Cut section image of lucida elytron (**a**), Notched cuticle sample, cut from elytron to perform single edge notched tension test using nano-mechanical testing fixture (**b**), OM image of notched cuticle in 2D (**c**), and µCT image of notched cuticle in 3D (**d**) [108]

3.1 Three-dimensional imaging techniques

Figure 17a and b show the comparison of different features and scanning capabilities of 3D NDT and DT techniques [77, 209, 210]. This section discusses the advantages and limitations of each technique.

Conical OM Advantages include non-destructive scanning and cost-effectiveness. However, it can be used only for non-transparent samples, and its penetration depth (z) is limited.

Electron tomography (ET) Transmission Electron Microscopy (TEM)/high-resolution TEM provides high-resolution 2D projection images, whereas ET uses a series of TEM projection images acquired at different tilt angles to reconstruct a 3D volume (3D structure). This technique can achieve the highest resolution and capture biological structures, as shown in Fig. 17. However, it is limited to small samples and is labor-intensive.

Photoacoustic tomography The advantage of photoacoustic tomography is its non-destructive scanning, though it can yield low resolution.

Neuron tomography Neuron tomography provides good contrast even for low-Z materials. However, it is much more expensive than other techniques.

Magnetic Resonance Imaging (MRI) NDT is widely used for soft tissues because it provides good contrast. MRI uses magnetic fields and radio waves; therefore, it is not suitable for studying ferromagnetic materials. This instrument costs millions of dollars ($). Imaging time is usually measured in hours.

3D SEM This instrument is less expensive than electron tomography (ET). It can achieve high resolution; however, it is slightly lower than ET resolution. This technique can capture biological structures, as shown in Fig. 18. However, it is destructive, requires only small samples, and is labor-intensive.

Computed tomography Based on resolution, it can be divided into micro-CT and nano-CT. High-resolution CT is generally called nano CT (nCT). This technique allows greater depth (z) and can scan a wide variety of samples. However, it is expensive, and image quality depends on several processing parameters, such as spatial

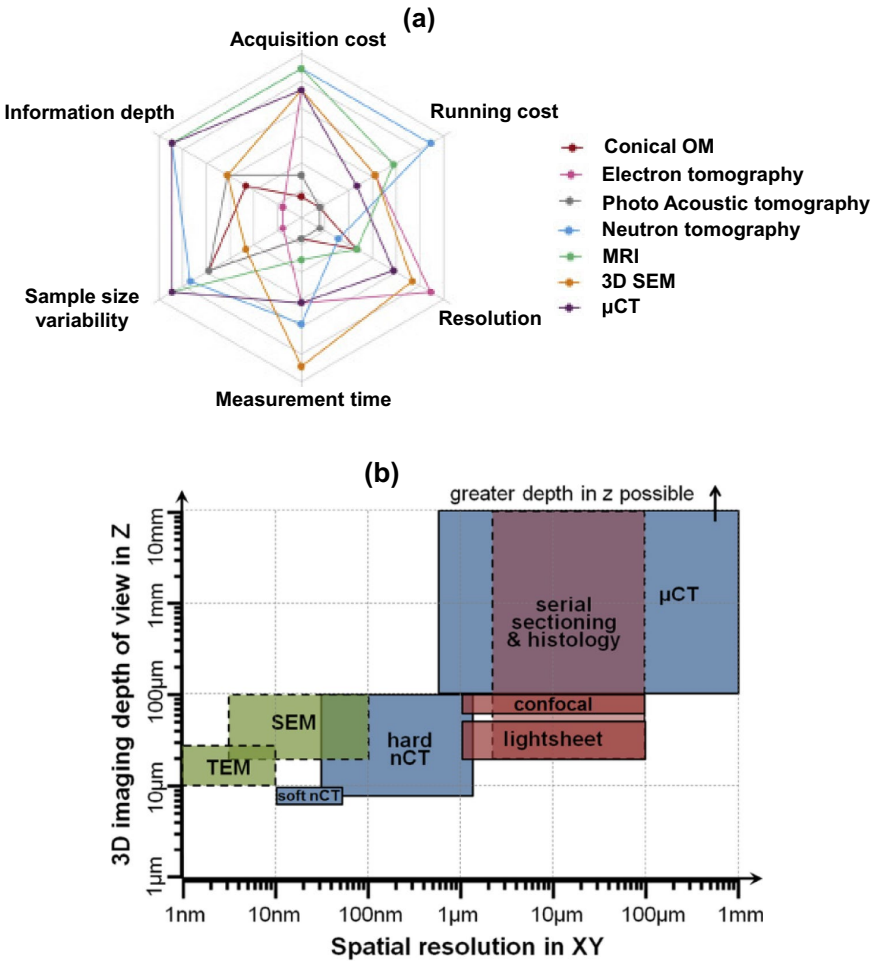


Fig. 17 Comparison of 3D microstructure investigation techniques [209, 210]

resolution (sample size), acquisition time and rotation steps, filtration, X-ray tube parameters, and sample-to-X-ray tube distance [134]. This instrument costs millions of dollars.

Light-sheet fluorescence microscopy Advantages include non-destructive scanning, higher resolution, faster imaging speed (i.e., imaging time is usually seconds), and lower cost than MRI and µCT [211]. However, it offers lower depth (z).

Confocal microscopy It offers non-destructive scanning and near-identical resolution; however, it provides greater depth than light-sheet fluorescence microscopy. However, this instrument costs approximately $200,000, while light-sheet fluorescence microscopy costs approximately $30,000 [211]. Sample preparation is tedious in both techniques because they require a smaller sample thickness for scanning than MRI and µCT [210].

3.2 Destructive and non-destructive scanning-assisted modeling of composites

Figure 19 shows the stepwise procedure for DT (OM)- and NDT (µCT)- aided FE modeling of composites [79]. The geometry of FE-simulated composites can be created using data from DT- and NDT-scanned images and

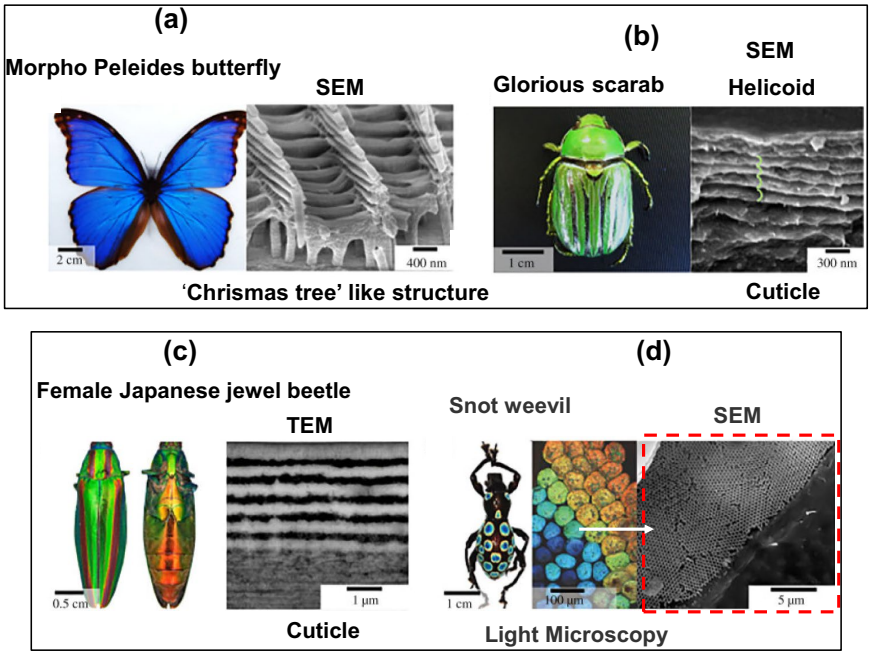


Fig. 18 Transverse section of butterfly wing scales and Cuticle of scarab [105, 107], beetle [109] and weevil [111], captured using DT techniques

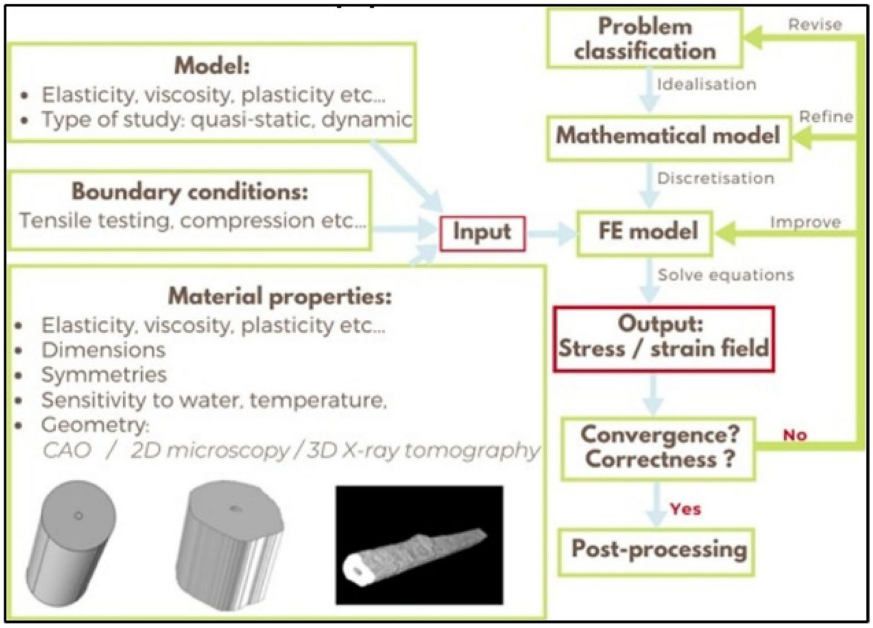


Fig. 19 Procedure to generate an FE model and FE-aided stress–strain field using destructive and non-destructive scanning: scanning, reconstruction, segmentation, and importing the geometry into FEA software; choosing the appropriate model, assigning material parameters and boundary conditions as inputs; running the simulation; and generating stress–strain fields [79]

geometric modeling software packages [78]. Geometric modeling details of helicoidal fiber architectures are discussed in detail by Wadekar et al. [212]. After that, FE simulations can be performed using various software packages, such as Abaqus, Ansys, LS-Dyna, SolidWorks, etc., to predict composite mechanical properties [213].

Figure 20 [19] and Figure 21 [81] show examples of FE-modeled composites in Abaqus. First, the representative volume element (RVE) model is created from scanned images using VG (volume graphics) Studio Max software, then imported into Abaqus to run an FEA simulation and measure mechanical properties [78, 91].

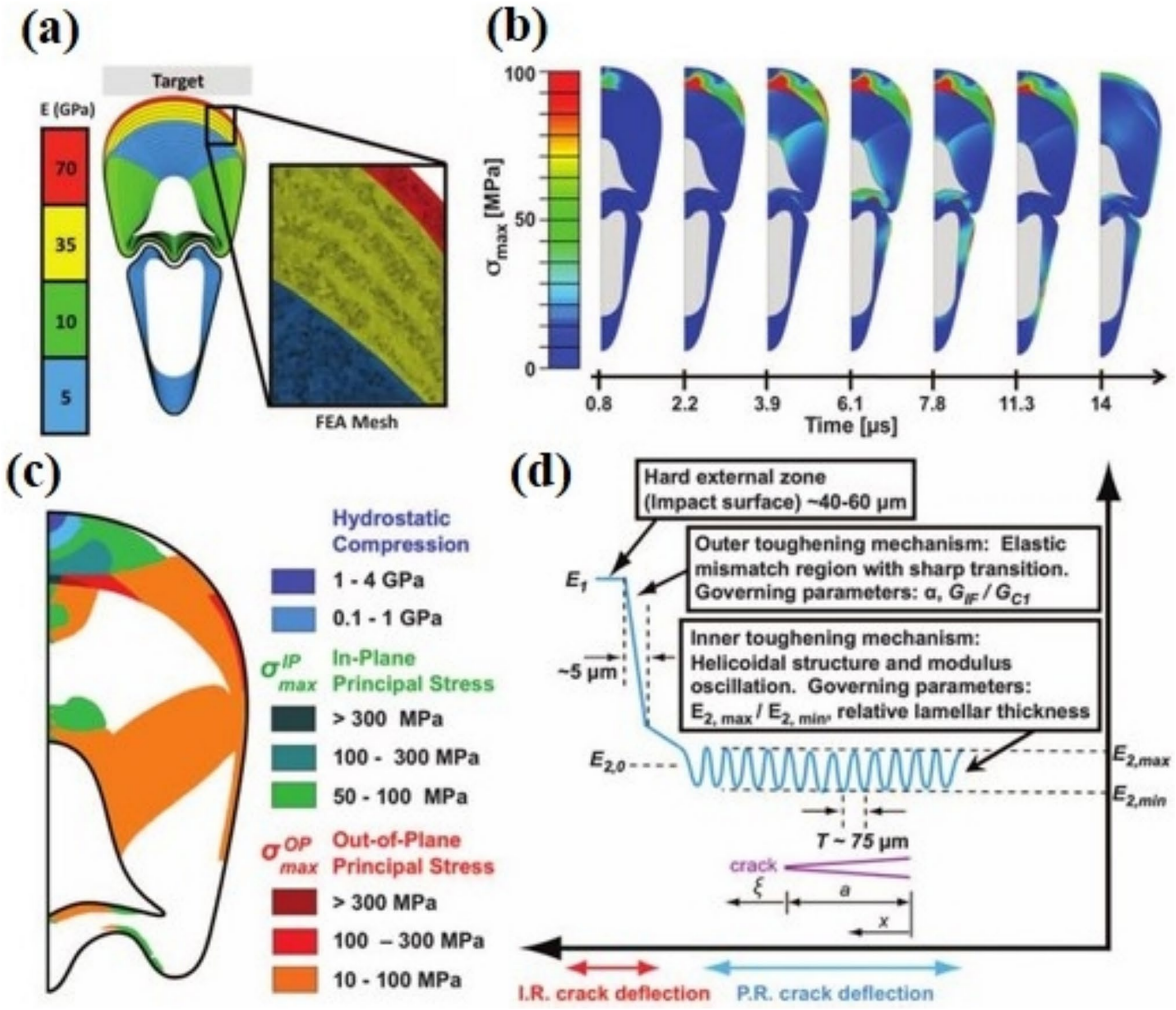


Fig. 20 Synchrotron X-ray transmission-aided FEA modeling: FEA mesh of the dactyl club with elastic modulus varying from hard outer layers (70 GPa) to soft inner layers (5 GPa) (**a**); FE simulation predicting maximum principal stress during the dactyl club impact event every 2 μs at 20 m/s (**b**); Predicted maximum principal stresses within the dactyl club after the impact event (**c**); Variation in elastic modulus due to changes in toughening mechanisms of the dactyl club from the hard outer impact region (I.R.) to the periodic region (P.R.) (**d**) [19]

Agez et al. [107] used confocal microscopy and spectrophotometry, SEM, and TEM in combination to measure the relationship between structural and optical properties. These properties were then used as input for numerical simulations. Numerical simulations were performed to predict the optical response of the Chrysina gloriosa (the cuticle of a scarab beetle) using the finite-difference time-domain method in the Meep software package. This software uses Maxwell's equations to run the simulation. Moreover, Aguilar Gutierrez et al. [188, 189] used these numerical simulation tools and found that complex pitch gradients are present in beetle cuticles. DT and NDT-aided modeling have certain limitations, which are: the size of the data is large, resulting in high computational time [214], and the quality of images sometimes decreases due to several issues (artifacts, noise, charging of samples, etc.) during scanning and post-processing [78, 131, 215]. To address these issues, artificial intelligence can be used, as discussed in the following section.

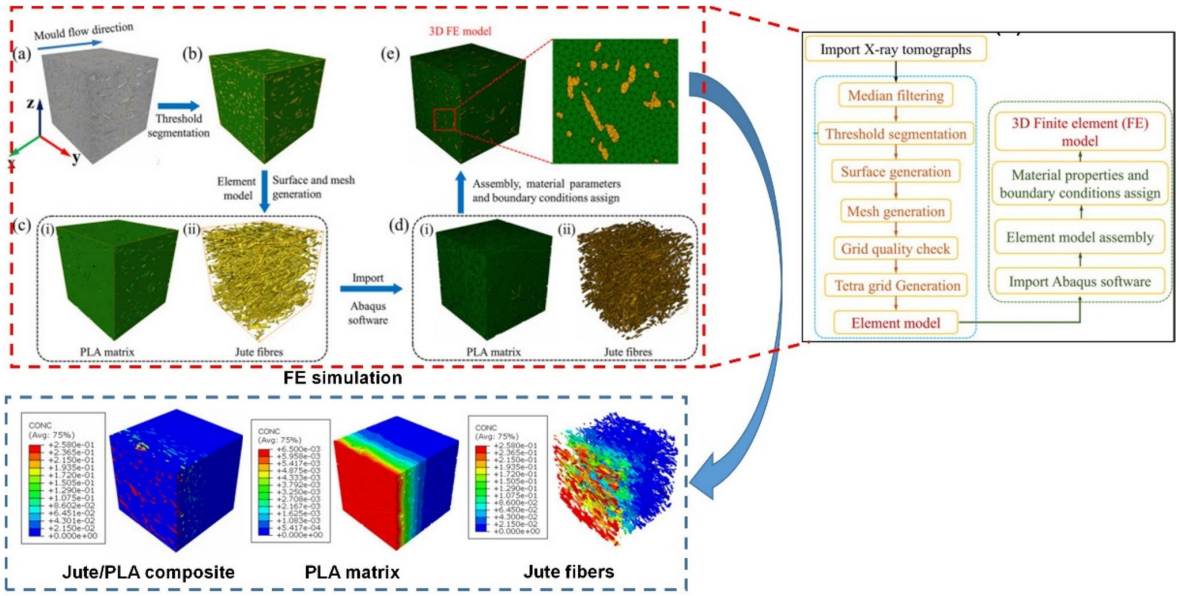


Fig. 21 μCT-aided FEA simulation in Jute/PLA biocomposites: composite volumetric sample in 3D after μCT scanning, followed by reconstruction (**a**), segmentation was performed to investigate the constituent matrix and fiber phases. **b** and **c**, importing the segmented geometry in Abaqus (**d**), assigning the material parameters and boundary conditions before running the FEA simulation, and the simulation results after the simulation (**e**) [81]

4 Modeling of composites using Artificial Intelligence (AI) technology

AI technology is widely applied across fields such as aerospace, automotive, and medicine. It is generally divided into two main categories: (i) machine learning (ML) and (ii) deep learning (DL) [216]. Amanullah et al. [190] reported that deep learning algorithms are becoming more popular than machine learning algorithms (Support Vector Machine, Decision Trees, K-means, and Logistic Regression) for certain tasks. DL models excel at handling large datasets, automatically learning complex feature representations, and delivering highly accurate results [217]. However, because DL is a subset of ML, certain architectures bridge both parameter optimization and image-processing roles when optimizing advanced manufacturing process parameters, such as those in AFP and AM. In recent years, many researchers have integrated ML and DL algorithms to optimize the process parameters of these advanced manufacturing techniques [147, 148]. Optimizing these process parameters is critical for minimizing defects and enhancing production efficiency [86]. Furthermore, this review discusses the application of DL to the preprocessing and post-processing of DT and NDT scanned images, as well as automated segmentation, to reduce overall computation time.

4.1 Optimization of process parameters using machine learning and deep learning

This section reviews process parameter optimization in advanced manufacturing (AFP and AM) using ML and DL techniques. The AI-driven material design workflow is illustrated in Fig. 22a–d [89]. As shown in Fig. 22a, material property data gathered from experiments, literature, and FEA digital twins are used to train various AI models, including Generative Adversarial Networks (GANs), Graph Neural Networks (GNNs), Convolutional Neural Networks (CNNs), and Bayesian frameworks. Following successful training, material properties can be predicted, validated, and optimized, with predictions benchmarked against FEA and experimental results

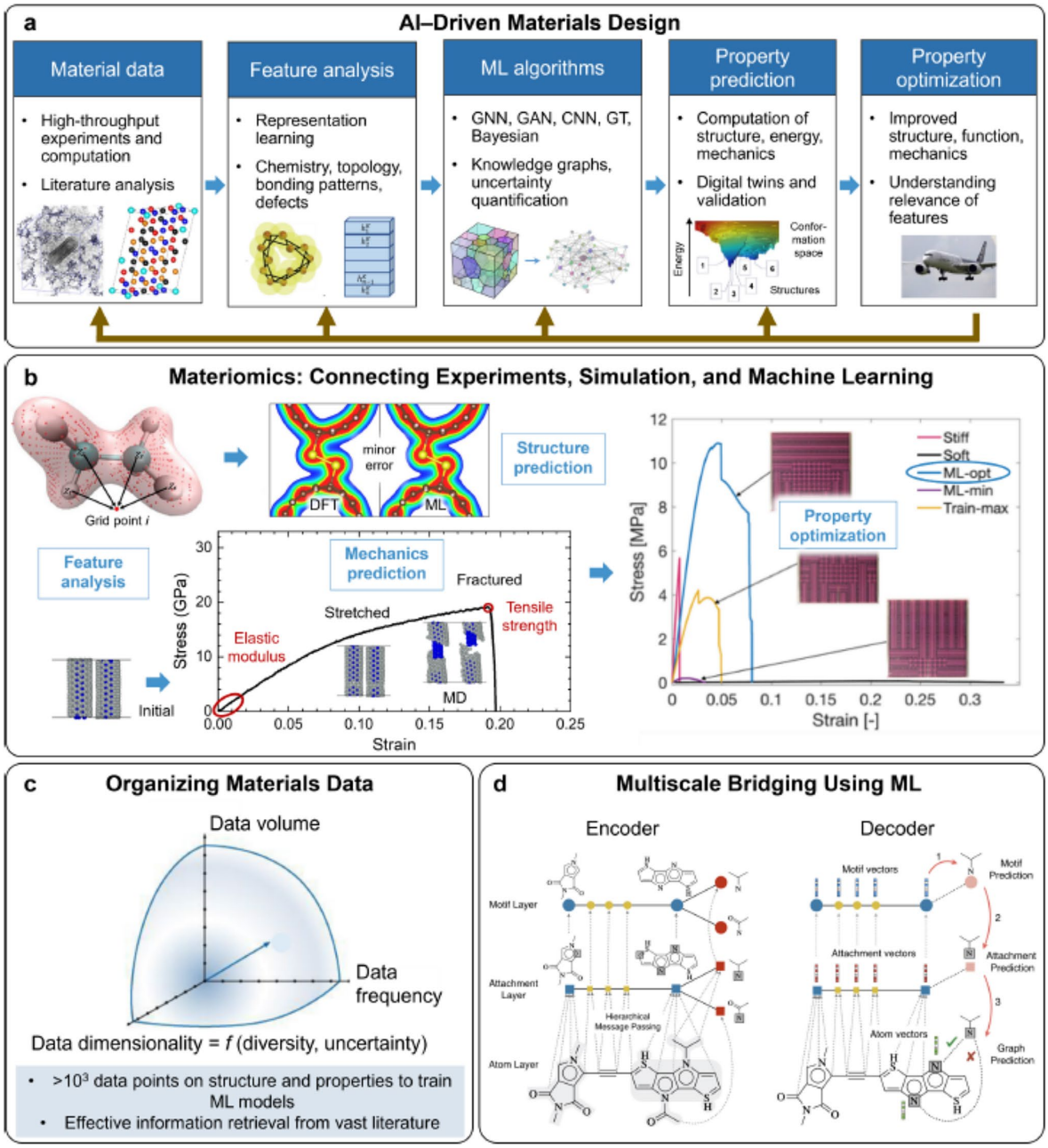


Fig. 22 AI-driven material design steps for property optimization using ML-based algorithms [88]

(Fig. 22b). Finally, Fig. 22c and d illustrate ML-enabled data organization strategies and multiscale bridging methodologies, respectively.

Common defects such as bridges, wrinkles, and gaps frequently occur during the AFP processing of composites, as illustrated in Fig. 23a, c, and e. Nonetheless, optimizing the AFP process can remove these defects from the composite part, as shown in Fig. 23b, d, and f [137]. Process optimization depends on several parameters,

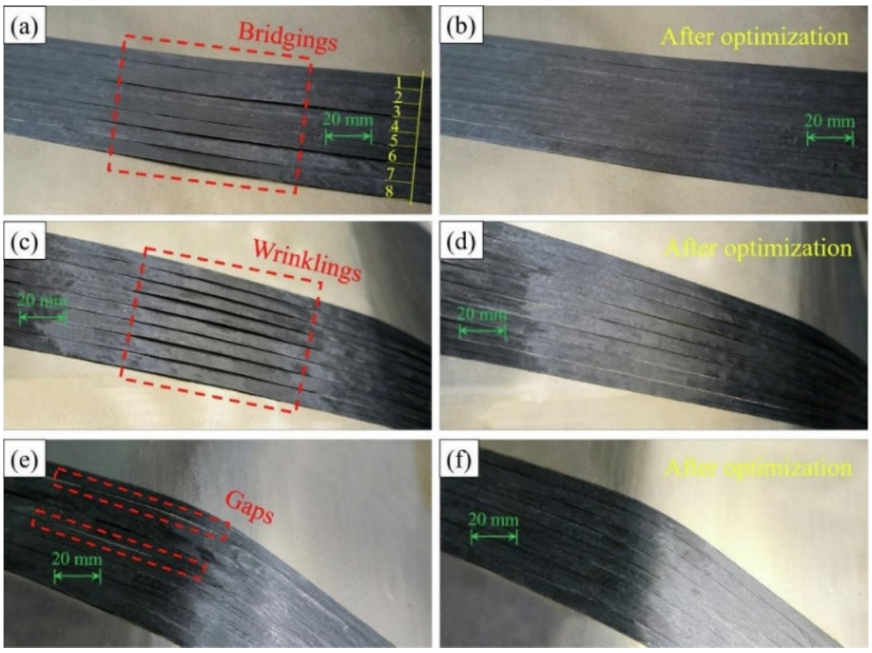


Fig. 23 Layup defects before optimization and after optimizing the AFP process parameters [137]

such as compaction pressure, temperature, and layup speed, and composite mechanical properties depend on these parameters, as shown in Fig. 24 [90]. Experimentally optimizing these parameters is time-consuming and expensive, but ML algorithms (GANs, GNNs, CNNs, Bayesian methods, etc.) can optimize them. The use of ML to optimize the lay-up process for AFP composites is shown in Fig. 25 [144]. Initially, AFP processing conditions (hot gas torch (HGT), compaction force, and layup speed) are used in experiments and FEA simulations to predict the composite strength. Moreover, the built-in scanner in the AFP instrument enables real-time monitoring, providing fiber orientation, defect information (gaps, overlaps, wrinkles, etc.), and in-situ thermal history [139]. These real-time monitoring data are important for measuring the experimental interlaminar shear strength (ILSS). Similarly, FEA-generated digital twins can predict ILSS [78]. Experimental and simulation data can also be used to train ML algorithms, as shown in Fig. 22a. After training, properties can be predicted and validated. After validation, the ML-based process optimizes material properties and predicts thermal profile parameters, which are used to create a graphical user interface (GUI)-based thermal profile prediction application.

Compared with conventional AFP inspection techniques such as laser profilometry and thermography, Tang et al. [145] developed a defect-detection algorithm using PointNet+ +, a convolutional neural network (CNN) tailored for 3D point cloud segmentation. The model was trained on a dataset of 3D point clouds representing intentional defects, fabricated on an AFP platform and captured with a structured-light camera. This approach offers a cost-effective, user-friendly alternative.

ML-based process optimization is also useful for developing 3D-printed bio-composites. Figure 26 shows the optimization of woodpecker-tongue-inspired hyper-elastic hybrid composite materials, developed by incorporating eggshell powder into a thermoplastic polyurethane (TPU)/polyhydroxyalkanoate (PHA) matrix using a ball mill homogenizer, followed by 3D printing [218]. Experimental testing, combined with FEA modeling and an ML-driven approach, can optimize the non-linear hyperelastic properties of hybrid biomaterials. Initially, the ML model can be trained on experimentally measured mechanical properties and FEA simulation results. After training and validation, the ML algorithms shown in Fig. 22a can optimize 3D printing process parameters (layer thickness, infill density, printing speed, and bed and nozzle parameters) and predict the hyperelastic Mode I

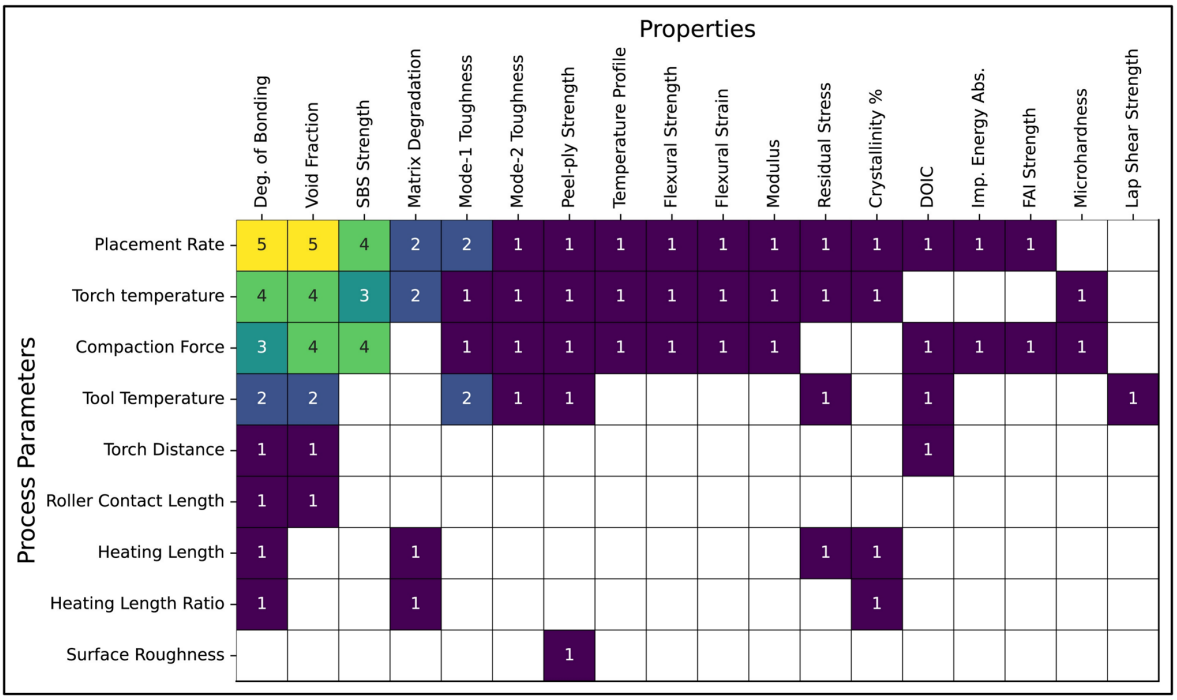


Fig. 24 Optimizing the AFP process parameters using ML methods to improve the mechanical properties of composites [90]

and Mode II properties. The resulting ML-generated force–displacement curves can then be compared with the experimental results.

4.2 Application of deep learning in composites

Deep learning models consist of multiple hidden layers, each containing neurons that predict the target output. These architectures resemble traditional artificial neural networks (ANNs) and are fundamentally inspired by the human brain [92, 219]. Deep learning methods fall into three broad categories: supervised, unsupervised, and hybrid learning frameworks. Common approaches include convolutional neural networks (CNNs), deep belief networks (DBNs), autoencoders (AEs), and recurrent neural networks (RNNs) [220, 221]. These networks are highly effective across several domains, particularly for improving the quality of DT and NDT images during preprocessing [222], reconstructing and post-processing DT and NDT images [223], enabling automated segmentation [224], and reducing overall computation time [214]. Furthermore, image-based deep learning tasks can be systematically classified into (i) low-level vision, (ii) high-level vision, and (iii) 3D data processing [225].

(i) Deep learning for low-level vision tasks

During 3D µCT scanning of composites, several process parameters influence image quality, including X-ray tube parameters (voltage and current), detector parameters, acquisition time, rotation steps, filtration, etc. Several image artifacts, such as beam drift, beam hardening, and ring artifacts, degrade image quality (blurring, noise, etc.) and can result from these parameters. Further details about the influence of these parameters on image quality can be found in our article [78]. The quality of these images can be improved using deep learning algorithms for low-level vision tasks, as shown in Fig. 27a.

(ii) Deep learning for high-level vision tasks

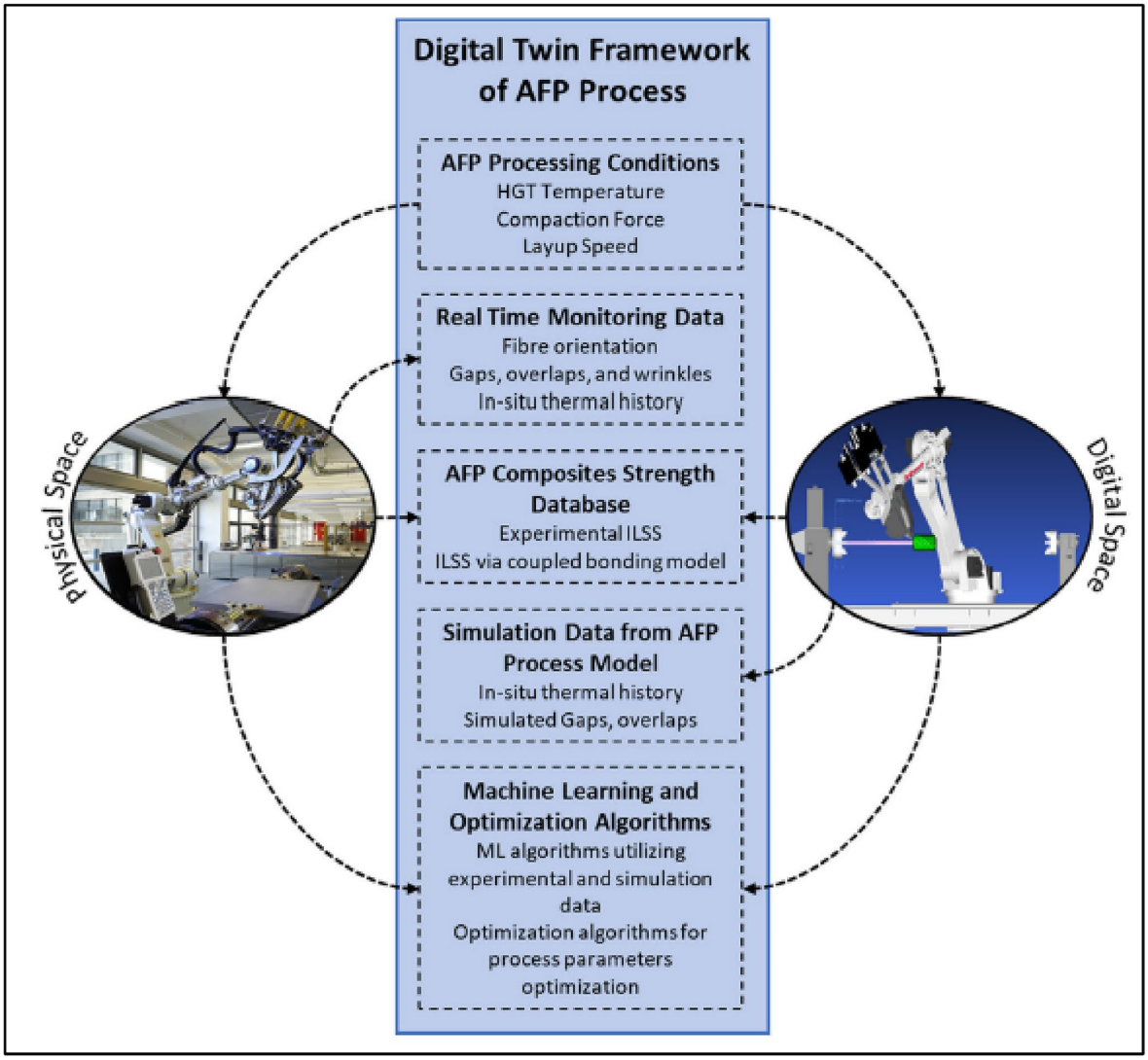


Fig. 25 ML-based process monitoring for AFP composite manufacturing [144]

Deep learning for high-level vision tasks achieves high accuracy in image analysis across various fields, such as medical imaging, airport security systems for face recognition, autonomous driving, and engineering (surface defect detection), as shown in Fig. 27b.

(iii) Deep learning for 3D data processing

The application of deep learning in composites can be divided into three groups, namely optimization, property prediction, and data processing, as shown in Fig. 27c. Deep learning is useful for reconstructing μCT images, enhancing 3D data processing of composite materials, reducing data volume, and more. Sinchuk et al. [226] employed deep learning algorithms to segment μCT data, even at very low contrast (noise), achieving accurate results using the U-Net architecture. Badran et al. [227, 228] automatically segmented the μCT images of FRP composites and validated the results with polished, high-resolution OM images.

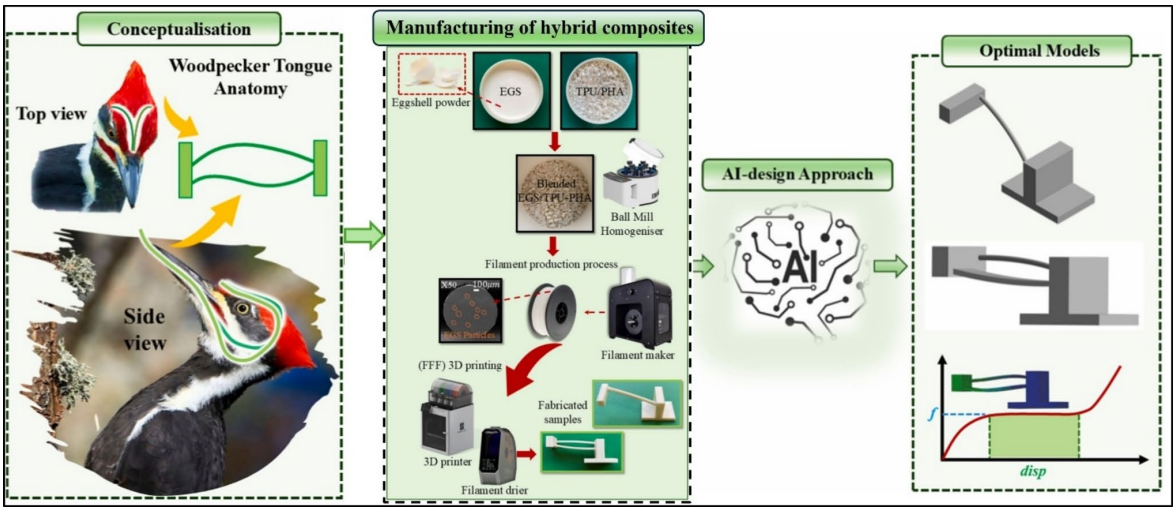


Fig. 26 ML-based process optimization for nature-inspired eggshell/TPU-PHA hybrid bio-composites fabricated by 3D printing

CNN is the most widely used deep learning approach for post-processing DT and NDT images and for automatically segmenting composite constituents, especially for void and defect characterization, compared with other approaches [229–231]. The automated segmentation of DT and NDT images can be performed using various software packages, such as Dragonfly and Geodict [227], which employ built-in architectures, including U-Net, LinkNet, etc., [91, 232]. A few hundred slices in a single scanned sample image stack can be trained using deep learning algorithms for automated segmentation of fibers, matrix, and voids; this approach can then be applied to similar scanned sample image stacks to automatically segment them, investigate defects, and measure porosity.

Also, CNN is used to predict the mechanical properties of composites [221]. Stress and strain contours can be predicted by importing 3D volumetric data into commercial FEA software packages (e.g., Abaqus, LS-DYNA) and running simulations [78, 92]. However, to the authors' knowledge, these deep learning approaches have not yet been employed to characterize helicoidal composite structures. Therefore, future deep learning studies are important to fill this gap.

5 Mechanical characterization of helicoidal composites

5.1 Quasi-static mechanical properties of helicoidal composites

Shang et al. [48] studied the quasi-static indentation (QSI) properties of different helicoidal ([0º/−18º/−36º/… −162º/−180º] and [0º/−10º/−20º/… −170º/−180º]) and cross-ply laminates, both experimentally and numerically. It was reported that the helicoidal laminates exhibited excellent quasi-static indentation (QSI) properties. In particular, the helicoidal laminate with a lower inter-ply angle variation (10º) exhibited higher maximum load and stiffness than the other laminates. Low fiber-failure and delamination regions are observed in helicoidal laminates, whereas the opposite trend is seen in cross-ply laminates. Luo et al. [23] reported a 62% drop in tensile strength as the inter-ply angle increased from 0º to 45º in a cross-ply laminate. However, the drop in tensile strength in helicoidal laminates was minimal as the inter-ply angle increased compared with cross-ply and quasi-isotropic laminate configurations, as shown in Fig. 28. This minimum drop is due to a crack-twisting mechanism that dissipates strain energy over a much larger surface area, preventing sudden failure under off-axis loading. As

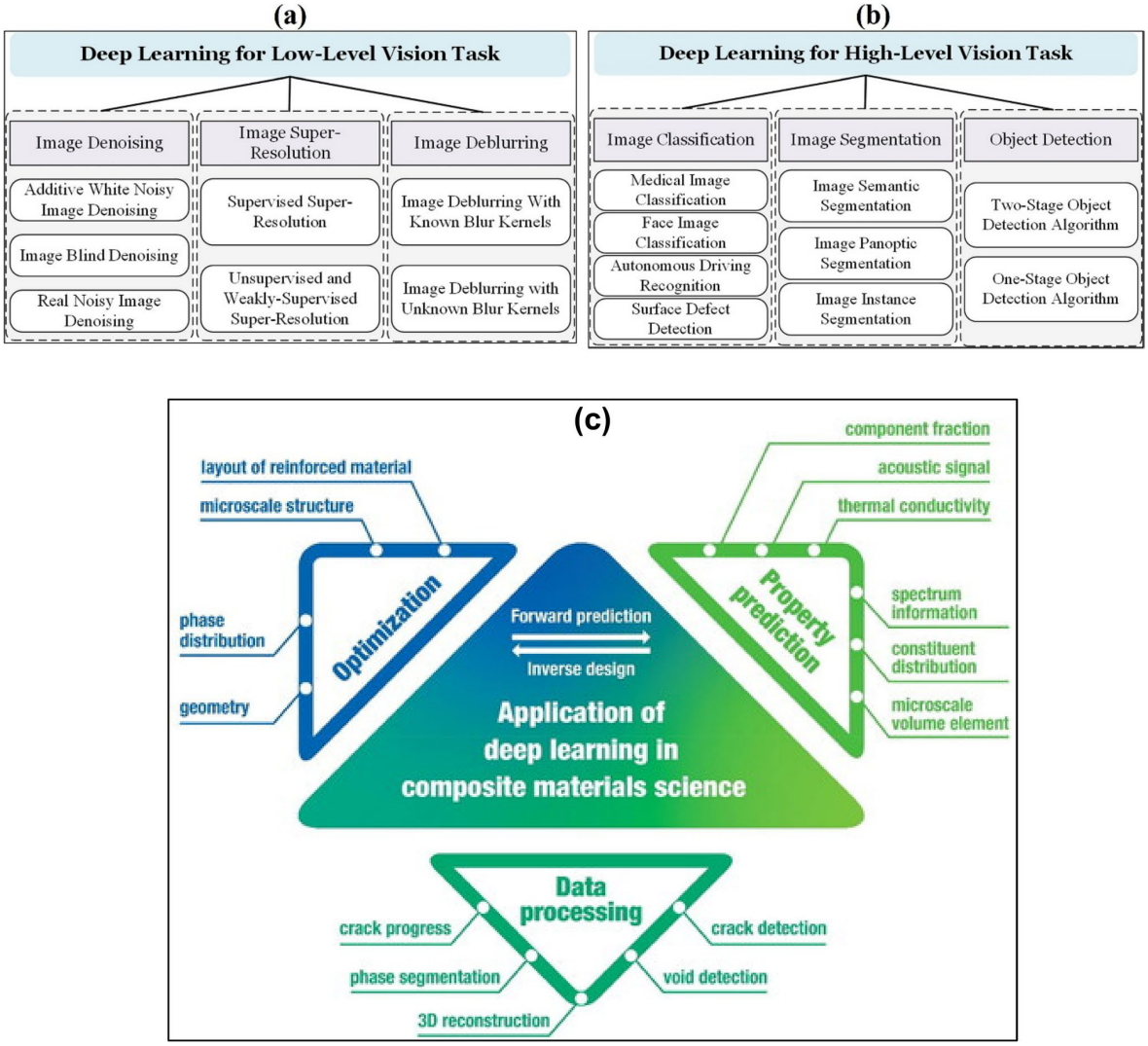


Fig. 27 Image-based deep learning methods (**a**,**b**), and Application of deep learning in composites (**c**) [233]

a crack propagates outward from the central hole's stress concentration, it encounters a constantly shifting fiber direction in adjacent layers, forcing continuous path deflection. The sudden drop in tensile strength in the cross-ply laminate resulted from a change in failure mode from brittle fiber failure to fiber pull-out.

However, in biological architecture, the inter-ply angle generally varies in the thickness direction. Instead, it varies gradually from the outer shell to the inner core, as shown in the Peacock mantis-shrimp and its telson in Fig. 29a-b and in its microstructure in Fig. 29c [159]. Using a helicoidal laminate with a smaller inter-ply angle variation keeps fibers closely aligned with the primary loading axis and minimizes mismatch between adjacent layers. Thus, the drop in fiber-direction stiffness reduces through the thickness. Moreover, small angular mismatch forces matrix cracks to twist along a longer helical path. Therefore, helicoidal laminates with a smaller inter-ply angle exhibited higher directional stiffness while simultaneously providing superior damage tolerance due to the enhanced crack-twisting mechanisms and increased interlaminar fracture toughness [160]. In contrast, helicoidal laminates with larger inter-ply angles show the opposite trend [163].

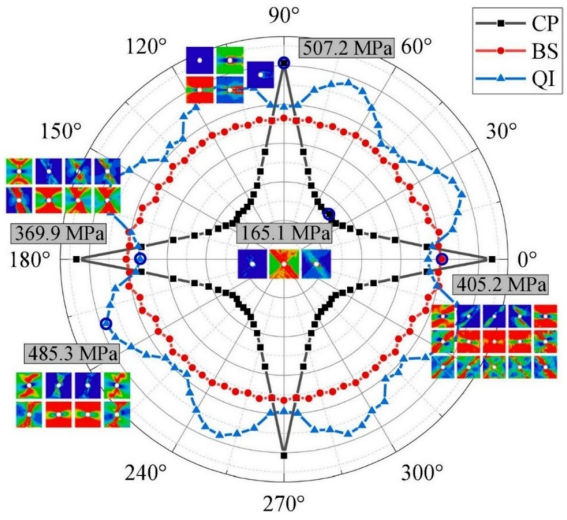
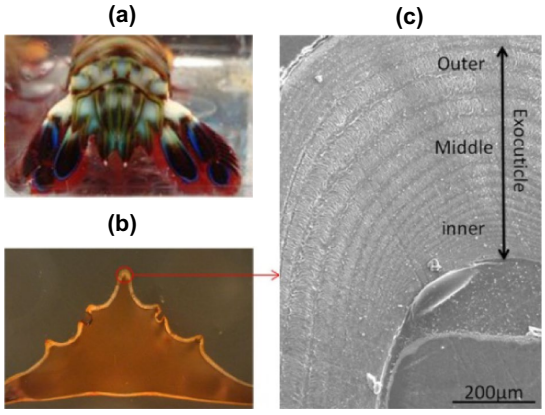


Fig. 28 Comparison of tensile strength distribution when increasing the inter-ply angle in cross ply, quasi-isotropic, and helicoidal laminates (Bouligand (BS)) [23]



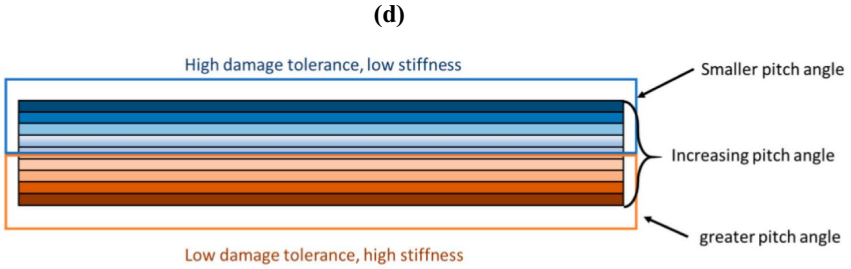


Fig. 29 Peacock mantis-shrimp (**a**) and section of its telson (**b**) and microstructure of telson captured using SEM (**c**) [159] and the effect of inter-ply angle on stiffness and damage tolerance of helicoidal laminate (**d**) [163]

5.1.1 Interlaminar shear properties

Investigating the interlaminar shear properties of helicoidal composites is important for understanding crack-twisting mechanisms, which can be studied using various experimental methods, such as the short-beam test [160] and the torsional test [234]. Figure 30a-d shows the through-thickness failure modes for symmetric helicoidal laminate configurations $[0/6/12/\ldots/84/90]_s$, $[0/9.1/18.2/\ldots\ 127.4/136.5]_s$, $[0/12/24/\ldots/168/180]_s$, and

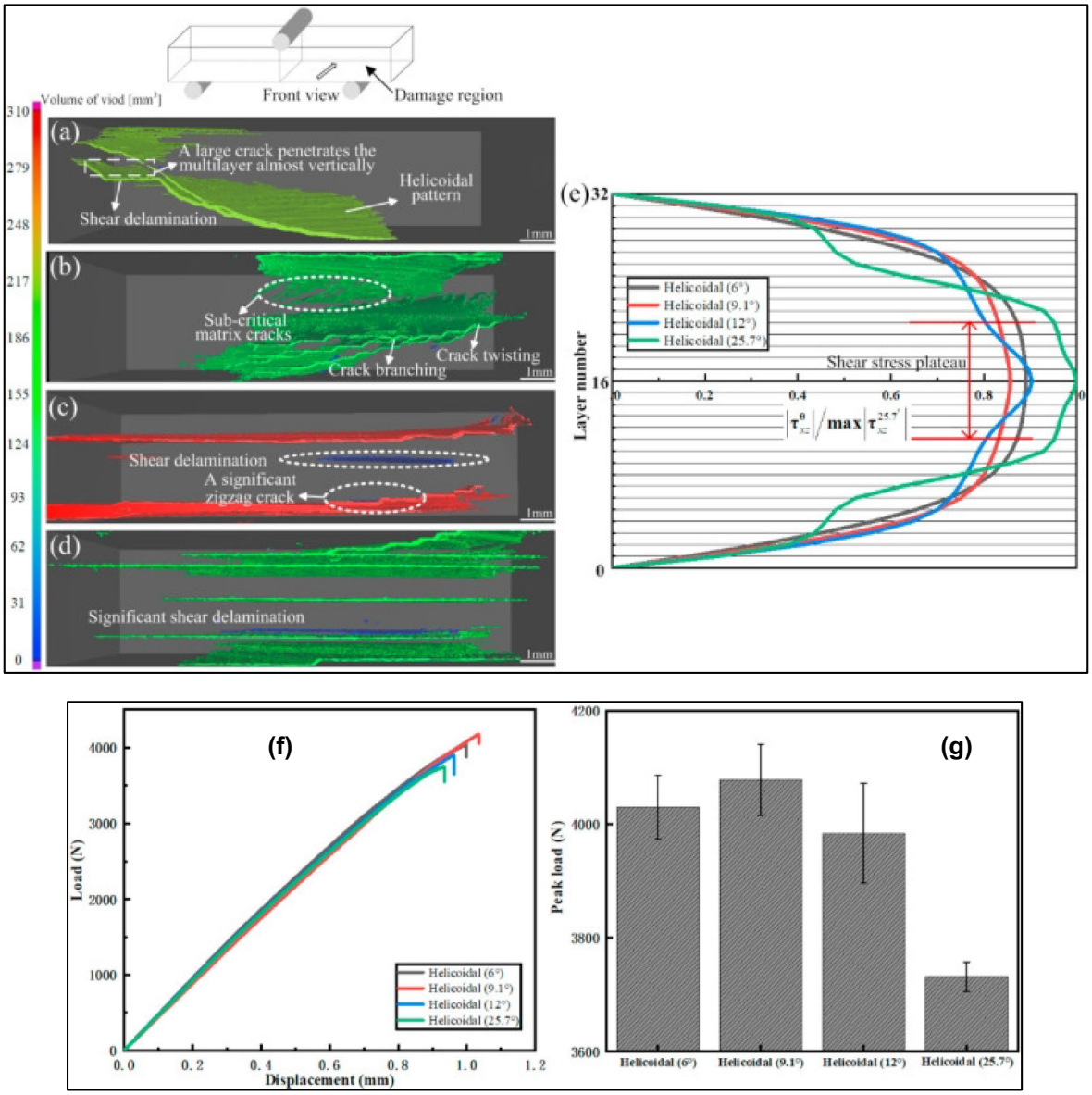


Fig. 30 Interlaminar shear properties of different symmetric helicoidal laminate configurations: through-thickness failure modes (**a**-**e**) and shear stress distribution (**e**); Load–Displacement curves (**f**) and Peak load (**g**) [160]

$[0/25.7/51.4/\ldots/154.2/180]_{2\ s}$, respectively, under bending. These failure mechanisms were captured using μCT, and the color maps of post-processed μCT images indicate delamination at a specific ply interface.

Figure 30e-g shows the through-thickness interlaminar shear stress distribution, load vs. displacement, and peak load for different symmetric helicoidal laminate configurations. From Fig. 30a-g, the laminate [0/9.1/18.2/…127.4/136.5]s, with an inter-ply angle of 9.1º between plies, effectively controls delamination through an appropriate crack-twisting mechanism. Therefore, a laminate with an inter-ply angle of 9.1º exhibits better mechanical properties than other symmetric helicoidal laminate configurations. These confirm that selecting the appropriate inter-ply angle is important for achieving optimal mechanical properties. This optimum value

is strongly dictated by system-specific variables, most notably the constituent fiber and matrix properties, the laminate thickness, and the orientation of the applied load [144, 147, 160].

5.2 Impact properties of helicoidal composites

Biomimetic structures can be used for different impact-loading applications (low velocity, high velocity, sharp impact, mobility, and movement), inspired by various biological materials, as shown in Fig. 31. These articles [235–237] discuss in detail the applications of these biomimetic structures in various defense-related products, such as body armor, vehicle armor, helmets, etc. This section discusses the low-velocity and high-velocity impact properties of helicoidal composites in detail.

5.2.1 Low velocity impact (LVI) properties of helicoidal composites

Meo et al. [163] manufactured functionally graded symmetric $[0/5/15/30/50/75/105/140/180]_s$ and asymmetric [0/1.2/3.5/…/160/180] helicoidal laminates with variable inter-ply angles between consecutive plies. Further, compared the LVI and flexural post-LVI properties of these laminates with those of the traditional (Benchmark) symmetric laminate $[0/0/+45/-45/90/0/+45/-45/90]_s$, as shown in Fig. 32a-b. The asymmetric helicoidal laminate showed higher maximum displacement and residual impact energy than the symmetric helicoidal laminate, followed by the traditional laminate. This can be attributed to changes in failure mechanisms: traditional laminates show peanut-shaped damage (larger through-thickness delamination regions), whereas crack twisting acts as a toughening mechanism, leading to smaller or no delamination regions in helicoidal laminates. The difference in properties between the two helicoidal laminates is due to variations in through-thickness stiffness based on their designs, which leads to a smaller damage area in the asymmetric helicoidal laminate, as shown in the 'C' scan images in Fig. 32c.

5.2.2 Self-healing helicoidal composites

Self-healing composites can autonomously repair internal microcracks and restore baseline mechanical properties without interrupting operational functionality. These materials are broadly categorized into intrinsic and extrinsic healing systems [238]. Intrinsic self-healing leverages reversible physical or dynamic chemical cross-links inherent to the polymer matrix, such as supramolecular interactions or thermally activated dynamic covalent bonds, to reform structural integrity across fractured interfaces [194]. Conversely, extrinsic self-healing relies on sequestered functional agents, such as microcapsules, hollow fibers, or vascular networks that rupture upon crack propagation to release a liquid healing agent into the damage site [239]. However, including liquid-filled capsules and vascular networks induces voids, thereby compromising composite strength. To overcome these issues, healable composites can also be fabricated by embedding solid thermoplastic microparticles, such as Nylon 6,

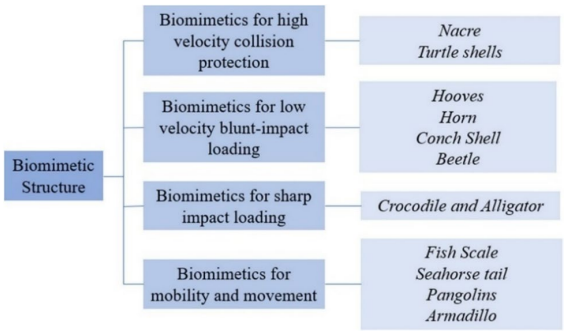


Fig. 31 Nature-inspired biomimetic structures for different impact loading applications [235]

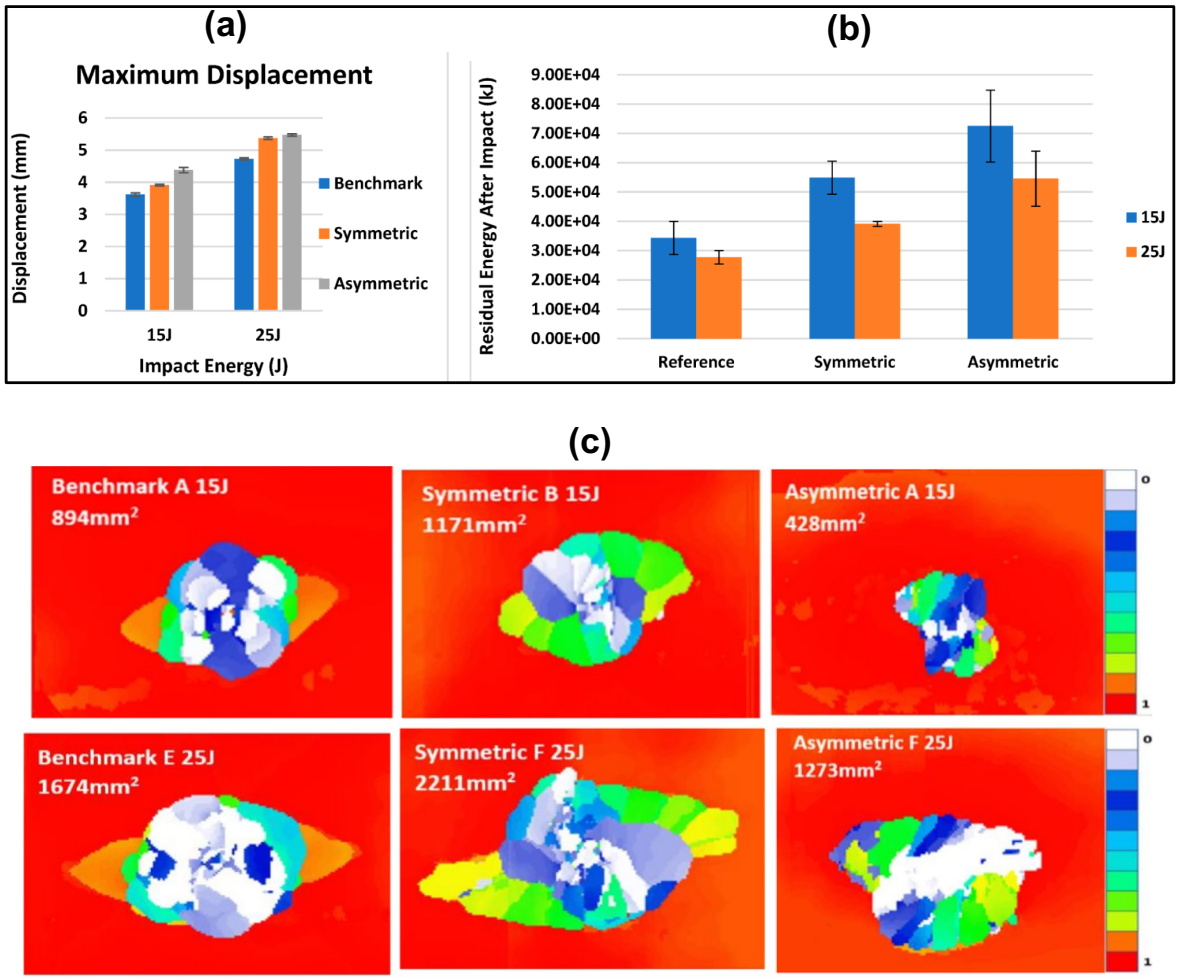


Fig. 32 Comparison of benchmark and helicoidal (Symmetric and Asymmetric) laminates: LVI (**a**) and flexural post-LVI (**b**) properties, and their failure mechanisms (**c**) [163]

ethylene-methacrylic acid copolymer (EMAA), and polyethylene-co-methacrylic acid agents, in the fibers. Utilizing solid microparticles avoids the undesirable voids typically introduced by capsules and vascular networks [97]. These thermoplastic particles can also be embedded in thermoset polymers (e.g., an epoxy matrix), as a result, both toughening and healing of the composite can be improved [240]. When damage occurs, controlled heating and pressure can melt these embedded thermoplastics to fill internal cracks; the healed sample is then tested, and its mechanical properties are compared with those of the corresponding initial (virgin) sample [171]. Healing efficiency (HE) of composites is typically defined as the percentage of a specific mechanical property (e.g., compressive strength, fracture toughness, or energy absorption) recovered relative to the virgin sample, and is given by [194],

$$\mathrm{HE}\,(\%) = \frac{(\mathrm{Mechanicalproperty})_{(\mathrm{Healedsample})}}{(\mathrm{Mechanicalproperty})_{(\mathrm{Virginsample})}} * 100 \tag{2}$$

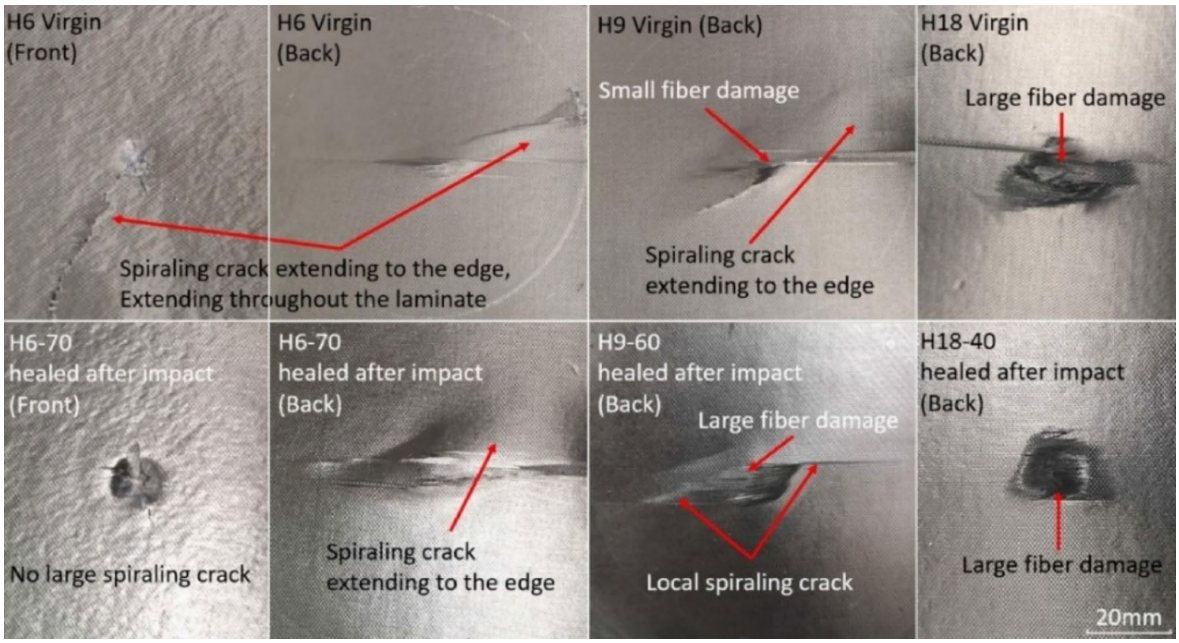


Fig. 33 Comparison of LVI damage mechanisms in virgin carbon/epoxy and self-healing carbon/epoxy/nylon microparticle helicoidal composite panels [97]

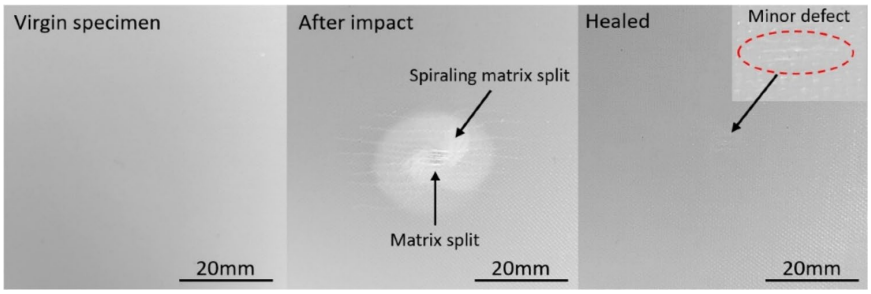


Fig. 34 Comparison of LVI damage mechanisms in virgin glass/epoxy and self-healing glass/epoxy/nylon microparticle helicoidal composite panels [98]

Nylon-based thermoplastic composites exhibit self-healing properties that enhance impact resistance by increasing toughness [171]. Liu et al. [97, 98] reported that incorporating nylon 6 powder microparticles into each prepreg ply of carbon/epoxy (Fig. 33) and glass/epoxy (Fig. 34) helicoidal hybrid composites subjected to LVI significantly improves their toughness through self-healing, compared with virgin helicoidal composites. From Fig. 33, it is observed that carbon/epoxy helicoidal composites with low inter-ply angles (H6 and H9) are affected by more matrix cracking and small fiber damage. In contrast, the high inter-ply angle (H18) helicoidal laminate exhibited the opposite trend. Self-healing in carbon/epoxy composites also helps minimize matrix cracking but does not reduce fiber damage. Figure 34 shows that self-healing significantly decreases damage in glass/epoxy composites. Additionally, self-healing is more effective at eliminating damage in glass/epoxy than in carbon/epoxy, mainly because the former exhibits higher ductility (% elongation) than the latter.

5.2.3 High velocity impact (HVI) properties of helicoidal composites

High-velocity impact tests of composites can be performed using an air gun [241]. In this test, three parameters, such as ballistic limit (V_b), residual velocity (V_r), and energy absorption (EA), are important to measure. Energy absorption depends on the projectile's mass, the impact velocity, and the residual velocity, which is given by [195],

$$EA = \frac{1}{2} m_p \left(V_i^2 - V_r^2 \right) \tag{3}$$

where m_p is the mass of the projectile; V_i and V_r are the impact and residual velocities, respectively. If the projectile does not penetrate the sample and instead rebounds, the sample's residual velocity is zero. A high-speed camera can monitor the projectile's velocity [108]. The failure mechanisms of composites under HVI depend on the projectile nose shape. Very recently, Hu et al. [38] reported the HVI performance of UHMWPE composites with different lay-up orientations (cross-ply, helicoidal, and quasi-isotropic) at an impact velocity of 500 m/s, as shown in Fig. 35. At this velocity, the cross-ply UHMWPE laminate performed well, as shown by a lower residual velocity. This was due to fiber recoil, sublayer folding on the impacted face, and localized bulge deformation on the back face, with cross-sectional failure mainly caused by localized progressive failure. Under high-velocity impact with flat-nosed projectiles, cross-ply UHMWPE laminates outperform double-helicoidal layups, as these projectiles induce high-rate localized shear punching, where continuous orthogonal fiber alignment (0°/90°) along the principal stress axes optimizes tensile membrane stretching. UHMWPE composites have exceptionally low inter-ply shear strength and high axial tensile strength [39, 242]. Under high-velocity flat impacts, encouraging excessive inter-ply delamination weakens structural integrity faster than the fiber tensile failure can absorb energy. For the same impact velocity, the double-helicoidal (HTS, HTM) and quasi-isotropic UHMWPE laminates performed worse in impact tests than the cross-ply laminates. Their failure patterns included fiber peeling, splitting, and extensive fiber fractures near perforations. However, the helicoidal configuration (HTS) exhibited superior performance under hemispherical and truncated nose-shaped projectiles compared with other laminate configurations. Hemispherical projectiles induce out-of-plane bending and contact stresses, where helicoidal pitch rotations effectively suppress catastrophic delamination growth.

Abir et al. [243] experimentally and numerically studied the high-velocity impact performance of carbon/epoxy composite samples with 37 layers and different fiber orientations, namely cross-ply, helicoidal, and quasi-isotropic. It was found that the ballistic limit (Fig. 36a) and absorbed energy (Fig. 36b) of helicoidal laminates are significantly higher compared to cross-ply (0/90) and quasi-isotropic laminates. This is because helicoidal laminates exhibit distributed damage, whereas cross-ply and quasi-isotropic laminates show concentrated damage.

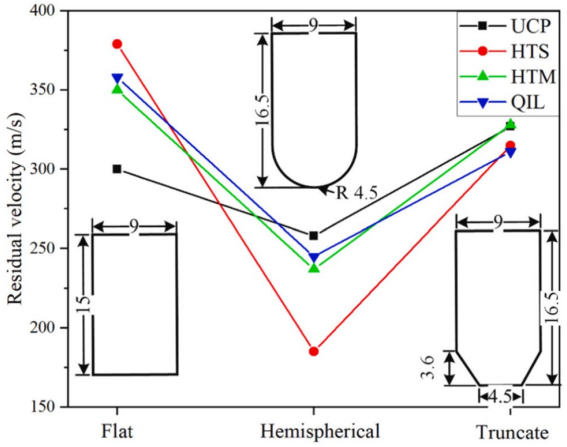


Fig. 35 Effect of different nose shapes of projectiles on residual velocities of different laminate configurations: cross-ply $[0°/90°]_{32\,s}$ (UCP), double-helicoidal (11.25° in lay-up HTS, and 22.5° in lay-up HTM), and quasi-isotropic laminate (QIL) composites tested at an impact velocity of 500 m/s [38]

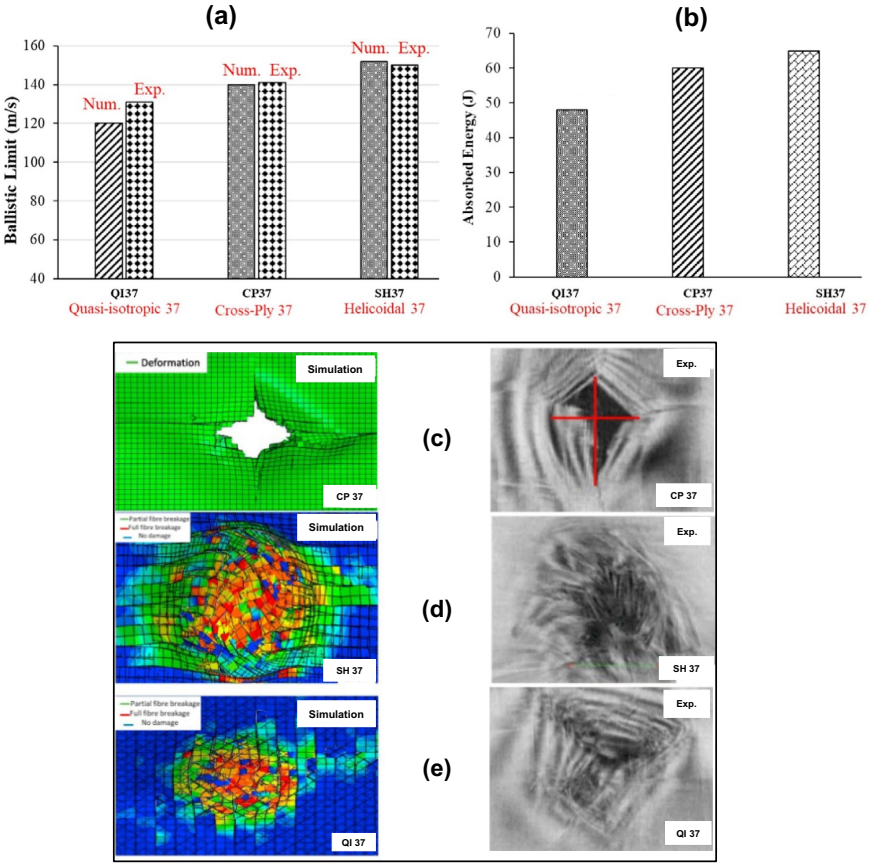


Fig. 36 Comparison of high-velocity impact properties between cross-ply, helicoidal, and quasi-isotropic carbon/epoxy composite samples: ballistic limit (**a**), absorbed energy (**b**), and failure mechanisms (**c**-**e**) [243]

Moreover, the helicoidal laminate shifts fiber failure from matrix splitting to matrix splitting, thereby improving impact performance. The thickness damage pattern observed in the helicoidal laminate is spiraling delamination.

In contrast, cross-ply delamination is observed in the cross-ply laminate, and the damage pattern is in between that of the quasi-isotropic laminate, as shown in Fig. 36c-e. The failure mechanisms observed in both µCT experiments and the numerical predictions from the Abaqus simulation correlate well. Liu et al. [244] compared the high-velocity impact properties of carbon/epoxy prepregs laminates with the same number of 37 layers and fiber orientations (cross-ply, helicoidal, and quasi-isotropic) to their Kevlar/epoxy prepregs and Endumax® tape counterparts, and found that Kevlar/epoxy laminates exhibited higher energy absorption capability. Cross-ply, quasi-isotropic, and large-angle helicoidal laminates fail primarily through fiber damage; consequently, designers should use these configurations with tough fibers (Kevlar and Endumax® tape). In contrast, brittle laminates perform better with bioinspired, small-angle helicoidal lay-ups. The study also found that absorbed energy increased through hybridization of helicoidal and cross-ply configurations. I.e., a hybrid (helicoidal and cross-ply) carbon/epoxy laminate, by replacing 7 plies of the helicoidal configuration (SH37) on the back side with a cross-ply configuration, exhibited 10% and 33% higher absorbed energy than SH37 and CP37, respectively.

µCT images in Fig. 37a-d show the through-thickness damage mechanisms of different laminate configurations (cross-ply (CP), quasi-isotropic (QI), 3H, and 9H) of flax/epoxy composites subjected to HVI. 3H (0/−3/−6 … −177/−180) and 9H (0/−9/−18 … −531/−540) are helicoidal laminate designs based on variations in inter-ply angles. The kinetic energy required to perforate the projectile through the helicoidal laminates 3H (59.5 J) and 9H (61.4) is significantly higher than that for the cross-ply (47.3) and quasi-isotropic (52 J) counterparts. This can be attributed to the projectile's easy penetration through the CP and QI laminates, owing to the dominance

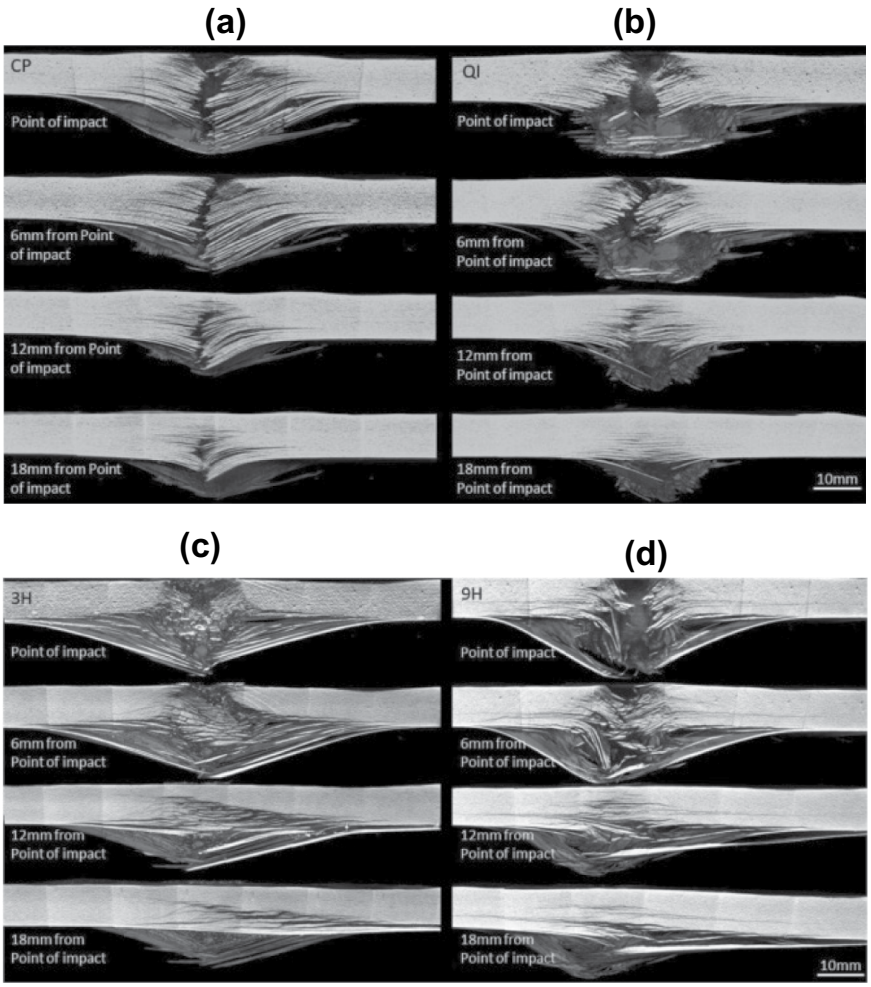


Fig. 37 The through-thickness damage mechanisms of flax/epoxy composites captured using μCT under HVI [44]

of fiber failure modes. Most of the energy dissipated in these laminates is due to fiber breakage and delamination (Fig. 37a-b). However, fiber failure can also be observed in 3H and 9H helicoidal laminates, but most of the energy dissipated in these laminates is due to matrix splitting rather than fiber failure. Among the two helicoidal laminates, a very low variation in inter-ply angle (3º) is not desirable for withstanding higher impact load and energy, compared to a helicoidal laminate that has a medium variation in inter-ply angle (9º).

5.3 High-strain-rate properties of helicoidal composites

High-strain-rate studies of composites can be conducted using a Split-Hopkinson Pressure Bar (SHPB), a drop-tower apparatus, and other methods. The SHPB is widely used to generate nominal strain rates above 1000 s^{-1} [4]. Papers on high-strain-rate studies of helical composites are scarce, except for these two papers [84, 99]. Investigating the high-strain-rate behavior of helicoidal composites is essential to understand dynamic loading events, such as hailstone impacts on wind turbine blades and tool drops on automotive parts.

Various mechanical properties and microstructural investigation techniques for helicoidal composites and polymers are summarized in Table 3, and those for hybrid and particle-filled helicoidal composites are summarized in Table 4.

Table 3 Mechanical and microstructural investigation of helicoidal composites

Material	Lay-up configuration	Manufacturing technique	Mechanical characterization	Micro-structure investigation technique	Summary of key trends based on mechanical properties	Reference	Year
Carbon/epoxy	CP, QI, and helicoidal	Hand-layup + hot press	HVI	μCT and FEA	The 37-ply CFRP helicoidal sample exhibited an 8% and 15% higher V_b compared to its CP and QI counterparts, respectively. By replacing seven plies on the back side of a helicoidal configuration with a CP configuration, the resulting hybrid carbon/epoxy laminate absorbed 10% more energy than the pure helicoidal laminate and 33% more than the pure CP laminate	[243, 244]	2019, 2020
UHMWPE	CP, QI, and helicoidal	Hand-layup + hot press	HVI	High speed camera and FEA	Under high-velocity flat-nose projectile impacts, double-helicoidal UHMWPE laminates performed worse than cross-ply configurations, but they exhibited superior resistance against hemispherical nose projectiles	[38]	2026
Carbon/epoxy	CP and helicoidal	Hand-layup + autoclave	LVI	μCT and FEA	At 20 J, the 12° double-helicoidal (DH) configuration exhibits a slightly lower peak force and higher absorbed energy than its CP counterpart; however, at 40 J, this trend reverses. To overcome the limitations of DH laminates, cross-helicoidal laminates were developed, which exhibited a significantly reduced damage area at both impact energies. Consequently, this design represents a viable approach to enhancing the impact resistance of helicoidal laminates	[168]	2023
Carbon/epoxy	CP and helicoidal	AFP + Autoclave	LVI, HVI, and Compression after Impact (CAI)	C-scan and DIC	Combining repeated segment stacking (RSS) and AFP enables tailorable, through-thickness fiber reinforcement that enhances impact resistance by increasing delamination fracture toughness. Compared to traditional laminates, the RSS concept successfully restricts damage propagation, resulting in reduced delamination footprints during both HVI and LVI testing	[5]	2025

Table 3 (continued)

Material	Lay-up configuration	Manufacturing technique	Mechanical characterization	Micro-structure investigation technique	Summary of key trends based on mechanical properties	Reference	Year
Carbon/epoxy	QI and helicoidal	AFP+Hot press	LVI and CAI	FEA	Compared to the standard QI benchmark, the variable-stiffness curvilinear helicoidal (VSCH) architecture enhanced impact mechanical performance by 30% and damage tolerance by 32%	[65]	2026
UHMWPE	CP and helicoidal	Hand-layup+hot press	LVI	VI	Absorbed energy and back-face signature (BFS) increased with an increase in impact energy from 50 to 250 J across all laminates. However, the helicoid laminates showed higher absorbed energy and lower BFS values than the CP laminate, while the performance difference between the 30° and 45° helicoid laminates was minimal	[37]	2023
Carbon/epoxy	CP and helicoidal	Hand layup+HAO	QSI	OM, MCT and FEA	Helicoidal laminates with a 19° inter-ply angle (SH-19) exhibited a higher maximum force and stiffness than their CP counterparts. However, FEA models comparing the SH-11 and SH-19 configurations revealed that a smaller inter-ply angle (e.g., 10° or less) is required to optimize stress distribution and eventually maximize load-bearing capacity	[48]	2016
Carbon/epoxy	CP and helicoidal	Hand-layup+HAO	QSI	VI and μCT	In thin helicoidal laminate configurations (19 and 37 plies), as the inter-ply angle was reduced from 40° to 5°, the maximum transverse load increased monotonically and outperformed its CP counterpart. Conversely, the thick 73-ply laminates showed a non-monotonic trend: narrowing the angle from 20° to 10° increased the maximum load, but further reductions to 5° and 2.5° dropped the performance below the CP baseline	[157]	2018

Table 3 (continued)

Material	Lay-up configuration	Manufacturing technique	Mechanical characterization	Micro-structure investigation technique	Summary of key trends based on mechanical properties	Reference	Year
Carbon/PA6	QI and helicoidal	Hand-layup + hot press	QSI, LVI, healing efficiency test	VI, SEM and μCT	Ply-blocking significantly reduces fiber damage in carbon-thermoplastic laminates following out-of-plane impact, with the extent of blocking playing a critical role regardless of whether a helicoidal or QI configuration is used. Post-healing mechanical recovery differs distinctly between the two architectures: QI laminates restore out-of-plane strength but not stiffness, whereas helicoidal laminates recover stiffness but not strength	[171]	2022
PLA	Helicoidal	FDM	High strain rate	High speed camera, DIC, and FEA	Unidirectional 19-ply helicoidal PLA samples were prepared with different helicoidal angles (0/15/30/45/60/75/90) using FDM technology, and SHPB tests were performed at 700 and 1000 1/s. The results showed higher strain-rate sensitivity in the 60° sample	[84]	2021
PLA/thermoplastic polyurethane (TPU)	Helicoidal	FDM	Flexural, LVI, HVI	High speed camera, and FEA	Utilizing multi-material FDM using stiff PLA and soft TPU, a compositionally gradient, double-twisted Bouligand structure (DT-Bou-G) was successfully fabricated. Dynamic testing showed that this architecture exhibits exceptional impact mitigation across multiple loading regimes, from quasi-static (0.5 mm/min) to high-velocity ballistic (120 m/s) impacts	[245]	2025
Functionally graded (FG) CFRP	QI and helicoidal	Hand-layup + autoclave	Flexural, LVI and Flexural After Impact (FAI)	C-scan	FG helicoidal laminates outperformed the benchmark QI under LVI (15 J and 25 J) and three-point bending. FG asymmetric exhibited better mechanical properties compared with FG symmetric helicoidal composites	[163]	2021
CFRP	Helicoidal	Hand-layup + autoclave	LVI and compression after LVI	VI, C-scan, SEM	The effect of the inter-ply angle (2.5° to 45°) on mechanical properties was investigated. The highest maximum force and its corresponding displacement were observed at 2.5°, while the highest absorbed energy was recorded at 20°	[20, 49]	2020, 2019

Table 3 (continued)

Material	Lay-up configuration	Manufacturing technique	Mechanical characterization	Micro-structure investigation technique	Summary of key trends based on mechanical properties	Reference	Year
Flax/epoxy	CP, QI and helicoidal	Hand-layup + autoclave	QSI and HVI	VI and μCT	The helicoidal laminate with a 9° inter-ply angle (SH-9) exhibited the highest absorbed energy, measuring 61.4 J, followed by the 3° laminate (SH-3) with 59.5 J. In contrast, the CP and QI laminates exhibited lower values of 47.3 J and 52.0 J, respectively	[44]	2021
Basalt/epoxy	CP and Helicoidal	Resin infusion	Pendulum impact test	SEM and FEA	The 15° helicoidal composite demonstrates superior impact resistance, achieving a toughness of 199.8 kJ/m^2, approximately 45% higher than traditional laminate alternatives	[246]	2023
Glass/epoxy, Glass/urethane, Kevlar/epoxy Kevlar/urethane	QI and helicoidal	Wet layup + HAO	LVI and compression after LVI	SEM, OM and VI	Epoxy-based composites exhibited higher maximum loads than urethane-based composites, but suffered severe external damage (delamination and fiber breakage), while urethane showed none. The QI laminate exhibited a higher maximum load compared to helicoidal laminates. Crucially, all helicoidal epoxy-matrix panels demonstrated significantly reduced dent depth compared to the quasi-isotropic baseline, indicating superior resistance to through-thickness damage, with the small-angle panels performing best. Furthermore, most helicoidal epoxy composites showed substantial improvements in residual compressive strength over the quasi-isotropic design, led by the large-angle glass–epoxy laminates, which reported an increase of over 60%. Kevlar/epoxy composites with small (7.5°), medium (15°), and large-angle (30°) helicoidal geometries achieved residual strength improvements of 17%, 25%, and 8%, respectively, compared to the quasi-isotropic laminate	[51]	2020
Carbon/epoxy	QI and helicoidal	Numerical study	LVI	FEA	High energy absorption values were recorded for the helicoidal-recursive, helicoidal-exponential, and helicoidal-semicircular laminates compared to the QI laminate	[129]	2019

Table 3 (continued)

Material	Lay-up configuration	Manufacturing technique	Mechanical characterization	Micro-structure investigation technique	Summary of key trends based on mechanical properties	Reference	Year
Carbon/PA6	Helicoidal	Hand-layup + Hot press	Charpy impact, Flexural	SEM, OM, and FEA	Double-helicoidal (DH-20) configurations significantly outperformed single-helicoidal architectures (SH-10, SH-20), increasing specific energy absorption by 122.5% and 26.5%, respectively. In both single-and double-helicoidal configurations, interlaminar stress governed the failure mechanism. However, the higher interlaminar stress in double-helicoidal designs triggered multiple, highly predictable delaminations, driving the superior energy dissipation	[21]	2020
CFRP (USN 15000/6511/RC33	Helicoidal	Hand-layup + autoclave	Short beam (Interlaminar shear)	μCT	The helicoidal laminate with a 9.1° inter-ply angle exhibited a higher maximum load and a delayed catastrophic failure compared with other helicoidal configurations (6°, 12°, and 25.7° plies) due to crack twisting and branching mechanisms	[160]	2021

Tables 3 and 4 demonstrate that the optimal helicoidal stacking sequence shifts based on the target performance metric. For instance, certain helicoidal configurations optimize maximum force, while others are tuned for maximum displacement or enhanced damage tolerance. At the same time, certain helicoidal configurations perform worse than conventional layup configurations (e.g., cross-ply and quasi-isotropic). The mechanical properties of the optimal helicoidal stacking sequence depend on parameters such as fiber and matrix types, manufacturing techniques, laminate configurations, inter-ply angles, and loading conditions. Therefore, no single overall trend applies to helicoidal configurations as a universal design; rather, their effectiveness depends entirely on the intended application and performance requirements.

6 Future perspectives

This section highlights significant research gaps that future studies can address across different applications of helicoidal FRP composites.

7 Research gaps in manufacturing and mechanical characterization of helicoidal composites

- High-velocity impact studies on helicoidal UHMWPE composites are limited, with only a few available [2, 38, 155]. Further studies on bio-inspired interleaved hybrid designs using Titanium/CFRP/Zylon fiber (PBO)/CFRP/PBO (Fig. 38), combined with UHMWPE, are recommended to improve ballistic impact performance for aerospace engine containment casing applications. More importantly, further studies on advanced

Table 4 Mechanical and microstructural investigation of hybrid and particle-filler helicoidal composites

Material	Lay-up configuration	Manufacturing technique	Mechanical characterization	Micro-structure investigation technique	Summary of key trends based on mechanical properties	Reference	Year
Flax/epoxy Glass/epoxy, and hybrid flax/glass/epoxy	QI and helicoidal	Hand-layup + autoclave	LVI	VI	The perforation energy of the hybrid helicoidal laminate (30 wt% GFRP/70 wt% flax fiber-reinforced polymer (FFRP)) outperforms plain GFRP by 11.7% and plain FFRP by 143.8%	[47]	2024
Carbon/epoxy/nylon 6	CP and helicoidal	Hand-layup + hot press	Mode I and QSI	VI and μCT	Helicoidal laminates experienced significantly less fiber damage than CP laminates, allowing them to recover up to 91% of their out-of-plane strength upon healing, compared to only 56% for the CP baseline. Because damage in helicoidal configurations with small inter-ply angles is dominated by extensive spiraling matrix splits rather than permanent fiber breakage, these laminates successfully eliminated major fiber damage, restoring most of their peak load and stiffness even after catastrophic failure. Conversely, while helicoidal laminates with larger inter-ply angles increased the virgin peak load, they induced greater fiber damage, which significantly limited healing efficiency	[158]	2020
Glass/epoxy/nylon 6	QI and helicoidal	Hand-layup + autoclave	LVI	VI	The perforation energy of the 61-ply helicoidal GFRP laminate is 48% higher than that of its QI counterpart. Notably, the 49-ply helicoidal laminate exhibited the same energy absorption as the 61-ply QI laminate, indicating a 20% weight reduction achieved by the helicoidal architecture. Moreover, incorporating polyamide 6 (PA6) into the glass/epoxy can completely heal impact damage in these helicoidal GFRP composites	[98]	2022

Table 4 (continued)

Material	Lay-up configuration	Manufacturing technique	Mechanical characterization	Micro-structure investigation technique	Summary of key trends based on mechanical properties	Reference	Year
Carbon/epoxy/nylon 6	QI and helicoidal	Hand-layup + autoclave	QSI, mode II fracture toughness, and LVI	VI and μCT	Helicoidal carbon/epoxy laminates with small inter-ply angles divert impact damage to the matrix. Incorporating Nylon6 powder allows specimens with intact fibers to fully recover or exceed their virgin out-of-plane strength. A 6° laminate (H6) achieves a full-recovery impact threshold 75% higher than quasi-isotropic laminates. However, this recovery depends strictly on the angle: H6 fully recovers from a 43.4 J impact, while an 18° laminate only recovers up to 24.8 J	[97]	2023
Carbon/PP, glass/PP, and hybrid carbon/glass/PP	Helicoidal	Hand-layup + hot press	Tensile, compressive, shear, and LVI	VI, SEM, μCT, 'C' scan, FEA	A multi-objective optimization was performed to optimize the material cost and LVI resistance of helicoidal CFRP/GFRP hybrid composites under multiple impact loads. Compared to the baseline design, the optimized configuration increased peak energy absorption by 31%, while reducing material cost by 33%	[151]	2022
Al_2O_3/epoxy	Helicoidal	Ball miller + DIW	Rheology, flexural, and fracture toughness	SEM, OM and μCT	Quasi-static loading tests demonstrated that infusing epoxy resin significantly reinforces the bionic gradient Al_2O_3 ceramic structure. This configuration activates multiple synergistic toughening mechanisms, including crack deflection and interfacial debonding	[206]	2025

Table 4 (continued)

Material	Lay-up configuration	Manufacturing technique	Mechanical characterization	Microstructure investigation technique	Summary of key trends based on mechanical properties	Reference	Year
Carbon/epoxy/Al_2O_3	Helicoidal	Ball miller + Vat photopolymerization (VPP)	Rheology, flexural, and fracture toughness	SEM, VI and, FEA	Investigating the effects of fiber initiation and rotation angles revealed that continuous carbon fibers significantly enhance mechanical properties compared to epoxy/Al_2O_3 counterparts. Specifically, fiber reinforcement increased average bending strength by 12% and fracture toughness by 62%	[192]	2024
Short carbon fiber/Al powder/polymer	Helicoidal	Ball miller + DIW	Rheology, flexural,, fracture toughness, LVI, HVI and high strain rate	SEM, VI, high speed camera and, FEA	A short carbon fiber/Al powder/polymer composite with a 15° twisted helicoidal configuration exhibited exceptional strength and toughness. Compared to the baseline Al powder/polymer composite, its maximum toughness (32 kJ/m^3), flexural strength (8.86 MPa), and flexural toughness (472 kJ/m^3) increased by 170%, 64%, and 300%, respectively. Impact tests also confirmed that the helicoidal architecture enhanced both peak stress and total energy absorption (~10.08 MJ/m^3)	[99]	2025
Stainless steel fibers/photosensitive resin	Helicoidal	DLP—Magnetically assisted 3D-printing	Tensile, compressive, and friction (wear)	SEM and OM	The composite displayed anisotropic behavior, with maximum tensile and compressive strengths occurring in the longitudinal (aligned) fiber direction and optimal tribological performance in the transverse direction. Regarding fiber loading, the 5% composite outperformed both the 10% and 15% variants in mechanical and frictional efficiency	[204]	2020

Table 4 (continued)

Material	Lay-up configuration	Manufacturing technique	Mechanical characterization	Micro-structure investigation technique	Summary of key trends based on mechanical properties	Reference	Year
MWCNTs/photo-curable resin	Helicoidal	DMD—electrically assisted 3D-printing	Tensile and compressive	SEM, OM and, FEA	Helicoidal-type MWCNTs were synthesized to mimic the helicoidal collagen or chitin fibers found in nature. The maximum load capacity is greatly enhanced by the exceptional fracture resistance inherent to the helicoidal pattern, mirroring natural armor architectures. Furthermore, minimizing the rotation angle increases energy dissipation and improves impact resistance	[203]	2017

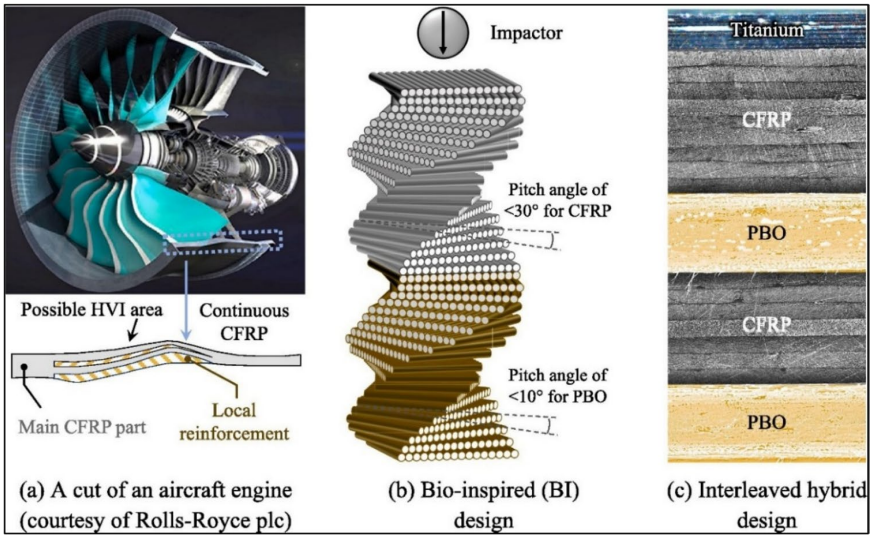


Fig. 38 Combination of bio-inspired helicoidal and interleaved hybrid design concept for aerospace engine containment casing, as these structures are subjected to high-velocity impact (HVI) [254]

manufacturing techniques, such as AFP and AM, are needed to prevent defects when fabricating helicoidal layups.

- To the best of our knowledge, Elium® is the only infusible thermoplastic resin currently available on the market that can be infused into different types of fabrics using vacuum-assisted resin transfer molding to fabricate thermoplastic fiber-reinforced polymer composites [247, 248]. Elium® resin-based thermoplastic synthetic fiber-reinforced polymer composites are widely used in various ballistic impact applications because of their self-healing properties [247, 249]. Self-healing composites significantly enhance toughness [239]. No studies are available on the helicoidal fiber orientation of Elium® resin-based infusible thermoplastic composites. Further studies are required to fill the research gap in the ballistic impact response of Elium® thermoplastic composites reinforced with helically oriented high-performance fibers, such as Kevlar and polyethylene.

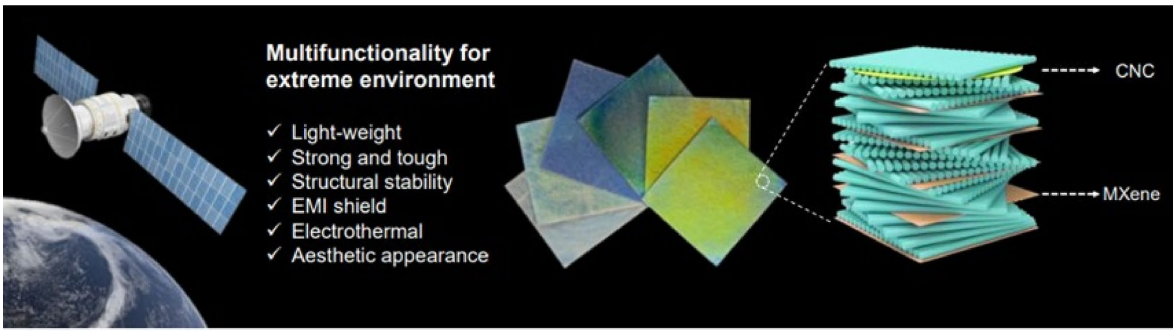


Fig. 39 Biomimetic cellulose nanocrystal (CNC) and MXene-based helicoidal composites for space applications [250]

- Mechanical characterization studies of helicoidal composites related to NFRCs are much more limited than those of SFRCs; therefore, further studies are needed to improve biodegradability. Moreover, studies on hybrid synthetic and natural fiber-reinforced helicoidal composite structures are very limited [47]. Such studies are important for enhancing mechanical performance by addressing the undesirable properties of both fiber types.
- Further studies are recommended on biomimetic cellulose nanocrystal (CNC) and MXene-based helicoidal composites for space applications, as shown in Fig. 39, owing to their multifunctional properties, including lightweight, high strength and toughness, excellent structural stability, and effective electromagnetic interference (EMI) shielding [43, 250, 251].
- Studies on the self-healing of helicoidal composites are limited to synthetic fiber-reinforced thermoset-thermoplastic composites (carbon/epoxy/nylon 6 [158] and glass/epoxy/nylon [98]). Therefore, further studies are required on natural fiber-reinforced thermoset-thermoplastic composites.
- The effect of ply blocking on minimizing fiber damage and maximizing the healing efficiency of thermoplastic helicoidal composites warrants investigation. Under impact testing, laminates with high levels of ply blocking fully recovered their strength and stiffness after healing. Those with lower levels of ply blocking sustained fiber damage but still recovered their stiffness [171]. Moreover, studies on HVI tests remain very limited [223]; therefore, further research is needed on this topic.
- Studies on fiber-metal hybridization of helicoidal composites remain limited because manufacturing stiffness-mismatched materials is challenging and often leads to premature interfacial failure. However, Dai et al. [5] recently developed aluminum-CFRP fiber-metal helicoidal and quasi-isotropic samples using a bio-inspired interface-structure synergy (BISS) approach. Then they performed LVI tests at an impact energy of 100 J. The energy absorption ratio and damage resistance increased by 45% and 77%, respectively. However, further studies are needed on this topic.
- High-strain-rate studies of helicoidal composites are very limited, except for this study performed recently by Liu et al. [84]. These studies are important for understanding the performance of helicoidal composites under dynamic loading at different strain rates and for minimizing catastrophic failure [4, 252].
- Studies on the fatigue behavior, environmental durability, and scaling challenges of helicoidal composites remain limited. Understanding helicoidal composite behavior under repeated cycles is important for assessing multi-impact resistance [253]; therefore, further studies are needed.
- Few experimental studies are available on the free-vibration response of helicoidal laminates [164]. These studies are important for ground vibration testing during aircraft assembly.
- Time-lapse in-situ mechanical tests are important for biological structures to understand failure mechanisms progressively; these studies remain limited [108].

8 Research gaps in optical property characterization of helicoidal composites:

- Zhang et al. [11] reviewed micro/nano-manufacturing strategies for bio-inspired hybrid nanocomposites with hierarchical architectures, highlighting applications in biomedical implants (nacre/bone), adhesives (petals/gecko feet), superhydrophobic surfaces (lotus/mosquito eyes), and photonic coatings (brittlestars/Morpho butterflies). Building on these insights, future research can expand into optically active helicoidal hybrid nanocomposites tailored for optical and polarized-light applications [19, 120]. Moreover, multilayer helicoidal architectures and 3D photonic crystals (e.g., single diamond or gyroid structures) in beetle cuticles grant exceptional reflectivity and full photonic bandgaps [111, 255]. However, optical data on bio-inspired helicoidal composites remain sparse. Further research is necessary to explore the periodicity of these composites for photonic, sensing, and additive manufacturing (e.g., laser lithography) applications. Additionally, while the shear-wave filtering parameter and gap-midgap ratio depend on the shear modulus ratio (C44/C66) and interply angle [221], further theoretical studies are required to predict the normalized first bandgap size across varying FRP composites.

9 Research gaps in artificial intelligence-based modeling of helicoidal composites

- Future studies on artificial intelligence-based modeling, including machine and deep learning techniques for particle-filled helicoidal nanocomposite structures, are needed to optimize process parameters, including rheology-based viscoelastic properties for ball milling and printing parameters for DLP and DIW 3D printing techniques. As a result, process time and process-induced defects can be reduced.

10 Conclusions

This review highlights a decade of advances in bio-inspired helicoidal composites. Specifically, integrating hybrid natural/synthetic fibers or nanoparticle reinforcements (graphene, Al_2O_3, and MWCNTs) with advanced manufacturing techniques, such as automated fiber placement and additive manufacturing, enables scalable, cost-effective production of complex geometries while incorporating real-time defect tracing. Machine learning and deep learning algorithms further optimize these process parameters, refine destructive and non-destructive testing data, and advance computational modeling. Helicoidal composites with low inter-ply angles (5° to 20°) consistently outperform conventional lay-ups under quasi-static and impact loading. This superior performance occurs because they minimize fiber-direction stiffness drops across the thickness and force matrix cracks to twist along extended helical paths, dramatically enhancing damage tolerance and interlaminar fracture toughness. Furthermore, thermoplastic helicoidal laminates with high ply blocking achieve complete strength and stiffness recovery after healing because fiber damage is minimized and healing efficiency is maximized, highlighting their potential for next-generation structural applications.

In the end, the following future perspectives are recommended for further studies, including: (i) High-strain-rate and fatigue behavior of helicoid composites remain major research gaps; therefore, further studies are important to fill this gap. (ii) Bio-inspired interleaved hybrid designs using Titanium/CFRP/Zylon fiber (PBO)/CFRP/PBO, combined with UHMWPE to improve ballistic impact performance for aerospace engine containment casing applications, and (iii) Biomimetic cellulose nanocrystal (CNC) and MXene-based helicoidal composites for space applications.

Acknowledgements This work was supported by the University of California, Irvine, USA.

Author contribution NK—Conceptualization, Methodology, Writing —Original Draft, Writing—Review and Editing, Data Curation, Investigation, Visualization AN—Data Curation, Investigation, Formal Analysis, Validation ES—Data Curation, Investigation, Formal Analysis, Validation DK—Conceptualization, Writing—Review and Editing, Supervision, Project Administration, Funding Acquisition, Validation, Resources.

Funding D.K. gratefully acknowledges the financial support from the Air Force Office of Scientific Research, Grant No. FA9550-23–1-0209 and FA9550-24–1-0283, and support from a JSPS Fellowship (Fellowship ID L26554) from the Japan Society for the Promotion of Science.

Data availability No datasets were generated or analysed during the current study.

Declarations

Competing interests The authors declare no competing interests.

Open Access This article is licensed under a Creative Commons Attribution 4.0 International License, which permits use, sharing, adaptation, distribution and reproduction in any medium or format, as long as you give appropriate credit to the original author(s) and the source, provide a link to the Creative Commons licence, and indicate if changes were made. The images or other third party material in this article are included in the article's Creative Commons licence, unless indicated otherwise in a credit line to the material. If material is not included in the article's Creative Commons licence and your intended use is not permitted by statutory regulation or exceeds the permitted use, you will need to obtain permission directly from the copyright holder. To view a copy of this licence, visit http://creativecommons.org/licenses/by/4.0/.

References

1. Plocher J, Mencattelli L, Narducci F, Pinho S (2021) Learning from nature: bio-inspiration for damage-tolerant high-performance fibre-reinforced composites. Compos Sci Technol. https://doi.org/10.1016/j.compscitech.2021.108669
2. Joshi A, Mishra A, Saxena VK (2024) Impact response and energy absorption mechanisms of UHMWPE fabric and composites in ballistic applications: a comprehensive review. Compos A Appl Sci Manuf 185.
3. Ao X, Zarzoso M, Collado I, Vázquez-López A, Sánchez del Río Sáez J, Plaza Gallardo B et al (2026) Laser-induced-graphene on Kevlar fabric as multifunctional reinforcement layer for basalt fiber/biobased epoxy composites: in-situ strain sensing, electromagnetic shielding and De-icing. Compos Part B Eng 322.
4. Naresh K, Shankar K, Velmurugan R, Gupta NK (2020) High strain rate studies for different laminate configurations of bi-directional glass/epoxy and carbon/epoxy composites using DIC. Structures 27:2451–2465
5. Whitehouse AD, Molla S, Médeau V, Mencattelli L, Finlayson J, Pinho ST (2025) Tailorable through-thickness fibre reinforcement in CFRP laminates with AFP via Repeated Segment Stacking. Compos Part C Open Access 17.
6. Natarajan B, Gilman JW (2018) Bioinspired Bouligand cellulose nanocrystal composites: a review of mechanical properties. Philos Trans R Soc A Math Phys Eng Sci. https://doi.org/10.1098/rsta.2017.0050
7. Egan P, Sinko R, LeDuc PR, Keten S (2015) The role of mechanics in biological and bio-inspired systems. Nat Commun 6:7418
8. Xu Y, Feng D (2024) Enhancing impact resistance of fiber-reinforced polymer composites through bio-inspired helicoidal structures: a review. Polym Compos. https://doi.org/10.1002/pc.29352
9. Wu H, Guo A, Kong D, Li X, Wu J, Wang H et al (2024) Nacre-like carbon fiber-reinforced biomimetic ceramic composites: fabrication, microstructure, and mechanical performance. Ceram Int 50(14):25388–25399
10. Häsä R, Pinho ST (2020) Bio-inspired armour: CFRP with scales for perforation resistance. Mater Lett. https://doi.org/10.1016/j.matlet.2020.127966
11. Zhang C, McAdams DA 2nd, Grunlan JC (2016) Nano/micro-manufacturing of bioinspired materials: a review of methods to mimic natural structures. Adv Mater 28(30):6292–6321
12. Ning H, Monroe C, Gibbons S, Gaskey B, Flater P (2024) A review of helicoidal composites: from natural to bio-inspired damage tolerant materials. Int Mater Rev 69(3–4):181–228
13. Wei Z, Hu X, Hu X, Yu Y (2026) A comparative experimental investigation of the static flexural behavior of five typical bio-inspired composite structures. J Compos Sci. https://doi.org/10.3390/jcs10080440
14. Bouligand Y (1972) Twisted fibrous arrangements in biological materials and cholesteric mesophases. Tissue Cell 4(2):189–217
15. Caviness C, Chen Y, Yang Z, Wang H, Wu Y, Meng Z (2024) Improved ballistic impact resistance of nanofibrillar cellulose films with discontinuous fibrous bouligand architecture. J Appl Mech 91(2).

16. Cheng L, Thomas A, Glancey JL, Karlsson AM (2011) Mechanical behavior of bio-inspired laminated composites. Compos Part A Appl Sci Manuf 42(2):211–220
17. Yaraghi NA, Guarin-Zapata N, Grunenfelder LK, Hintsala E, Bhowmick S, Hiller JM et al (2016) A Sinusoidally Architected Helicoidal Biocomposite. Adv Mater 28(32):6835–6844
18. Quan H, Yang W, Schaible E, Ritchie RO, Meyers MA (2018) Novel defense mechanisms in the armor of the scales of the "living fossil" coelacanth fish. Adv Funct Mater. https://doi.org/10.1002/adfm.201804237
19. Weaver JC, Milliron GW, Miserez A, Evans-Lutterodt K, Herrera S, Gallana I et al (2012) The stomatopod dactyl club: a formidable damage-tolerant biological hammer. Science 336(6086):1275–1280
20. Mencattelli L, Pinho ST (2019) Realising bio-inspired impact damage-tolerant thin-ply CFRP Bouligand structures via promoting diffused sub-critical helicoidal damage. Compos Sci Technol. https://doi.org/10.1016/j.compscitech.2019.107684
21. Yin S, Chen H, Yang R, He Q, Chen D, Ye L et al (2020) Tough nature-inspired helicoidal composites with printing-induced voids. Cell Rep Phys Sci. https://doi.org/10.1016/j.xcrp.2020.100109
22. Patek SN, Korff WL, Caldwell RL (2004) Deadly strike mechanism of a mantis shrimp. Nature 428:819–820
23. Luo H, Wang H, Zhao Z, Xue H, Li Y (2023) Experimental and numerical investigation on the failure behavior of Bouligand laminates under off-axis open-hole tensile loading. Compos Struct 313.
24. Bert A, Mencattelli L, Kisailus D, Wasilenkoff C High impact-resistant, reinforced fiber for leading edge protection of aerodynamic structures. US Patent 11,952,1032024.
25. Ouyang W, Gao X, Yan L, Gong B, Wang H, Peng H-X (2024) Biomimetic approach to gradient-helicoidal laminates for impact-resistant applications. Adv Compos Hybrid Mater 7(6):217
26. https://wwwcompositesworldcom/articles/creating-stronger-composites-through-nature-inspired-helicoid-designs.
27. Guarin-Zapata N, Gomez J, Yaraghi N, Kisailus D, Zavattieri PD (2015) Shear wave filtering in naturally-occurring Bouligand structures. Acta Biomater 23:11–20
28. Suksangpanya N, Yaraghi NA, Kisailus D, Zavattieri P (2017) Twisting cracks in Bouligand structures. J Mech Behav Biomed Mater 76:38–57
29. Wu K, Song Z, Liu M, Wang Z, Chen SM, Yu SH et al (2025) Distorting crack-front geometry for enhanced toughness by manipulating bioinspired heterogeneity. Nat Commun 16(1):194
30. Sokolova L, Infante D, Vladimir J, Ermakova E (2020) Helical surfaces and their application in engineering design. Int J Adv Sci Technol 29:1839–1846
31. Inzerillo L (2012) Helicoid and Architectural application. Disegnarecon 5(10):219–224
32. Lynch P (2016) Vincent Callebaut Architectures' Double Helix Eco-Tower Takes Shape in Taiwan. https://wwwarchdailycom/800209/vincent-callebaut-architectures-double-helix-eco-tower-takes-shape-in-taiwan.
33. https://wwwaboutamazoncom/news/job-creation-and-investment/building-on-progress-at-amazons-hq2-in-arlington-virginia.
34. Arc https://wwwarc-magazinecom/meixi-urban-helix-china/.
35. https://wwwmathcurvecom/surfacesgb/helicoiddeveloppable/helicoiddeveloppableshtml.
36. Jean PV (2018) A Review of geometry investigations of helicoids. IOP Conf Ser Mater Sci Eng 371:012029
37. Madhu V, Reddy PRS, Reddy TS (2023) Effect of temperature and ply angle on performance of ultra high molecular weight polyethylene (UHMWPE) laminates under low velocity impact. Def Sci J 73(2):163–170
38. Hu P, Li X, Chen W, Ge X, Hu Z, Zhang Y et al (2026) Ballistic behavior of bionic UHMWPE laminates with double-helicoidal lay-ups. Thin-Walled Struct 218.
39. Aziz AR, Al Abdouli H, Kakur N, Ramos H, Savioli R, Guan Z et al (2025) The effects of high strain-rate and temperature on tensile properties of UHMWPE composite laminates. Compos Part C Open Access 16.
40. Ghazlan A, Ngo T, Tan P, Xie YM, Tran P, Donough M (2021) Inspiration from Nature's body armours – A review of biological and bioinspired composites. Compos Part B Eng 205.
41. Recommended pressure cycle for Dyneema HB UD grades (metric). https://wwwdyneemacom/our-products/dyneema-ud.
42. Eckhoff D, Thomesen S, Heisserer U, Børvik T (2025) Ballistic response behaviour of Dyneema® HB210 curved armour plates: an experimental and numerical study. Thin-Walled Struct 213.
43. Khan MKA, Mujahid Y, Alahmed N, Khan KA (2026) A review of multifunctional hybrid fiber-reinforced polymer (HFRP) composites for aerospace applications. Adv Compos Hybrid Mater 9(2).
44. Chew E, Liu JL, Tay TE, Tran LQN, Tan VBC (2021) Improving the mechanical properties of natural fibre reinforced laminates composites through biomimicry. Compos Struct 258:113208
45. Han Q, Shi S, Liu Z, Han Z, Niu S, Zhang J et al (2020) Study on impact resistance behaviors of a novel composite laminate with basalt fiber for helical-sinusoidal bionic structure of dactyl club of mantis shrimp. Compos B Eng 191:107976
46. Han Q, Qin H, Han Z, Zhang J, Niu S, Sun Y et al (2020) Study on mechanical properties of multi-structure dactyl-inspired sandwich honeycomb with basalt fiber. Compos Struct. https://doi.org/10.1016/j.compstruct.2020.112467

47. Liu JL, Pham VNH, Mencattelli L, Chew E, Chua PY, Shen J et al (2024) Improving the impact performance of natural fiber reinforced laminate through hybridization and layup design. Compos Sci Technol. https://doi.org/10.1016/j.compscitech.2024.110585
48. Shang JS, Ngern NHH, Tan VBC (2016) Crustacean-inspired helicoidal laminates. Compos Sci Technol 128:222–232
49. Mencattelli L, Pinho ST (2020) Ultra-thin-ply CFRP Bouligand bio-inspired structures with enhanced load-bearing capacity, delayed catastrophic failure and high energy dissipation capability. Compos Part A Appl Sci Manufact 129.
50. Mencattelli L, Pinho ST (2020) Herringbone-Bouligand CFRP structures: a new tailorable damage-tolerant solution for damage containment and reduced delaminations. Compos Sci Technol. https://doi.org/10.1016/j.compscitech.2020.108047
51. Rivera J, Yaraghi NA, Huang W, Gray D, Kisailus D (2020) Modulation of impact energy dissipation in biomimetic helicoidal composites. J Mater Res Technol 9(6):14619–14629
52. Ighalo JO, Adeyanju CA, Ogunniyi S, Adeniyi AG, Abdulkareem SA (2020) An empirical review of the recent advances in treatment of natural fibers for reinforced plastic composites. Compos Interfaces 28(9):925–960
53. Keerthi Gowda BS, Naresh K, Ilangovan S, Sanjay MR, Siengchin S (2021) Effect of fiber volume fraction on mechanical and fire resistance properties of basalt/polyester and pineapple/polyester composites. J Nat Fibers. https://doi.org/10.1080/15440478.2021.1904479
54. Srisuk R, Techawinyutham L, Vinod A, Mavinkere Rangappa S, Siengchin S (2023) Agro-waste from *Bambusa flexuosa* stem fibers: a sustainable and green material for lightweight polymer composites. J Build Eng. https://doi.org/10.1016/j.jobe.2023.106674
55. Huda MS, Drzal LT, Ray D, Mohanty AK, Mishra M (2008) Natural-fiber composites in the automotive sector. In Properties and Performance of Natural-Fibre Composites. Woodhead Publishing: Oxford, UK, ISBN 9781845692674.
56. Pecas P, Carvalho H, Salman H, Leite M (2018) Natural Fibre Composites and Their Applications: A Review. J Compos Sci 2(4):66
57. Li M, Pu Y, Thomas VM, Yoo CG, Ozcan S, Deng Y et al (2020) Recent advancements of plant-based natural fiber–reinforced composites and their applications. Compos Part B Eng. https://doi.org/10.1016/j.compositesb.2020.108254
58. Ilangovan S, Kumaran SS, Vasudevan A, Naresh K (2019) Effect of silica nanoparticles on mechanical and thermal properties of neat epoxy and filament wounded E-glass/epoxy and basalt/epoxy composite tubes. Mater Res Express. https://doi.org/10.1088/2053-1591/ab2601
59. Ilangovan S, Senthil Kumaran S, Naresh K (2020) Effect of nanoparticles loading on free vibration response of epoxy and filament winding basalt/epoxy and E-glass/epoxy composite tubes: experimental, analytical and numerical investigations. Mater Res Express. https://doi.org/10.1088/2053-1591/ab6e36
60. Ramesh M (2019) Flax (*Linum usitatissimum* L.) fibre reinforced polymer composite materials: a review on preparation, properties and prospects. Prog Mater Sci 102:109–66
61. Gowda D, Bhat RS (2024) Bio-inspired helicoidal hemp/basalt/polyurethane rubber bio-composites: Experimental, numerical and analytical ballistic impact study with residual velocity prediction using artificial neural network. Ind Crops Prod 222.
62. Sanjeevi S, Shanmugam V, Kumar S, Ganesan V, Sas G, Johnson DJ et al (2021) Effects of water absorption on the mechanical properties of hybrid natural fibre/phenol formaldehyde composites. Sci Rep 11(1):13385
63. Wolter N, Beber VC, Sandinge A, Blomqvist P, Goethals F, Van Hove M et al (2020) Carbon, glass and basalt fiber reinforced polybenzoxazine: the effects of fiber reinforcement on mechanical, fire, smoke and toxicity properties. Polymers 12(10):2379
64. Bouvier M, Guiheneuf V, Jean-marie A (2019) Modeling and simulation of a composite high-pressure vessel made of sustainable and renewable alternative fibers. Int J Hydrogen Energy 44(23):11970–11978
65. Liu C, Jiang L, Liu H, Feng J, Li Y, Fu A et al (2026) Bio-inspired composite design with variable-stiffness curvilinear helicoidal layup for enhanced impact resistance. Compos Part B Eng 309.
66. Xiang GuG, Su I, Sharma S, Voros JL, Qin Z, Buehler MJ (2016) Three-Dimensional-Printing of Bio-Inspired Composites. J Biomech Eng 138(2):021006
67. Zaheri A, Fenner JS, Russell BP, Restrepo D, Daly M, Wang D et al (2018) Revealing the mechanics of helicoidal composites through additive manufacturing and beetle developmental stage analysis. Adv Funct Mater. https://doi.org/10.1002/adfm.201803073
68. Chanraksmey L, Zhao W, Han Y, Chen Y, Ghita O, Chen B (2026) Recent advances in additive manufacturing of impact-resistant structures with high-performance polymers and their composites. Addit Manuf Front. https://doi.org/10.1016/j.amf.2025.200276
69. Carosella S, Hügle S, Helber F, Middendorf P (2024) A short review on recent advances in automated fiber placement and filament winding technologies. Compos Part B Eng. https://doi.org/10.1016/j.compositesb.2024.111843
70. https://www.compositesworld.com/news/afp-with-very-thin-plies-of-carbon-fiberlmpaek-prepreg-for-sustainable-helicopter-structures-.
71. https://wwwaddcompositescom/post/design-for-manufacturing-composite-helicopter-tailboom-afp.

72. Torres JJ, Simmons M, Sket F, González C (2019) An analysis of void formation mechanisms in out-of-autoclave prepregs by means of X-ray computed tomography. Compos A Appl Sci Manuf 117:230–242
73. Goh GD, Yap YL, Agarwala S, Yeong WY (2019) Recent Progress in Additive Manufacturing of Fiber Reinforced Polymer Composite. Adv Mater Technol 4(1):1800271
74. Towsyfyan H, Biguri A, Boardman R, Blumensath T (2019) Successes and challenges in non-destructive testing of aircraft composite structures. Chinese J Aeronaut 33:771–791
75. Hanhan I, Agyei R, Xiao X, Sangi MD (2019) Comparing non-destructive 3D X-ray computed tomography with destructive optical microscopy for microstructural characterization of fiber reinforced composites. Compos Sci Technol 184:107843
76. Naresh K, Salem A, Khan KA, Cantwell WJ, Umer R (2022) Isothermal compaction-creep-recovery behavior and statistical void analysis of prepregs under various process parameters. Compos Part A Appl Sci Manuf. https://doi.org/10.1016/j.compositesa.2021.106663
77. Inês Silva M, Malitckii E, Santos TG, Vilaça P (2023) Review of conventional and advanced non-destructive testing techniques for detection and characterization of small-scale defects. Progress Mater Sci 138.
78. Naresh K, Khan KA, Umer R, Cantwell WJ (2020) The use of X-ray computed tomography for design and process modeling of aerospace composites: a review. Mater Des. https://doi.org/10.1016/j.matdes.2020.108553
79. Richely E, Bourmaud A, Placet V, Guessasma S, Beaugrand J (2022) A critical review of the ultrastructure, mechanics and modelling of flax fibres and their defects. Prog Mater Sci. https://doi.org/10.1016/j.pmatsci.2021.100851
80. David Muzel S, Bonhin EP, Guimaraes NM, Guidi ES (2020) Application of the Finite Element Method in the Analysis of Composite Materials: A Review. Polymers (Basel) 12(4).
81. Jiang N, Li Y, Li D, Yu T, Li Y, Xu J et al (2020) 3D finite element modeling of water diffusion behavior of jute/PLA composite based on X-ray computed tomography. Compos Sci Technol. https://doi.org/10.1016/j.compscitech.2020.108313
82. Ren Y, Yang C, Li L, Deng Y (2025) Multi-scale analysis of low-velocity impact resistance of bionic helicoidal composite laminates with void defects. Eng Fail Anal 182.
83. Liu JL, Lee HP, Tan VBC (2018) Failure mechanisms in bioinspired helicoidal laminates. Compos Sci Technol 157:99–106
84. Liu Y, Shen J, Li Y, Ge X, Li Y (2021) Enhanced high-strain-rate impact resistance of helicoidal composites by fused deposition modelling. Mech Adv Mater Struct:1–13.
85. Jespersen KM, Glud JA, Zangenberg J, Hosoi A, Kawada H, Mikkelsen LP (2018) Ex-situ X-ray computed tomography, tension clamp and in-situ transilluminated white light imaging data of non-crimp fabric based fibre composite under fatigue loading. Data Brief 21:228–233
86. Azimi M, Eslamlou AD, Pekcan G (2020) Data-driven structural health monitoring and damage detection through deep learning: state-of-the-art review. Sensors (Basel). https://doi.org/10.3390/s20102778
87. Jia Z, An L, Du Z, Wu X, Zhao Z, Li R et al (2025) Machine learning assisted design of bioinspired double helicoidal composites under dynamic three-point bending. Multidiscip Model Mater Struct 21(6):1602–1617
88. Nepal D, Kang S, Adstedt KM, Kanhaiya K, Bockstaller MR, Brinson LC et al (2023) Hierarchically structured bioinspired nanocomposites. Nat Mater 22(1):18–35
89. Arora G, Sharma H, Bhowmik P, Singh MK, Ayyappan V, Rangappa SM et al (2026) Recent Studies on Multiscale Modeling of Natural Fiber-Reinforced Composites. Arch Comput Methods Eng 33(4):5339–5367
90. Mittal S, Gangadhara Prusty B (2026) Artificial intelligence-enabled material design for automated manufacturing of tailored composites – a review. Compos Part B Eng. https://doi.org/10.1016/j.compositesb.2026.113658
91. Preethikaharshini J, Naresh K, Rajeshkumar G, Arumugaprabu V, Khan MA, Khan KA (2022) Review of advanced techniques for manufacturing biocomposites: non-destructive evaluation and artificial intelligence-assisted modeling. J Mater Sci 57(34):16091–16146
92. Yang Z, Yu C-H, Buehler MJ (2021) Deep learning model to predict complex stress and strain fields in hierarchical composites. Sci Adv 7:1–10
93. Huang W, Restrepo D, Jung J-Y, Su FY, Liu Z, Ritchie RO et al (2019) Multiscale toughening mechanisms in biological materials and bioinspired designs. Adv Mater 31(43):1901561
94. Selvan DK, Noor Mohamed MR, Lakshminarasimhan R, Arora G, Kumar M, Ayyappan V et al (2026) Investigation of tribological behaviour of B4C–graphene glass fiber composites using Taguchi, multi-criteria decision making, and machine learning approaches. J Compos Mater 0(0):00219983261450597
95. Yashas Gowda TG, Vinod A, Madhu P, Kushvaha V, Sanjay MR, Siengchin S (2021) A new study on flax-basalt-carbon fiber reinforced epoxy/bioepoxy hybrid composites. Polym Compos 42(4):1891–1900
96. Moorthy JSN, Chandran MS (2026) A comprehensive review on the influence of surface treatment and 3D printing of natural fiber composites. Compos Interfaces 33(2):399–434
97. Liu JL, Pham VNH, Tay TE, Huang J, Chew E, Tan VBC (2023) Bio-inspired helicoidal thin-ply carbon fiber reinforced epoxy laminates with nylon microparticles for improved toughness and healing. Compos Part A Appl Sci Manuf. https://doi.org/10.1016/j.compositesa.2023.107588

98. Liu JL, Mencattelli L, Zhi J, Chua PY, Tay TE, Tan VBC (2022) Lightweight, Fiber-Damage-Resistant, and Healable Bio-Inspired Glass-Fiber Reinforced Polymer Laminate. Polymers 14(3):475
99. Yang L-F, Zhang X-S, Huang X-Y, Chen J, Mao Y-F, Wang J et al (2025) Biomimetic Bouligand structure assisted mechanical enhancement of highly particle-filled polymer composites. Addit Manuf. https://doi.org/10.1016/j.addma.2025.104666
100. Chen S-M, Wen S-M, Zhang S-C, Wang C-X, Yu S-H (2024) Biological and bioinspired Bouligand structural materials: Recent advances and perspectives. Matter 7(2):378–407
101. Wan G, Jin C, Trase I, Zhao S, Chen Z (2018) Helical Structures Mimicking Chiral Seedpod Opening and Tendril Coiling. Sensors 18(9):2973
102. Spinks GM (2020) Advanced actuator materials powered by biomimetic helical fiber topologies. Adv Mater 32(18):e1904093
103. Raney JR, Compton BG, Mueller J, Ober TJ, Shea K, Lewis JA (2018) Rotational 3D printing of damage-tolerant composites with programmable mechanics. Proc Natl Acad Sci U S A 115(6):1198–1203
104. Wilts BD, Whitney HM, Glover BJ, Steiner U, Vignolini S (2014) Natural Helicoidal Structures: Morphology, Self-assembly and Optical Properties. Mater Today Proc 1:177–185
105. Hou J, Aydemir BE, Dumanli AG (2021) Understanding the structural diversity of chitins as a versatile biomaterial. Philos Trans A Math Phys Eng Sci 379(2206):20200331
106. Sharma V, Crne M, Park JO, Srinivasarao M (2014) Bouligand Structures Underlie Circularly Polarized Iridescence of Scarab Beetles: A Closer View. Mater Today Proc 1:161–171
107. Agez G, Bayon C, Mitov M (2017) Multiwavelength micromirrors in the cuticle of scarab beetle Chrysina gloriosa. Acta Biomater 48:357–367
108. Sykes D, Hartwell R, Bradley RS, Burnett TL, Hornberger B, Garwood RJ et al (2019) Time-lapse three-dimensional imaging of crack propagation in beetle cuticle. Acta Biomater 86:109–116
109. Schenk F, Wilts BD, Stavenga DG (2013) The Japanese jewel beetle: a painter's challenge. Bioinspir Biomim 8(4):045002
110. van de Kamp T, Riedel A, Greven H (2016) Micromorphology of the elytral cuticle of beetles, with an emphasis on weevils (Coleoptera: Curculionoidea). Arthropod Struct Dev 45(1):14–22
111. Wilts BD, Saranathan V (2018) A literal elytral rainbow: tunable structural colors using single diamond biophotonic crystals in *Pachyrrhynchus congestus* weevils. Small 14(46):e1802328
112. Zimmermann EA, Gludovatz B, Schaible E, Dave NK, Yang W, Meyers MA et al (2013) Mechanical adaptability of the Bouligand-type structure in natural dermal armour. Nat Commun 4:2634
113. Yang W, Sherman VR, Gludovatz B, Mackey M, Zimmermann EA, Chang EH et al (2014) Protective role of Arapaima gigas fish scales: structure and mechanical behavior. Acta Biomater 10(8):3599–3614
114. Zhang Y, Tan G, Zhang M, Yu Q, Liu Z, Liu Y et al (2022) Bioinspired tungsten-copper composites with Bouligand-type architectures mimicking fish scales. J Mater Sci Technol 96:21–30
115. Sutcharit C, Naggs F, Ablett J, Sang PV, Van Luong H, Panha S (2019) Notes on the sinistral helicoid snail Bertia cambojiensis (Reeve, 1860) from Vietnam (Eupulmonata, Dyakiidae). Zookeys 885:1–14
116. Greenfeld I, Kellersztein I, Wagner HD (2020) Nested helicoids in biological microstructures. Nat Commun 11(1):224
117. Nikolov S, Fabritius H, Petrov M, Friak M, Lymperakis L, Sachs C et al (2011) Robustness and optimal use of design principles of arthropod exoskeletons studied by ab initio-based multiscale simulations. J Mech Behav Biomed Mater 4(2):129–145
118. Ashby M, Cebon D (1993) Materials selection in mechanical design. J Phys IV Colloq 3:1–9
119. Nikolov S, Petrov M, Lymperakis L, Friak M, Sachs C, Fabritius HO et al (2010) Revealing the design principles of high-performance biological composites using ab initio and multiscale simulations: the example of lobster cuticle. Adv Mater 22(4):519–526
120. Lizundia E, Nguyen T-D, Winnick RJ, MacLachlan MJ (2021) Biomimetic photonic materials derived from chitin and chitosan. J Mater Chem C 9(3):796–817
121. Song Z, Ni Y, Cai S (2019) Fracture modes and hybrid toughening mechanisms in oscillated/twisted plywood structure. Acta Biomater 91:284–293
122. Bert A, Mencattelli L, Kisailus D, Wasilenkoff C High impact-resistant, reinforced fiber for leading edge protection of aerodynamic structures. US Patent 11,952,103 B2. 2024.
123. CCM Hochey Industry. https://us.ccmhockey.com/homepage.html.
124. Li S, Tang B, Cai X, Zhang P, Zhou G (2025) Inspired by G-quadruplex DNA: a multi-degree-of-freedom actuator driven by a magnetic soft composite. Compos Part B Eng. https://doi.org/10.1016/j.compositesb.2025.112470
125. Perricone V, Sarmiento E, Nguyen A, Hughes NC, Kisailus D (2024) The convergent design evolution of multiscale biomineralized structures in extinct and extant organisms. Commun Mater. https://doi.org/10.1038/s43246-024-00669-z
126. Bu D, Zhang J, Wu G, Xia Z, Zhang H, Lu C et al (2025) Impact performance of 3D printed ECC inspired by biological Bouligand structure. Constr Build Mater. https://doi.org/10.1016/j.conbuildmat.2025.143826

127. Sharma A, Shukla NK, Belarbi M-O, Abbas M, Garg A, Li L et al (2023) Bio-inspired nacre and helicoidal composites: from structure to mechanical applications. Thin-Walled Struct. https://doi.org/10.1016/j.tws.2023.111146
128. Grunenfelder LK, Suksangpanya N, Salinas C, Milliron G, Yaraghi N, Herrera S et al (2014) Bio-inspired impact-resistant composites. Acta Biomater 10(9):3997–4008
129. Jiang H, Ren Y, Liu Z, Zhang S, Lin Z (2019) Low-velocity impact resistance behaviors of bio-inspired helicoidal composite laminates with non-linear rotation angle based layups. Compos Struct 214:463–475
130. Razali N, Mansor MR, Omar G, Kamarulzaman SAFS, Zin MH, Razali N (2021) Out-of-autoclave as a sustainable composites manufacturing process for aerospace applications. Design for sustainability. pp 395–413
131. Ud Din I, Naresh K, Umer R, Khan KA, Drzal LT, Haq M et al (2020) Processing and out-of-plane properties of composites with embedded graphene paper for EMI shielding applications. Compos A Appl Sci Manuf 134:105901
132. Littner L, Protz R, Kunze E, Bernhardt Y, Kreutzbruck M, Gude M (2023) Flow front monitoring in high-pressure resin transfer molding using phased array ultrasonic testing to optimize mold filling simulations. Materials (Basel). https://doi.org/10.3390/ma17010207
133. Ekuase OA, Anjum N, Eze VO, Okoli OI (2022) A review on the out-of-autoclave process for composite manufacturing. J Compos Sci. https://doi.org/10.3390/jcs6060172
134. Naresh K, Khan KA, Umer R, Cantwell WJ (2020) The use of X-ray computed tomography for design and process modeling of aerospace composites: a review. Mater Des 190:108553
135. Naresh K, Salem A, Khan KA, Cantwell WJ, Umer R (2021) Isothermal compaction-creep-recovery behavior and statistical void analysis of prepregs under various process parameters. Compos Part A Appl Sci Manuf. https://doi.org/10.1016/j.compositesa.2021.106663
136. Mencattelli L, Ouches P, Bert A Realising Impact Damage Tolerant Helicoid Bioinspired Composites with Automated Fiber Placement – from Coupon Testing to Three-Dimensional Preforms 2021.
137. Xu X, Cheng L, Cai Z, Li J, Ke Y (2025) Multi-source lay-up error analysis and lay-up pressure optimization for robotic automated fiber placement (AFP). Compos Part A Appl Sci Manuf. https://doi.org/10.1016/j.compositesa.2025.108825
138. Kukwi T, Shan C, Pengfei L, Zhang B, Leiyang G, Wang Z (2025) Continuous Improvement in Composite Manufacturing: A Review of Automated Fiber Placement Process Evolution and Future Research Prospects. Appl Compos Mater 32(4):1267–1314
139. Ji Y, Luan C, Cheng L, Yao X, Ding Z, Niu C et al (2024) Real-time in-situ process monitoring method based on the self-conductivity of carbon fiber prepreg for automated fiber placement (AFP). Compos Part B Eng. https://doi.org/10.1016/j.compositesb.2024.111356
140. Carbon Fiber Rapid Prototyping: Methods, Tooling, Cost, And The Path To Mass Production - NEXWAVE. https://nexwavecarboncom/blog/carbon-fiber-rapid-prototyping-methods-tooling-cost-and-the-path-to-mass-production/.
141. https://eurekapatsnapcom/report-comparison-of-fiber-volume-fraction-between-resin-liquid-infusion-and-prepreg.
142. Taskin EG, Üstün GE (2026) Comparative life cycle assessment of composite fuel tanks manufactured using filament winding. Clean Technol Environ Policy. https://doi.org/10.1007/s10098-026-03521-9
143. Arsenyeva A, Duddeck F, Thompson HM (2024) An iso-contour method for automated fiber placement optimization of composite structures. Compos Struct. https://doi.org/10.1016/j.compstruct.2023.117628
144. Mujtaba A, Islam F, Kaeding P, Lindemann T, Gangadhara PB (2023) Machine-learning based process monitoring for automated composites manufacturing. J Intell Manuf 36(2):1095–1110
145. Tang C, Sun D, Zou J, Xiong Y, Fang G, Zhang W (2025) Lay-up defects inspection for automated fiber placement with structural light scanning and deep learning. Polym Compos 46(12):11089–11099
146. Mahapatra S, Chen S, Chiappini A, Hallett SR, Belnoue JPH (2024) Model based data-driven optimisation of automated fibre placement set up. Manuf Lett 40:150–153
147. Cardoso D, Silva AR, Correia N (2026) Automated fiber placement gap width prediction using a transformer-based deep learning approach. Processes. https://doi.org/10.3390/pr14040609
148. Tang Y, Wang Q, Cheng L, Li J, Ke Y (2022) An in-process inspection method integrating deep learning and classical algorithm for automated fiber placement. Compos Struct. https://doi.org/10.1016/j.compstruct.2022.116051
149. Santiago RC, Aziz AR, Han F, Kakur N, Savioli R, Alameri R et al (2026) Design and development of ceramic/metal/UHMWPE hybrid ballistic panels for ground combat vehicle applications: experimental testing and numerical modeling. Int J Prot Struct. https://doi.org/10.1177/20414196261443541
150. García-Martínez Á, Fernández-Jiménez A, Sánchez JMG-C, Gutiérrez-Trashorras AJ (2025) Thermal effects of cooling dynamics in autoclave processing on composite materials. Int J Adv Manuf Technol 137(5–6):2979–2989
151. Wang Z, Luo Q, Li Q, Sun G (2022) Design optimization of bioinspired helicoidal CFRPP/GFRPP hybrid composites for multiple low-velocity impact loads. Int J Mech Sci. https://doi.org/10.1016/j.ijmecsci.2022.107064
152. Xin Z-Y, Zhu G-Q, Gattas JM, Luo D (2025) Automated large-scale additive manufacturing of structural formwork with rapid fibre-reinforced polymer tape lamination. Autom Constr. https://doi.org/10.1016/j.autcon.2025.105978
153. Rakhshbahar M, Sinapius M (2018) A novel approach: combination of automated fiber placement (AFP) and additive layer manufacturing (ALM). J Compos Sci. https://doi.org/10.3390/jcs2030042

154. Yin S, Yang R, Huang Y, Guo W, Chen D, Zhang W et al (2021) Toughening mechanism of coelacanth-fish-inspired double-helicoidal composites. Compos Sci Technol. https://doi.org/10.1016/j.compscitech.2021.108650
155. K K, Kazemahvazi S, Russell BP (2016) Optimal fibre architecture of soft-matrix ballistic laminates. Int J Impact Eng 88:227–237
156. Wang H, Wang C, Hazell PJ, Wright A, Zhang Z, Lan X et al (2021) Insights into the high-velocity impact behaviour of bio-inspired composite laminates with helicoidal lay-ups. Polym Test. https://doi.org/10.1016/j.polymertesting.2021.107348
157. Liu JL, Lee HP, Tan VBC (2018) Effects of inter-ply angles on the failure mechanisms in bioinspired helicoidal laminates. Compos Sci Technol 165:282–289
158. Liu JL, Lee HP, Tay TE, Tan VBC (2020) Healable bio-inspired helicoidal laminates. Compos Part A Appl Sci Manuf. https://doi.org/10.1016/j.compositesa.2020.106024
159. Liu JL, Lee HP, Kong SHR, Tan VBC (2019) Improving laminates through non-uniform inter-ply angles. Compos Part A Appl Sci Manuf. https://doi.org/10.1016/j.compositesa.2019.105625
160. Ouyang W, Gong B, Wang H, Scarpa F, Su B, Peng H-X (2021) Identifying optimal rotating pitch angles in composites with Bouligand structure. Compos Commun. https://doi.org/10.1016/j.coco.2020.100602
161. Huang W, Montroni D, Wang T, Murata S, Arakaki A, Nemoto M et al (2022) Nanoarchitected tough biological composites from assembled chitinous scaffolds. Acc Chem Res. https://doi.org/10.1021/acs.accounts.2c00110
162. Huang X, Xiang D, Xie G, Gong Y, Harkin-Jones E, Wang M et al (2025) Improving the impact resistance of basalt fiber-reinforced polymer composites via a biomimetic nacre structure. Compos Commun. https://doi.org/10.1016/j.coco.2024.102233
163. Meo M, Rizzo F, Portus M, Pinto F (2021) Bioinspired helicoidal composite structure featuring functionally graded variable ply pitch. Materials (Basel) 14(18):5133
164. Garg A, Li L, Zheng W, Belarbi M-O, Raman R (2024) Free vibration behaviour of bio-inspired helicoidal laminated composite panels of revolution under thermal conditions: multi-output machine learning approach. Eng Anal Bound Elem. https://doi.org/10.1016/j.enganabound.2024.106024
165. Garg A, Belarbi MO, Chalak HD, Li L, Sharma A, Avcar M et al (2023) Buckling and free vibration analysis of bio-inspired laminated sandwich plates with helicoidal/Bouligand face sheets containing softcore. Ocean Eng. https://doi.org/10.1016/j.oceaneng.2023.113684
166. Wang D, Zaheri A, Russell B, Espinosa H, Zavattieri P (2020) Fiber reorientation in hybrid helicoidal composites. J Mech Behav Biomed Mater 110:103914
167. Suksangpanya N, Yaraghi NA, Pipes RB, Kisailus D, Zavattieri P (2018) Crack twisting and toughening strategies in Bouligand architectures. Int J Solids Struct 150:83–106
168. Ouyang W, Wang H, Dong J, Gong B, Scarpa F, Peng H-X (2023) Cross-helicoidal approach to the design of damage-resistant composites. Compos Struct. https://doi.org/10.1016/j.compstruct.2022.116577
169. Bayat MJ, Kalhori A, Babaei M, Asemi K (2025) Buckling characteristics of bio-inspired helicoidal laminated composite spherical shells under external normal and torsional loads subjected to elastic support. Buildings. https://doi.org/10.3390/buildings15173165
170. Liu JL, Singh AK, Lee HP, Tay TE, Tan VBC (2020) The response of bio-inspired helicoidal laminates to small projectile impact. Int J Impact Eng. https://doi.org/10.1016/j.ijimpeng.2020.103608
171. Liu JL, Mazeli ZAB, Tay TE, Tan VBC (2022) Strength and healing efficiency of helicoidal carbon fiber reinforced thermoplastic laminates. Compos Part A Appl Sci Manuf. https://doi.org/10.1016/j.compositesa.2022.106903
172. Yu Z, Du X, Liu R, Xie Q, Zhang X, Zhu Q (2023) Increasing the compressive strength of helicoidal laminates after low-velocity impact upon mixing with 0° orientation plies and its analysis. Materials (Basel). https://doi.org/10.3390/ma16134599
173. Zhang X, Sun X, Zhang L, Shao Z, Dong Y (2026) Penetration resistance characteristics of bioinspired helical laminated composite structures against projectile impact. Defence Technol 61:234–249
174. Khotjanta P, Aimmanee S (2024) Optimal interply angle of bio-inspired composite curved panels with helicoidal fiber architecture. Compos Struct. https://doi.org/10.1016/j.compstruct.2024.118269
175. Gao Y, Li B, Wang J, Feng X-Q (2021) Fracture toughness analysis of helical fiber-reinforced biocomposites. J Mech Phys Solids. https://doi.org/10.1016/j.jmps.2020.104206
176. Bhowmik P, Sharma H, Arora G, Kumar M, Dhiman B, Ayyappan V et al (2026) Advances in thermoplastic composites focusing on processing, recyclability, and performance. Discov Mech Eng. https://doi.org/10.1007/s44245-026-00238-3
177. Bahrami M, Abenojar J, Martinez MA (2020) Recent progress in hybrid biocomposites: mechanical properties, water absorption, and flame retardancy. Materials (Basel) 13(22):5145
178. Mohanty AK, Vivekanandhan S, Pin J-M, Misra M (2018) Composites from renewable and sustainable resources: Challenges and innovations. Science 362:536–542
179. Asyraf MRM, Ishak MR, Syamsir A, Nurazzi NM, Sabaruddin FA, Shazleen SS et al (2022) Mechanical properties of oil palm fibre-reinforced polymer composites: a review. J Mater Res Technol 17:33–65

180. Norrrahim MNF, Ariffin H, Yasim-Anuar TAT, Hassan MA, Ibrahim NA, Yunus W et al (2021) Performance evaluation of cellulose nanofiber with residual hemicellulose as a nanofiller in polypropylene-based nanocomposite. Polymers (Basel). https://doi.org/10.3390/polym13071064
181. Norrrahim MNF, Ariffin H, Yasim-Anuar TAT, Ghaemi F, Hassan MA, Ibrahim NA et al (2018) Superheated steam pretreatment of cellulose affects its electrospinnability for microfibrillated cellulose production. Cellulose 25(7):3853–3859
182. Mishra G, Mohapatra SR, Behera PR, Dash B, Mohanty UK, Ray BC (2010) Environmental stability of GFRP laminated composites: an emphasis on mechanical behaviour. Aircr Eng Aerosp Technol 82(4):258–266
183. Kumar M, Ayyappan V, Kumar R, Singh MK, Rangappa SM, Siengchin S (2026) Performance of strategically interleaved continuous sisal fiber core 3D printed PLA composites for engineering applications. Int J Adv Manuf Technol 143(7):3601–3616
184. Mwaikambo LY, Ansell MP (2002) Chemical modification of hemp, sisal, jute, and kapok fibers by alkalization. J Appl Polym Sci 84(12):2222–2234
185. Sanjay MR, Siengchin S, Parameswaranpillai J, Jawaid M, Pruncu CI, Khan A (2019) A comprehensive review of techniques for natural fibers as reinforcement in composites: Preparation, processing and characterization. Carbohydr Polym 207:108–21
186. Gupta MK, Ramesh M, Thomas S (2021) Effect of hybridization on properties of natural and synthetic fiber-reinforced polymer composites (2001–2020): A review. Polym Compos 42:4981–5010
187. Arora G, Sharma H, Bhowmik P, Kumar M, Ayyappan V, Singh MK et al (2026) From plant fiber to product: fabrication, properties, and circular pathways of bio-based composites. J Compos Mater 0(0):00219983261425772
188. Kenned JJ, Sankaranarayanasamy K, Kumar CS (2020) Chemical, biological, and nanoclay treatments for natural plant fiber-reinforced polymer composites: A review. Polym Polym Compos 29(7):1011–1038
189. Nurazzi NM, Asyraf MRM, Athiyah SF, Shazleen SS, Rafiqah SA, Harussani MM et al (2021) A review on mechanical performance of hybrid natural fiber polymer composites for structural applications. Polymers. https://doi.org/10.3390/polym13132170
190. Wegst UGK, Ashby MF (2004) The mechanical efficiency of natural materials. Phil Mag 84(21):2167–2186
191. Wegst UG, Bai H, Saiz E, Tomsia AP, Ritchie RO (2015) Bioinspired structural materials. Nat Mater 14(1):23–36
192. Wu H, Guo A, Kong D, Wu J, Qu P, Wang S et al (2024) Preparation of Bouligand biomimetic ceramic composites and the effect of different fiber orientations on mechanical properties. J Manuf Process 132:789–801
193. Das R, Sahu DP, Ayyappan V, Raghunathan V, Yorseng K, Rangappa SM et al (2026) MWCNTs Modified Epoxy Composites Reinforced With Kapok Fiber: Mechanical and Vibrational Study for Automotive Applications. Polym Compos 47(6):5255–5270
194. Luan Y, Gao F, Li Y, Yang J, Hu Y, Guo Z et al (2018) Healing mechanisms induced by synergy of Graphene-CNTs and microwave focusing effect for the thermoplastic polyurethane composites. Compos Part A Appl Sci Manuf 106:34–41
195. Murugan P, Naresh K, Shankar K, Velmurugan R, Balaganesan G (2018) High velocity impact damage investigation of carbon/epoxy/clay nanocomposites using 3D computed tomography. Mater Today Proc 5(9):16946–16955
196. Raghunathan V, Sathyamoorthy G, Ayyappan V, Gapsari F, Mavinkere Rangappa S, Siengchin S (2026) Development of Calcium Sulphate Fiber-Reinforced Polymeric Brake Pads for Vehicle Applications: Next-Generation Friction Materials. Polym Compos 47(7):5943–5963
197. Peng X, Kuang X, Roach DJ, Wang Y, Hamel CM, Lu C et al (2021) Integrating digital light processing with direct ink writing for hybrid 3D printing of functional structures and devices. Addit Manuf. https://doi.org/10.1016/j.addma.2021.101911
198. Yi J, Yang S, Yue L, Lei IM (2025) Digital light processing 3D printing of flexible devices: actuators, sensors and energy devices. Microsyst Nanoeng 11(1):51
199. Shi X, Sun Y, Tian H, Liu H (2024) Evaluation of direct ink write processing parameter window via machine learning. Mater Today Commun 38.
200. Khecho A, Rahman MMT, Reddy D, El-Ghannam A, Joyee EB (2025) DLP-based additive manufacturing of hollow 3D structures with surface activated silicone carbide-polymer composite. Compos Part B-Eng. https://doi.org/10.1016/j.compositesb.2025.112236
201. Alparslan C, Bayraktar S (2025) Advances in digital light processing (DLP) bioprinting: a review of biomaterials and its applications, innovations, challenges, and future perspectives. Polymers (Basel). https://doi.org/10.3390/polym17091287
202. Jang S, Boddorff A, Jang DJ, Lloyd J, Wagner K, Thadhani N et al (2021) Effect of material extrusion process parameters on filament geometry and inter-filament voids in as-fabricated high solids loaded polymer composites. Addit Manuf. https://doi.org/10.1016/j.addma.2021.102313
203. Yang Y, Chen Z, Song X, Zhang Z, Zhang J, Shung KK et al (2017) Biomimetic anisotropic reinforcement architectures by electrically assisted nanocomposite 3D printing. Adv Mater. https://doi.org/10.1002/adma.201605750
204. Ma Y, Wu Q, Duanmu L, Wu S, Liu Q, Li B et al (2020) Bioinspired composites reinforced with ordered steel fibers produced via a magnetically assisted 3D printing process. J Mater Sci 55(32):15510–15522

205. Wen S-M, Chen S-M, Gao W, Zheng Z, Bao J-Z, Cui C et al (2023) Biomimetic gradient bouligand structure enhances impact resistance of ceramic-polymer composites. Adv Mater 35(21):2211175
206. Wang Z, Jiang B, Liu Y, Xin Z, Jiao Z (2025) Three-dimensional printing of rigid-flexible ceramic-epoxy composites with excellent mechanical properties. Materials (Basel). https://doi.org/10.3390/ma18071479
207. Naresh K, Khan KA, Cantwell WJ, Umer R (2022) Rate and temperature dependent compaction-creep-recovery and void analysis of compression molded prepregs. Compos Part B Eng. https://doi.org/10.1016/j.compositesb.2022.109757
208. Karam FK, Zancope K, Carneiro T, Oliviera M, Resende CCD, Neves F (2017) Comparative analysis of optical microscopy, scanning electron microscopy, and micro-computed tomography on measurements. Braz J Oral Sci 16:1–9
209. Vasarhelyi L, Kónya Z, Kukovecz Á, Vajtai R (2020) Microcomputed tomography–based characterization of advanced materials: a review. Mater Today Adv 8:100084
210. Rawson SD, Maksimcuka J, Withers PJ, Cartmell SH (2020) X-ray computed tomography in life sciences. BMC Biol 18(1):21
211. Santi PA (2011) Light sheet fluorescence microscopy: a review. J Histochem Cytochem 59(2):129–138
212. Wadekar P, Goel P, Amanatides C, Dion G, Kamien RD, Breen DE (2020) Geometric modeling of knitted fabrics using helicoid scaffolds. J Eng Fibers Fabrics 15.
213. Elkolali M, Nogueira LP, Ronning PO, Alcocer A (2022) Void content determination of carbon fiber reinforced polymers: a comparison between destructive and non-destructive methods. Polymers (Basel) 14(6).
214. Caglar B, Broggi G, Ali MA, Orgéas L, Michaud V (2022) Deep learning accelerated prediction of the permeability of fibrous microstructures. Compos Part A Appl Sci 106973.
215. Naresh K, Shankar K, Velmurugan R (2018) Digital image processing and thermo-mechanical response of neat epoxy and different laminate orientations of fiber reinforced polymer composites for vibration isolation applications. Int J Polym Anal 23(8):684–709
216. Boon YD, Joshi SC, Bhudolia SK, Gohel G (2020) Recent Advances on the Design Automation for Performance-Optimized Fiber Reinforced Polymer Composite Components. J Compos Sci 4(2):61
217. Guo Y, Liu Y, Oerlemans A, Lao S, Wu S, Lew MS (2016) Deep learning for visual understanding: A review. Neurocomputing 187:27–48
218. Ravanbod S, Rahmani K, Branfoot C, Karmel S, Haque A, Lidgett M et al (2025) Biomimetic composite metastabilisers with programmable multi-directional quasi-zero stiffness and vibration isolation. Mater Today Adv. https://doi.org/10.1016/j.mtadv.2025.100661
219. Wang C, Dong S, Zhao X, Papanastasiou G, Zhang H, Yang G (2020) SaliencyGAN: Deep Learning Semisupervised Salient Object Detection in the Fog of IoT. IEEE Trans Industr Inf 16(4):2667–2676
220. Wang J, Ma Y, Zhang L, Gao RX, Wu D (2018) Deep learning for smart manufacturing: Methods and applications. J Manuf Syst 48:144–156
221. Jiang F, Guan Z, Wang X, Li Z, Tan R, Qiu C (2021) Study on Prediction of Compression Performance of Composite Laminates After Impact Based on Convolutional Neural Networks. Appl Compos Mater 28(4):1153–1173
222. Xu C, Xie J, Wu C, Gao L, Chen G, Song G (2018) Enhancing the Visibility of Delamination during Pulsed Thermography of Carbon Fiber-Reinforced Plates Using a Stacked Autoencoder. Sensors 18(9):2809
223. Pain CD, Egan GF, Chen Z (2022) Deep learning-based image reconstruction and post-processing methods in positron emission tomography for low-dose imaging and resolution enhancement. Eur J Nucl Med Mol Imaging. https://doi.org/10.1007/s00259-022-05746-4
224. Badrinarayanan V, Kendall A, Cipolla R (2017) SegNet: a deep convolutional encoder-decoder architecture for image segmentation. IEEE Trans Pattern Anal Mach Intell 39(12):2481–2495
225. Tian C, Cheng T, Peng Z, Zuo W, Tian Y, Zhang Q et al (2025) A survey on deep learning fundamentals. Artif Intell Rev. https://doi.org/10.1007/s10462-025-11368-7
226. Sinchuk Y, Kibleur P, Aelterman J, Boone MN, Van Paepegem W (2020) Variational and deep learning segmentation of very-low-contrast x-ray computed tomography images of carbon/epoxy woven composites. Materials (Basel) 3(4).
227. Badran A, Marshall D, Legault Z, Makovetsky R, Provencher B, Piché N et al (2020) Automated segmentation of computed tomography images of fiber-reinforced composites by deep learning. J Mater Sci 55(34):16273–16289
228. Badran A, Parkinson D, Ushizima D, Marshall D, Maillet E (2022) Validation of deep learning segmentation of CT images of fiber-reinforced composites. J Compos Sci. https://doi.org/10.3390/jcs6020060
229. Sammons D, Winfree WP, Burke E, Ji S (2016) Segmenting delaminations in carbon fiber reinforced polymer composite CT using convolutional neural networks.
230. Machado JM, Tavares JMRS, Camanho PP, Correia N (2022) Automatic void content assessment of composite laminates using a machine-learning approach. Compos Struct. https://doi.org/10.1016/j.compstruct.2022.115383
231. Marani R, Palumbo D, Galietti U, D'Orazio T (2021) Deep learning for defect characterization in composite laminates inspected by step-heating thermography. Opt Lasers Eng 145.
232. Vaidyanathan A, van der Lubbe M, Leijenaar RTH, van Hoof M, Zerka F, Miraglio B et al (2021) Deep learning for the fully automated segmentation of the inner ear on MRI. Sci Rep 11(1):2885

233. Wang Y, Soutis C, Ando D, Sutou Y, Narita F (2022) Application of deep neural network learning in composites design. Eur J Mater 2:118–171
234. Ribbans B, Li Y, Tan T (2016) A bioinspired study on the interlaminar shear resistance of helicoidal fiber structures. J Mech Behav Biomed Mater 56:57–67
235. Islam MK, Hazell PJ, Escobedo JP, Wang H (2021) Biomimetic armour design strategies for additive manufacturing: a review. Mater Des. https://doi.org/10.1016/j.matdes.2021.109730
236. Biradar A, Arulvel S, Kandasamy J (2023) Significance of ballistic parameters and nanohybridization in the development of textile-based body armor: a review. Int J Impact Eng. https://doi.org/10.1016/j.ijimpeng.2023.104700
237. Bezerra WBA, Lazarus BS, Costa UO, Figueiredo ABS, Lima EP Jr, Luz FSD et al (2023) Energy absorption and ballistic performance of epoxy composite reinforced with arapaima scales. Polymers (Basel). https://doi.org/10.3390/polym15071614
238. Durao ML, Nobre L, Mota C, Bessa J, Cunha F, Fangueiro R (2024) Self-healing composites: a path to redefining material resilience-a comprehensive recent review. Materials (Basel). https://doi.org/10.3390/ma17194681
239. Paladugu SRM, Sreekanth PSR, Sahu SK, Naresh K, Karthick SA, Venkateshwaran N et al (2022) A comprehensive review of self-healing polymer, metal, and ceramic matrix composites and their modeling aspects for aerospace applications. Materials (Basel). https://doi.org/10.3390/ma15238521
240. Wang W-T, Yu H, Potter K, Kim BC (2020) Effect of the characteristics of nylon microparticles on mode-I interlaminar fracture toughness of carbon-fibre/epoxy composites. Compos Part A Appl Sci Manuf. https://doi.org/10.1016/j.compositesa.2020.106073
241. Velmurugan R, Naresh K, Shankar K (2017) Influence of fibre orientation and thickness on the response of CFRP composites subjected to high velocity impact loading. Adv Mater Process Technol 4(1):120–131
242. Thomas FD, Sockalingam S, Sutton MA, Gunnarsson CA, Weerasooriya T, Alexander SL (2026) Quasi-static mode II interlaminar shear behavior of ultrahigh molecular weight (UHMWPE) cross-ply film composites. Thin-Walled Struct. https://doi.org/10.1016/j.tws.2026.115070
243. Abir MR, Tay TE, Lee HP (2019) On the improved ballistic performance of bio-inspired composites. Compos A Appl Sci Manuf 123:59–70
244. Liu JL, Singh AK, Lee HP, Tay TE, Tan VBC (2020) The response of bio-inspired helicoidal laminates to small projectile impact. Int J Impact Eng 142:103608
245. Wen S-M, Gao W, Zhang S-C, Pang J, Cui C, Gao H-L et al (2025) Gradient double-twisted Bouligand structural design for high impact resistance over a wide range of loading velocities. Sci Adv 11:1–10
246. Zhang B, Yang J, Li Y, Zhang J, Niu S, Han Z et al (2023) Bioinspired basalt fiber composites with higher impact resistance through coupling sinusoidal and helical structures inspired by mantis shrimp. Int J Mech Sci. https://doi.org/10.1016/j.ijmecsci.2022.108073
247. Khan T, Irfan MS, Cantwell WJ, Umer R (2022) Crack healing in infusible thermoplastic composite laminates. Compos Part A Appl Sci Manuf. https://doi.org/10.1016/j.compositesa.2022.106896
248. Shah SZH, Megat-Yusoff PSM, Choudhry RS, Sajid Z, Din IU (2021) Experimental investigation on the quasi-static crush performance of resin-infused thermoplastic 3D fibre-reinforced composites. Compos Commun. https://doi.org/10.1016/j.coco.2021.100916
249. Bandaru AK, Chouhan H, Ma H, Kothandan DK, O'Higgins RM (2026) Ballistic impact response of Elium® thermoplastic composites reinforced with high-performance fibres in monolithic and hybrid configurations. Compos Part B Eng 309.
250. Wang Q, Wu B, Yu S, Xiong R (2026) Superstrong and supertough biomimetic nanocellulose composites with gradient bouligand architecture. Nat Commun 2026.
251. Irfan MS, Ali MA, Khan T, Anwer S, Liao K, Umer R (2023) MXene and graphene coated multifunctional fiber reinforced aerospace composites with sensing and EMI shielding abilities. Compos Part A Appl Sci Manufact 165.
252. Naresh K, Shankar K, Rao BS, Velmurugan R (2016) Effect of high strain rate on glass/carbon/hybrid fiber reinforced epoxy laminated composites. Compos B Eng 100:125–135
253. Mencattelli L, Jansen M (2023) Extending impact fatigue life of thermoplastic fibre-reinforced composites via multi-impact resistant nature-inspired Helicoid fibre architectures. Conference: CAMX 2023.
254. Kazemi ME, Medeau V, Chen Y, Xu Z, Petrinic N, Greenhalgh E et al (2024) Ballistic performance of bio-inspired hybrid interleaved composite structures suitable for aerospace applications. Compos Part A Appl Sci Manuf. https://doi.org/10.1016/j.compositesa.2023.107992
255. Stavenga DG, Wilts BD, Leertouwer HL, Hariyama T (2011) Polarized iridescence of the multilayered elytra of the Japanese jewel beetle, Chrysochroa fulgidissima. Philos Trans R Soc Lond B Biol Sci 366(1565):709–723

Publisher's Note Springer Nature remains neutral with regard to jurisdictional claims in published maps and institutional affiliations.

Authors and Affiliations

Naresh Kakur[1,2] · Andrew Tran Nguyen[1] · Ezra Sarmiento[1] · David Kisailus[1]

✉ Naresh Kakur
naresh.kakur@gmail.com

✉ David Kisailus
david.k@uci.edu

[1] Department of Materials Science and Engineering, University of California, Irvine, CA, USA

[2] Advanced Materials Research Center, Technology Innovation Institute, Abu Dhabi, United Arab Emirates